The APOBEC3G-regulated host factors REDD1 and KDELR2 restrict measles virus replication

Die durch APOBEC3G-regulierten Wirtsfaktoren REDD1 und KDELR2 restringieren die Masernvirus Replikation

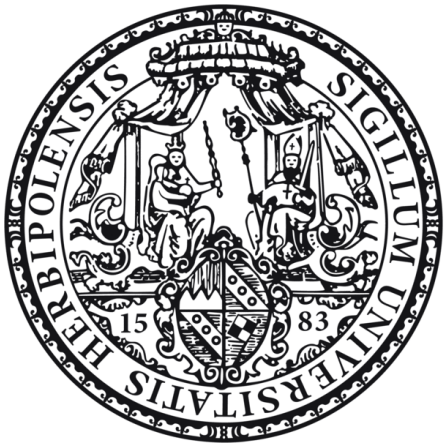

Dissertation

For

Doctoral degree at the Graduate School of Life Sciences

Julius-Maximilians-Universität Würzburg

Section: Infection and Immunity

submitted by

Vishakha Rakesh Tiwarekar

From

Ratnagiri, India

Würzburg, 2018

Submitted on:

Office stamp

Members of the Thesis Committee:

Chairperson: Prof. Dr. Georg Gasteiger, Institute for System Immunology, Julius-Maximilians Universität Würzburg, Germany

Primary Supervisor: Prof. Dr. Jürgen Schneider-Schaulies, Institute of Virology and Immunobiology, Julius-Maximilians-Universität Würzburg, Germany.

Supervisor (Second): Prof. Dr.med. Niklas Beyersdorf, Institute of Virology and Immunobiology, Julius-Maximilians-Universität Würzburg, Germany.

Supervisor (Third): Prof. Dr. Antje Gohla, Department of Pharmacology, Julius-Maximilians-Universität Würzburg, Germany

Date of Public Defence:

Date of Receipt of Certificates:

Affidavit

I hereby confirm that my thesis entitled "**The APOBEC3G-regulated host factors REDD1 and KDELR2 restrict measles virus replication"** is the result of my own work. I did not receive any help or support from commercial consultants. All sources and/or materials applied are listed and specified in the thesis.

Furthermore, I also confirm that this thesis has not yet been submitted as part of another examination process neither in identical or similar form.

Würzburg, 2018 Vishakha Rakesh Tiwarekar

Eidesstattliche Erklärung

Hiermit erkläre ich an Eides statt, die Dissertation „ **Die durch APOBEC3G-regulierten Wirtsfaktoren REDD1 und KDELR2 restringieren die Masernvirus Replikation.**" eigenständig, d.h. insbesondere selbständig und ohne Hilfe eines kommerziellen Promotionsberaters, angefertigt und keine anderen als die von mir angegebenen Quellen und Hilfsmittel verwendet zu haben.
Ich erkläre außerdem, dass die Dissertation weder in gleicher noch in ähnlicher Form bereits in einem anderen Prüfungsverfahren vorgelegen hat.

Würzburg, 2018 Vishakha Rakesh Tiwarekar

To my beloved Dad and Mom
For giving dreams to live for

"Far better to live your own destiny imperfectly than to live an imitation of somebody else 's with perfection."
— The Bhagavad Gita

Acknowledgements

A long journey of hardship, courage and frustration has come to an end, with new challenges in the horizon. I take this opportunity to express my sincere and heartfelt gratitude to all of the amazing people, without whom this journey would have never been accomplished.

First and foremost, I am greatly indebted to my primary supervisor Prof. Dr. Jürgen Schneider-Schaulies, a patient mentor, a true guide and an inspiring Guru. I am grateful for all the guidance and helpful advices you gave me. I feel extremely fortunate to have a supervisor like you, who gave me the freedom to test my crazy ideas and at the same time being my north star to guide me in the correct direction. I sincerely thank you for everything that I have achieved in this journey.

My earnest thanks go to other members of thesis committee Prof. Dr.med Niklas Beyersdrof and Prof. Dr. Antje Gohla. Their valuable guidance, appreciation and constructive criticism have helped throughout the research. I would also like to extend my thanks to all co-authors of the paper for their help and critical reviewing of the research paper.

I am profoundly grateful for the support provided by all colleagues in Prof. Jürgen's lab, especially by Anika and Johannes during my thesis. I want to thank Prof. Dr. Sybille Schneider-Schaulies for involving me in her literature seminars as well as for peer reviewing of my research. I have greatly benefited from her advices and suggestions. Elita and Charlene deserve special thanks for their timely help and advice in the lab.

My research would have been impossible without funding and enormous support from the Graduate School of Life Science. Especially by Prof. Dr Gabriele Blum-Oehler and her team for providing all help possible to achieve my goals. I would also like to thank Prof. Dr Thomas Hünig and immunomodulation for their contribution and support in learning more about immunology.

My deepest appreciation goes to Vini, Hemant and Mohindar for their support and encouragement, I was fortunate to have friends like you who made my life easier in a constant struggle between motherhood and science.

Finally, my parents who mean the world to me, I am fortunate to have a mother and father like you, who always encouraged and supported my every decision. Thank you so much for teaching me what books could not. Your care and scarifies helped me to achieve my dreams. I love you both beyond words. Heartfelt thanks go to my crazy little sisters and best buddies Chaitali and Shraddha, without your endless love, well-wishes and chattering I would not have endured this journey. My deep regards go to my mother in law, father in law and Rohil for their love, encouragement and moral support. I owe my deepest of gratitude to my extended family members Miriam and Clara, you lived up to my trust and took care of my Vrehaa when I was away in the lab.

Last but not least, Rakesh, you are the strength of my thrives. Without your patience, trust and understanding this work would have never completed. During all the ups and downs your confidence in me helped to stay focused and pursue my research. My darling daughter Vrehaa, you are my source of inspiration. I have no word to express the amazing understanding and patience you showed during this period. I am blessed to have such a loving family.

Contents

Summary

Measles is an extremely contagious vaccine-preventable disease responsible for more than 90000 deaths worldwide annually. The number of deaths has declined from 8 million in the pre-vaccination era to few thousands every year due to the highly efficacious vaccine. However, this effective vaccine is still unreachable in many developing countries due to lack of infrastructure, while in developed countries too many people refuse vaccination. Specific antiviral compounds are not yet available. In the current situation, only an extensive vaccination approach along with effective antivirals could help to have a measles-free future. To develop an effective antiviral, detailed knowledge of viral-host interaction is required.

This study was undertaken to understand the interaction between MV and the innate host restriction factor APOBEC3G (A3G), which is well-known for its activity against human immunodeficiency virus (HIV). Restriction of MV replication was not attributed to the cytidine deaminase function of A3G, instead, we identified a novel role of A3G in regulating cellular gene functions. Among two of the A3G regulated host factors, we found that REDD1 reduced MV replication, whereas, KDELR2 hampered MV haemagglutinin (H) surface transport thereby affecting viral release. REDD1, a negative regulator of mTORC1 signalling impaired MV replication by inhibiting mTORC1. A3G regulated REDD1 expression was demonstrated to inversely correlate with MV replication. siRNA mediated silencing of A3G in primary human blood lymphocytes (PBL) reduced REDD1 levels and simultaneously increased MV titres. Also, direct depletion of REDD1 improved MV replication in PBL, indicating its role in A3G mediated restriction of MV. Based on these finding, a new role of rapamycin, a pharmacological inhibitor of mTORC1, was uncovered in successfully diminishing MV replication in Vero as well as in human PBL. The ER and Golgi resident receptor KDELR2 indirectly affected MV by competing with MV-H for cellular chaperones. Due to the sequestering of chaperones by KDELR2, they can no longer assist in MV-H folding and subsequent surface expression. Taken together, the two A3G-regulated host factors REDD1 and KDELR2 are mainly responsible for mediating its antiviral activity against MV.

Zusammenfassung

Masern ist eine extrem ansteckende, durch Impfung verhinderbare Infektionskrankheit, die für mehr als 90000 Todesfälle jährlich weltweit verantwortlich ist. Die Zahl der Todesfälle nahm von ca. 8 Millionen in der Prä-Impf-Ära auf wenige Tausend pro Jahr aufgrund dieses effizienten Impfstoffs ab. Dieser ist jedoch aufgrund mangelnder Infrastruktur in vielen Entwicklungsländern nicht ausreichend verfügbar, oder die Impfung wird – vor allem in entwickelten Ländern – verweigert. Spezifische antivirale Substanzen sind noch nicht verfügbar. So könnte nur eine extensive Impfkampagne zu einer Masern-freien Zukunft führen. Um antivirale Substanzen zu generieren wird detailiertes Wissen über Virus-Wirt-Interaktionen benötigt.

Diese Studie wurde unternommen um Interaktionen zwischen Masernviren (MV) und dem zellulären Restriktionsfaktor APOBEC3G (A3G), der allgemein bekannt für seine antivirale Wirkung gegen das humane Immundefizienzvirus (HIV) ist, zu charakterisieren. A3G hemmt die MV-Replikation nicht aufgrund seiner Cytidin-Desaminase-Funktion, sondern wir entdeckten eine neue Funktion des A3G, nämlich dass es die Expression zellulärer Faktoren reguliert. Wir fanden, dass unter den A3G-regulierten Wirtszellfaktoren REDD1 die MV-Replikation reduzierte, während KDELR2 den Transport des MV-Hämagglutinins (H) zur Zelloberfläche, und somit die Virusfreisetzung, inhibierte. REDD1, ein negativer Regulator des mTORC1-Signalübertragungswegs, reduzierte die MV-Replikation indem es mTORC1 inhibiert. Die Expression des durch A3G regulierten REDD1 korrelierte umgekehrt mit der MV Replikation. SiRNA-vermittelte Reduktion des A3G in primären humanen Lymphozyten des Bluts (PBL) führte zu einer Abnahme des REDD1 und gleichzeitig zu einer Zunahme des MV-Titers. Ebenso führte direktes Silencing des REDD1 zu einer verstärkten MV-Replikation in PBL, was seine Rolle bei der A3G-vermittelten Restriktion der MV-Replikation unterstreicht. Aufgrund dieser Befunde wurde auch eine neue Funktion des mTORC1-Inhibitors Rapamycin als Inhibitor der MV-Replikation in Vero-Zellen und primären PBL aufgedeckt. Der ER- und Golgi-residente Rezeptor KDELR2 wirkte sich indirekt auf die MV-Replikation aus, indem er mit dem MV-H um die Interaktion mit Chaperonen kompetiert. KDELR2 bindet Chaperone und

verhindert so deren Interaktion mit MV-H und den Transport zur Zelloberfläche. Zusammenfassend lässt sich sagen, dass die beiden A3G-regulierten Wirtszellfaktoren REDD1 und KDELR2 hauptsächlich für die antivirale Aktivität des A3G gegen MV verantwortlich sind.

List of Figures

List of Tables

INTRODUCTION

1. Introduction

1.1. Measles virus

More than 100 million viruses are estimated to colonize planet earth and significantly shaping past, present and future of evolution of life. Out of this colossal numbers, 320000 different viruses infect mammals [1]. Adolf Mayer pioneered the research on viruses in 1882 followed by Martinus Beijerinck who conceived the term 'Virus' in 1898. Baltimore classification categorized these viruses in seven different groups which was further developed by ICTV (International Committee on Taxonomy of Viruses).

The family of Paramyxoviridae comprises some unique and classical viruses such as measles virus (MV). Paramyxoviruses are known not only for their extensive disease burden on animal husbandry such as NDV (Newcastle disease Virus) but also for the recently identified deadly viruses such as Nipah and Hendra. MV is a highly infectious virus and assumed to have evolved from rinderpest virus (RPV) during early livestock farming and diverged around 11th century [2]. Antigenically and genetically it is closely related to RPV, a causative agent of a devastating cattle plague. Phylogenetic analysis of MV shows a genetic link to animal viruses such as RPV, peste des petits ruminants virus (PPRV), canine distemper virus (CDV) **(Figure 1.1).**

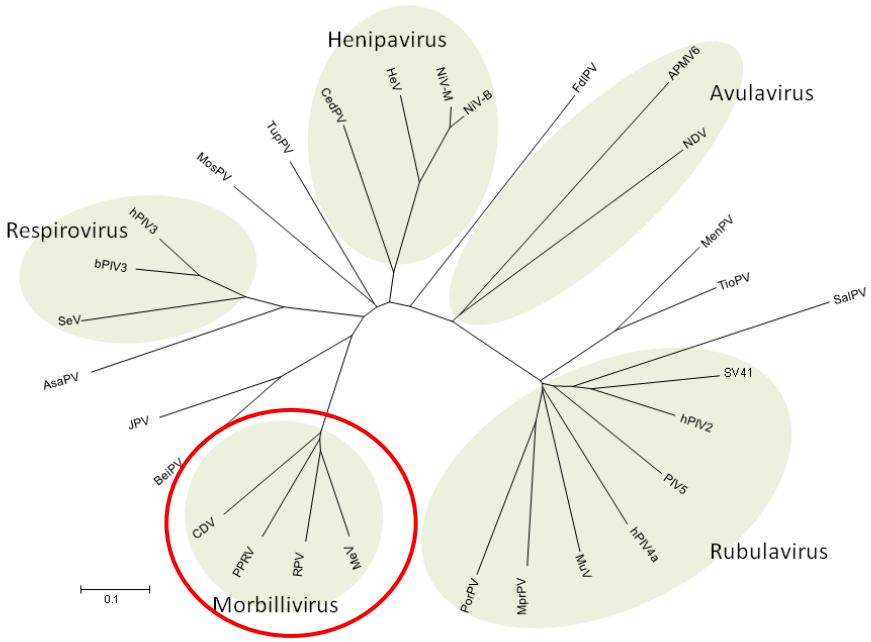

Figure 1.1. Genetic relationship between MV and other morbilliviruses (source [3]).
Measles virus phylogenetic tree based on N protein sequence.

Historic evidence dated back in the 9th century by Abu Becr who gave a scientific description of measles-like symptoms whereas, the earliest repeated epidemics were reported in the 11th and 12th centuries. In 1757, Scottish physician Francis Home shown that measles disease is caused by an infectious agent. It took around 200 years for isolation of MV in tissue culture. In 1954 Enders and Peebles isolated MV from the blood of David Edmonston, whereas, the measles-associated complications such as encephalomyelitis was described in 1790 by James Lucas and subacute sclerosing pan encephalitis (SSPE) by Dawson in 1933 [4].

MV cause acute infection resulting in a cough, fever, Kolpik's spots inside the mouth and flat skin rash. In 30% of cases complications such as diarrhoea, pneumonia and encephalitis appear. Although an effective vaccine is available, MV is still accountable as a major cause of child mortality and morbidity.

1.1.1. Taxonomy

Various morphological features define viruses in a subfamily of Paramyxovirinae such as an enveloped virus with negative stranded non-segmented RNA genome. The term 'myxovirus' implies an affinity for mucin and originally denoted to a large group of enveloped viruses that are able to attach to glycoprotein cell surface receptors. A detailed classification of MV is summarized in **Table 1.1.** The name *Measles* is derived from a word *masel* (Middle Dutch) or *maselen* (middle low German), which means blisters or sick skin spots.

Table 1.1: ICTV taxonomic classification of *Measles virus*

Domain	*Virus*
Group	*Group V (-) ssRNA*
Order	*Mononegavirales*
Family	*Paramyxoviridae*
Subfamily	*Paramyxovirinae*
Genus	*Morbillivirus*
Species	*Measles morbillivirus*

1.1.2. Morphology

MV is a pleomorphic virus of 100-900 nm in size **(Figure 1.2)**. The viral genome is a negative ss RNA of 16 kb, encoding eight viral proteins. The outermost lipid envelope is derived from the plasma membrane of the host cell. The viral genome is encapsidated by ribonucleoprotein (RNP) complex consisting of Nucleoprotein (N), phosphoprotein (P) and large protein (L) [5]. Two viral non-structural proteins V and C are expressed from P genes by RNA editing and alternative translational initiation respectively [6]. The viral RNP is packaged into a lipid envelope. Matrix protein (M) lines the interior of the envelope, whereas, the viral transmembrane glycoproteins hemagglutinin (H) and fusion (F) line the exterior of the envelope [7].

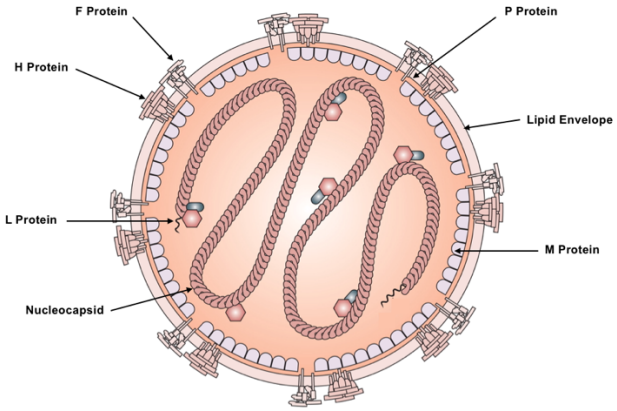

Figure 1.2. Schematic representation of MV virion (source: adapted from [8]).

1.1.3. Genome and Viral proteins

MV negative-stranded RNA genome length is 15,894 bp. Viral RNA is enclosed in nucleoprotein forming helical RNPs (ribonucleoprotein) to which Phosphoprotein (P protein) and Large polymerase proteins (L protein) are attached. The MV genome encodes for eight proteins **(Figure 1.3 and Table 1.2)** Conserved gene-end and gene-start transcriptional control sequences are located at both ends of each gene. The entire sequence is flanked with 52 nt non-coding 3' leader region and 37 nt non-coding trailer region which are essential for viral transcription and replication [9].

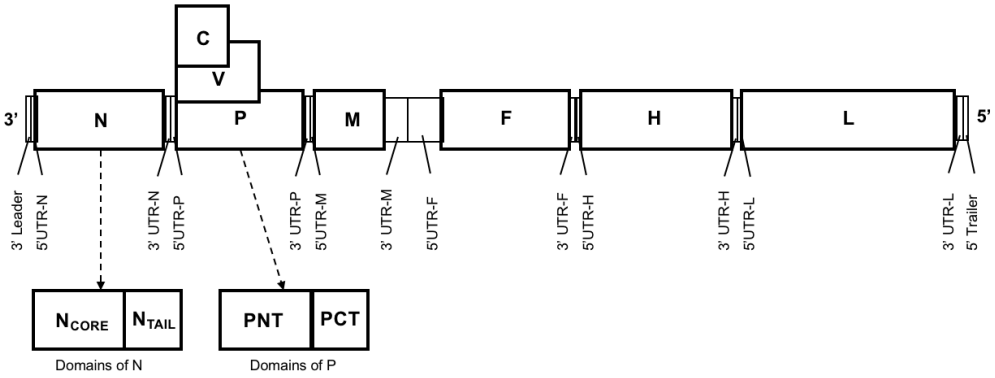

Figure 1.3. Genomic organization of MV (adapted from [10])
(UTR: untranslated regions, PNT: P protein N-terminal, PCT: P protein C-terminal)

Table 1.2: MV genome encoded transcripts and viral proteins (adapted from [9]**)**

Nucleotide number	mRNA	Proteins
1-52	Leader	-
56-1744	N	Nucleocapsid
1748–3402	P/V/C	Phosphoprotein/ V and C protein
3406–4872	M	Matrix protein
4876–7247	F	Fusion glycoprotein
7251–9208	H	Hemagglutinin glycoprotein
9212–15,854	L	Large protein
15,858–15,894	Trailer	-

Out of eight viral proteins, only six are part of the virion. The RNP is the template for transcription and replication. N protein is the first to be transcribed from the genome and a central player in replication of MV. The N-terminal domain of 400 amino acids forms a core region (N_{CORE}) which is important for self-assembly and RNA binding. It also contains a nuclear localization signal which is important for inhibition of IFN-α/β and γ signalling [11]. The C-terminal domain (N_{TAIL}) of 100 amino acids is intrinsically disordered and binds to M and P protein [12]. Apart from its interaction with viral proteins, N_{TAIL} interacts with various cellular proteins. It is also required for flexibility of viral nucleic acid [13].

The second gene transcribed from the genome encodes for the P protein. The P protein upon phosphorylation acts as a co-factor to form a replicase complex by linking L protein to N protein. A less conserved N-terminal domain (PNT) plays an important role in replication by preventing binding on N^0 to cellular RNAs and nuclear translocation. Whereas, the C terminal domain (PCT) is crucial for transcription as it helps for binding of polymerase L to its template [14].

Two more non-structural proteins V and C are transcribed from the P gene which is not detected in fully mature virion released from the cell [15]. The C protein affects interferon signalling and prevents cell death by regulation of viral RNA synthesis [16]. V and C are not required for MV replication in Vero cells, but it has been shown that the C protein is crucial for *in vivo* pathogenesis of measles [17][18].

Matrix (M) protein is the third protein translated. This hydrophobic protein lines the inner leaflet of the viral envelope thus playing a central role in viral assembly and pathogenesis [19]. Interaction of M protein with a cytoplasmic region of H and F glycoproteins regulates the fusogenic capacity of F protein and viral release from infected cells [20]. It also interacts with N protein to regulate viral RNA production [21]. Mutations in the M protein enhance cell to cell fusion and contribute to the establishment of persistent infection [22].

The next two genes encode for hemagglutinin (H) and fusion (F) protein **(Figure 1.4)**. Together with M protein, they form the viral fusion machinery. These highly conserved proteins are embedded in the viral envelope and bind to cellular receptors, and thus are responsible for MV infectivity.

The F protein is a type I transmembrane glycoprotein. It is glycosylated and oligomerized in Endoplasmic Reticulum (ER). F protein is synthesized as 60 kDa inactive precursor (F_0) which is cleaved by cellular furin in trans-Golgi network. The cleavage results in fusion competent mature F protein trimer composed of three monomers linked by disulphide bonds [6].

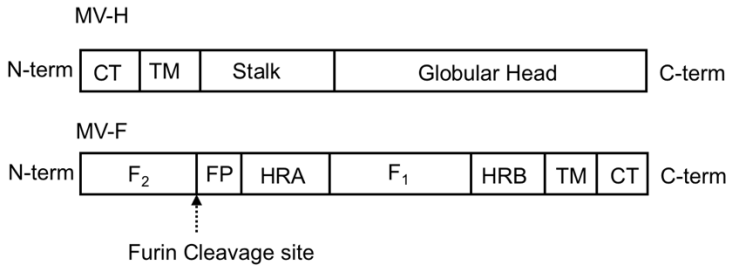

Figure 1.4. Schematic representation of MV glycoproteins.
CT: cytoplasmic tail; TM: Trans-membrane domain; FP: Fusion peptide; HRA: Heptad repeat A; HRB: Heptad repeat B (adapted from [23]).

H is a tetrameric type II transmembrane glycoprotein expressed on mature virions and the infected cell surface. The attachment protein H of MV is different than other Paramyxoviruses as it does not have neuraminidase activity. Instead of

sialic acid H uses CD46, SLAM and Nectin-4 as cellular receptors to determine the cellular tropism [24][25][26][27][28]. Upon binding to cellular receptors conformational changes are triggered in H and F proteins. The so-called fusion peptide of the F protein is inserted into the target cell membrane and fusion pore complex is formed which results in viral entry, or cell to cell fusion [29]. Similar to F protein, H is glycosylated and is oligomerized in the ER and crucial for particle assembly [30]. These glycoproteins are transported to the plasma membrane by cellular secretory pathway and expressed on the infected cell surface for particle assembly or cell to cell fusion [31].

The last gene encodes for a Large protein (L), a highly conserved 250 kDa viral protein which is present in small amounts in infected cells and in virions. Along with P protein L acts as RNA-dependent RNA polymerase (RdRp) and viral RNA is the template for transcription and replication [4][32]. L proteins carry out all essential functions of RNA synthesis such as polymerization, mRNA binding, polyadenylation and methylation [33].

1.1.4. Cellular Receptors

Binding of viral antigens to cellular receptors is a prerequisite for initiating infection in cells, thus, governing susceptibility of cells to a virus. As mentioned above, binding of H on cellular receptors triggers conformational changes in F and this facilitates pH-independent fusion of the viral envelope with the cellular plasma membrane.

Over the period of last 30 years, various groups identified three main cellular receptors for MV. CD46 was the first MV receptor identified in 1993 [24] followed by identification of SLAM/CD150 in 2000 [26] and recently Nectin-4 has been identified as an epithelial cell receptor [27][34]. All three important receptors are shown in **Figure 1.5**.

CD46 (Cluster of differentiation-46) or MCP (membrane cofactor protein) was the first receptor identified for Edmonston vaccine and lab adapted MV strains. It is an inhibitory complement regulatory receptor and expressed on all nucleated cells to protect from damage by complement system [35]. A tyrosine and glycine at position 481 and 546 determine the affinity of H to CD46 [36]. Although identified first, CD46 is less relevant pathologically since no wild-type MV uses

this receptor as efficiently as vaccine strains [9]. Clinical isolates of MV have been shown to prefer SLAM as a cellular receptor [37]thus, indicating that CD46 usage as a receptor reflects *in vitro* adaptation of MV rather than it's *in vivo* ability.

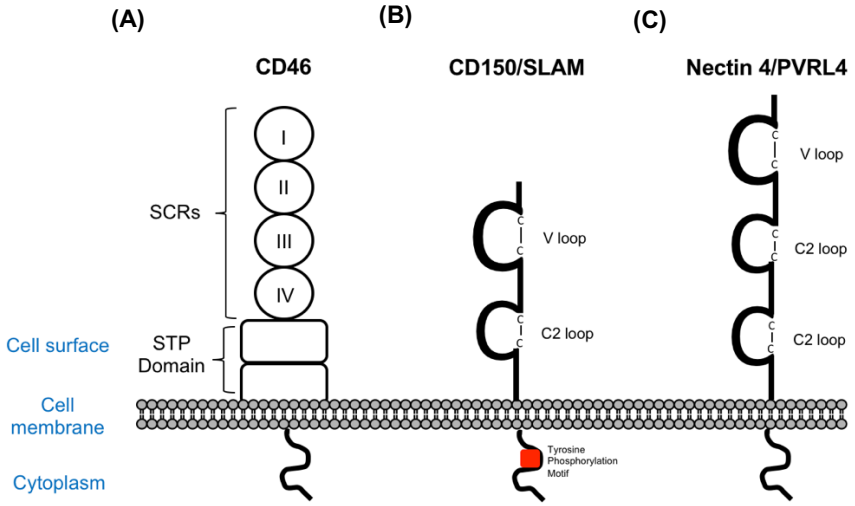

Figure 1.5. Structure of cellular surface receptors for MV (Source: adapted from [38])
(A) CD46 a type I glycoprotein with four SCRs (short consensus repeats), STP domain (Serine-Threonine-Proline), a transmembrane domain and a cytoplasmic domain. **(B)** CD150/SLAM (signalling lymphocyte-activation molecule) a membrane glycoprotein with a variable Ig-like V-type domain (V) and a constant Ig-like C-type domain (C2) domain, transmembrane domain and cytoplasmic domain with tyrosine phosphorylation site **(C)** Nectin-4/PVRL-4 (Polio virus receptor-like protein-4) is member of nectin family and contain one Ig-like V-type domain and two constant Ig-like C-type domain (C2) domain.

A second receptor, CD150 (Cluster of differentiation-150) or SLAM (signalling lymphocyte-activation molecule) is expressed on immune cells such as activated T and B-cells, thymocytes, macrophages and mature Dendritic cells. The distribution of SLAM on immune cells supports lymphotrophism of MV. Wildtype MV as well as Edmonston strains, use SLAM as a receptor but with fivefold higher affinity to SLAM than CD46 [39] [40] [41]. All MV strains ever reported have been shown to use SLAM as a receptor with exception of recombinant SLAM-blind viruses. It is also reported that three residues (Isoleucine 60, Histidine 61 and Valine 63) are critical for SLAM to function as a cellular receptor for MV [42]. However, the absence of SLAM on epithelial and neuronal cells indicated a requirement of another important 'receptor X' for MV entry.

In 2011 this 'receptor X' was identified to be Nectin-4/PVRL-4 (Polio virus receptor-like protein-4) [27][34] thus solved the mystery of MV infection of a respiratory epithelial cell. Nectin-4 is a 55 kDa transmembrane protein belonging to immunoglobulin superfamily [43]. Nectin-4 is expressed the basolateral side of

primary airway epithelial cells and many carcinoma cell lines. This receptor is responsible for mediating infection in respiratory epithelial cells and followed by subsequent amplification of MV and release from apical surfaces of epithelial cells [44].

However, identification of these receptors does not explain the ability of MV to infect neuronal and endothelial cells [45][46] indicating possible use of another unknown receptor by MV.

1.1.5. Viral replication

Viral replication is a biological process in which the virus enters the host cell and forms progeny virus. It is an indispensable step for viruses to establish infection and continuation of infection in the new host. Viruses are dependent on host cells for energy and cellular machinery to synthesize progeny virus, and therefore, can multiply only in living cells.

Viruses of different families have different replication strategies and different intracellular locations to replicate. MV like other members of the *Paramyxoviridae* family replicate entirely in the cytoplasm. The life cycle of MV in a cell is depicted in **Figure 1.6**.

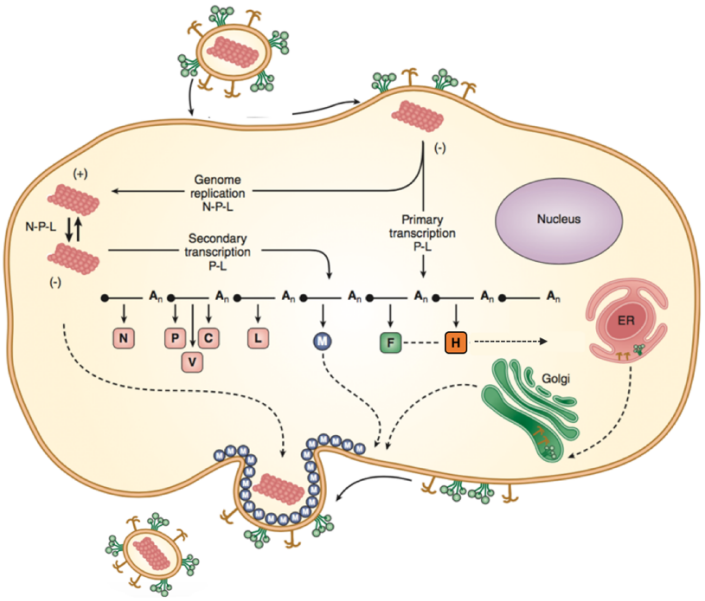

Figure 1.6. Schematic representation of replication of Measles virus (Source: [47] © G.D. Parks and R.A. Lamb 2006)
MV enters the cells by attachment of H on the cellular receptor and viral nucleic acid is released in the cytoplasm. (Solid line: transcription and replication; Dotted line: viral egress). The newly synthesised virus is assembled near the plasma membrane and then released by budding. (N: Nucleocapsid, P: Phosphoprotein, L: Large protein, F: Fusion protein, H: Hemagglutinin, ER: Endoplasmic Reticulum).

Tetrameric H proteins bind to the cellular receptors CD46, SLAM and nectin-4 and trigger conformational changes in H stalk carrying F triggering activity [48] [6][49]. Thus, initiating a series of spontaneous conformational changes in F protein eventually leading to insertion of the fusion peptide into the target membrane. Various models have been proposed to show F activation by H [6]. These structural rearrangements finally result in fusion pore formation via merging of viral and cell membranes. The viral nucleocapsid is then released into the cell cytoplasm for subsequent steps of viral replication.

Viral RdRp uses the negative-stranded non-segmented viral RNA as a template for both transcription to generate mRNA and for replication to generate progeny RNA. Obligatory sequential transcription begins at the 3' end and requires termination of each upstream gene to initiate transcription of the next downstream gene [50]. Thus, MV genes are transcribed sequentially. Each of six viral genes are flanked with 3' short leader sequences and 5' trailer sequences containing start and stop codons. Newly synthesized (+) mRNA is translated into viral proteins by cellular machinery. N protein is synthesized first and in highest amounts of the viral gene products and forms tight complexes with progeny RNA which serves as a functional template for subsequent viral transcription and replication [51][52].

After translation, the H and F proteins undergo post-translational modifications and oligomerization in the ER using cellular chaperones. Impaired ER retention of H and F has been shown to affect the cell to cell fusion ability of MV [30][31].

Newly synthesised viral proteins, the viral genomic RNA, and cellular membrane assemble to form infectious progeny virions which exit host cells by budding in order to infect other susceptible cells. The matrix protein is crucial in MV assembly and the budding process [53][54]. The location of M proteins at the inner leaflet of the viral envelope allows a close interaction not only with the viral RNP complex but also with cytoplasmic tails of H and F glycoproteins. This interaction aggregates them at the plasma membrane for viral assembly and release [55][21]. The M protein interacts with the C-terminal domain of the N

protein. Two leucines at position L523 and L524 of the N protein are important for this interaction. This interaction results in the retention of RNP at the plasma membrane and shifts the equilibrium from viral replication to virus assembly and release [21]. In addition, M proteins at inner leaflet regulate the fusogenic activity of the envelope proteins [56][57]. Taken together, the M protein orchestrates MV budding in an ESCRT (endosomal sorting complexes required for transport) independent manner [58].

1.1.6. Measles virus Pathogenesis

Although MV diverged relatively recently from a common ancestor with RPV [2], humans are the only natural host. Measles is a highly contagious disease with a secondary attack rate of more than 90% [59].

1.1.6.1. Entry into a susceptible host

MV enters a host by respiratory route via infectious droplets and aerosols. The primary site of virus replication was initially believed to be respiratory epithelial cells. However, recent evidence suggest that epithelial cells are infected from basolateral surface and not from apical surfaces [60], hence epithelial cells may get infected in later stages of infection. In non-human primate infection model, lung $CD150^+$ immune cells such as alveolar macrophages and DCs are the first cells reported to be infected by MV followed by significant viral multiplication in BALT (bronchus-associated lymphoid tissue) [61]. These cells then transport MV to local lymphatic tissue and in draining lymph node. Subsequent analysis of MV-infected blood cells and lymphoid tissue have shown a massive replication of MV in $CD150^+$ T and B cells [4][62][63]. Thus, measles is an acute viral infection resulting in the systemic spread of the virus in the host.

Measles has an incubation period of 10-14 days. The prodromal phase of 2-4 days is characterized by classical MV symptoms such as fever followed by running nose (coryza), cough and conjunctivitis. Two to three days later blue-white spots on red background appear inside the mouth which are known as Koplik's spots. Three to five days after onset of initial symptoms measles rash appears throughout the skin starting from hairline to face and neck **(Figure 1.7B)**. Then proceed to arms, legs and feet in the next 3-4 days [64]. The appearance of

symptoms coincides with a viral spread in lymphatic tissue, $CD4^+$ /$CD8^+$ immune response and with cytokine production **(Figure 1.7A).**

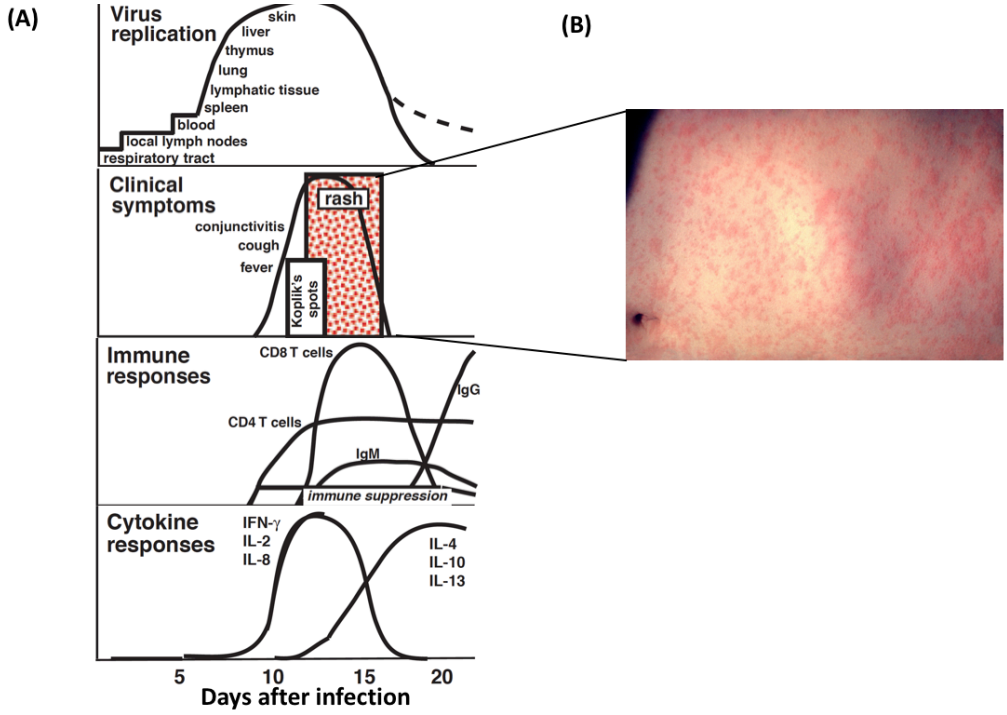

Figure 1.7. Measles virus Pathogenesis
(A) MV enters from the respiratory tract and gradually spread to other organs. Rash appears when MV-specific CD4 and CD8 T cells are activated and antibody response is triggered (adapted from [4]) **(B)** Classical MV rash. (source: CDC/ Heinz F. Eichenwald, MD).

1.1.6.2. Viral dissemination and transmission

Within 4-7 days the virus is detected in blood. Virus dissemination from the primary site of infection is shown in **Figure 1.8**. The viremia is often associated with leukopenia due to significant infection in T and B cells or due to the migration of T and B cells out of the blood vessels into organs. MV replicates in primary, secondary and tertiary lymphoid tissues and forms multinucleated giant cells (syncytia) known as Warthin-Finkeldey cells [4]. Increased LFA-1 (Leucocyte function-associated antigen-1) in MV-infected monocytes and lymphocytes leads to enhanced adherence and virus dissemination to endothelial cells via cell to cell transmission of the virus [65] [66]. MV then spreads systemically via blood to other organs such as kidney, liver, gastrointestinal tract, respiratory tract, genital mucosa, conjunctiva and skin.

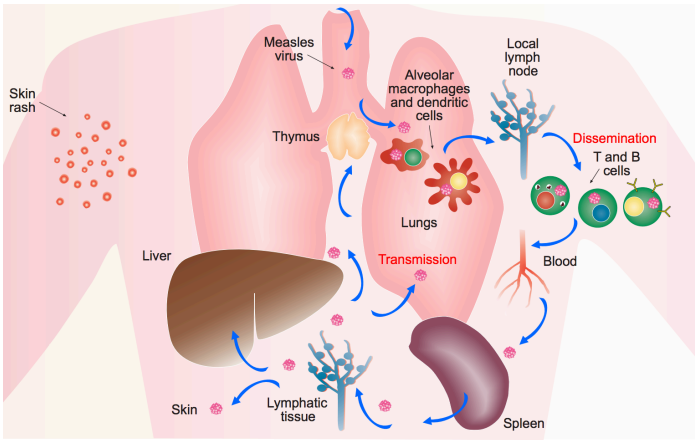

Figure 1.8. Measles virus dissemination cycle (Source: [67])

Epithelial cells of the respiratory tract are highly susceptible for MV infection. The virus is delivered to the basolateral side by infected myeloid cells [68] and then is spread as well as released from the apical surface of the cell [34] in mucus lining of the respiratory tract. These cell-free particles are then released as infectious droplets by coughing.

1.1.7. Immune response

Current knowledge of the immune response to MV is progressively increasing with new aspects of viral-host protein interactions being uncovered. Measles is a typical childhood disease conferring lifelong immunity. Along with the acute infection, MV is known to cause severe immunosuppression and may lead to persistent infections.

1.1.7.1. Innate immune response

The primary defence against all viral infections is mediated by interferons (IFNs). These potent pro-inflammatory cytokines not only play an important role in inhibiting viral replication but also govern host immunity. IFN response is triggered by recognition of viral proteins by cell surface or cytoplasmic PPRs (pattern recognition receptors). Subsequent signalling eventually activates the transcription factors IRF-3 (IFN regulatory factor-3) and NFκB (nuclear factor kappa-light chain enhancer of activated B cells). NFκB regulates different aspects of the innate and adaptive immune response leading to the induction of various proinflammatory cytokines, interferons and ISGs (Interferon-stimulated genes) which can suppress MV replication [69].

TLR (toll-like receptor) 7 and 9 mediated IFNα/β production is aptly shut down by MV [70]. The V protein inhibits IFN production by blocking intracellular sensing molecules such as RIG-I (retinoic acid-inducible gene I) and MDA-5 (melanoma differentiation associated gene 5) [71][72]. Several groups have reported inhibition of IFN and downstream JAK/STAT signalling pathway by P,C and V proteins [73][74][75][76] [77]. As a result, viral replication is not sufficiently suppressed by the innate immune response leading to the systemic spread of MV (reviewed in [78][79][80]).

1.1.7.2. Cellular immune response

Normally, acute MV infection is brief and the virus is cleared within months of onset of disease. Cellular immunity has been shown to be more critical in MV clearance than humoral immunity. Studies on immunodeficient or immunocompromised individuals have proven the importance of the cellular immune response. Individuals with deficient cellular immunity had prolonged infectious period and often died due to MV associated complications [81] [82] while children with agammaglobulinemia cleared the MV infection [83]. *In-vivo*, CD8+ T cell depleted Rhesus monkeys have shown uncontrolled viremia for a prolonged period, higher viral load and severe rash [84], whereas B cell depleted Rhesus monkeys cleared the virus effectively [85]. Similarly, *in-vitro* CD8+ T cells instead of CD4+ T cells controlled MV [86]. Fever and rash slowly resolve as CD8+ and CD4+ T cells infiltrate to infection sites. Follow-up studies on PBMC after recovery period have shown effective IFN-γ production and CD8+ T cell memory response [87].

Before the onset of the rash, effective early T_H1 response is engaged leading to the production of IFN-γ and IL-2, followed by increased IL-2, soluble CD4 and CD8 levels. During convalescence as rash fades, type II cytokines IL-4, IL-5, IL-10 and IL-13 are produced in high levels [88][89].

1.1.7.3. Humoral immune response

MV-specific neutralizing antibodies protect from the disease at the time of exposure, whereas antibody-mediated clearance of MV after the onset of disease has a minor role. Maternal antibodies have been shown to confer protection in infants [90]. Poor prognosis of MV has been shown to be associated with the absence of robust antibody response [91]. Therefore, the induction of neutralizing antibodies by vaccination certainly plays a significant role in the control of MV disease and spread.

Along with the initial onset of rash antibodies are detected in blood. MV-specific IgM dominates the early phase of infection followed by class switching to low avidity IgG2 and IgG3 isotypes. As infection progress the avidity of IgGs increase gradually. These antibodies are then also detected in mucosal secretions [92]. Antibodies are detected for all viral proteins and anti-N antibodies are most prevalent [93]. Antibodies targeting viral envelop glycoprotein H and F result in neutralization of viral infectivity by preventing fusion of viral envelop and cell membrane [94] and downregulate intracellular viral replication[95][96].

1.1.7.4. Immunosuppression

Immunosuppressive effects of MV are known to increase the susceptibility to other diseases and result in deaths due to complications such as pneumonia and diarrhoea [97].Several mechanisms have defined MV-induced immunosuppression such as, 1) short-term lymphopenia: in which due to lymphotrophism of MV, the T and B cells are primarily infected and result in CD95 mediated apoptosis [98][99][100]. Spontaneous apoptosis of uninfected T cells also has been observed [101]. 2) diminished Akt phosphorylation upon MV contact shown to affect T cell activation during immunosuppression [102]. 3) Type-2 cytokine response: during acute measles impaired IL-12 production leads to T_H2 response with increased IL-4, IL-10 and IL-13 production, however, this T_H2 cytokine dominance favours the establishment of humoral immunity during recovery [103][104].

1.1.7.5. ADME

ADME (acute disseminated encephalomyelitis) is an inflammatory demyelinating condition affecting white matter of CNS [105], a frequent complication (in more than 0.1% cases after natural infection) of MV which develop within 2-4 weeks after infection without the presence of virus in the brain [106]. The precise mechanisms of ADME progression are still poorly understood. Structural homology of myelin proteins with foreign epitopes or CNS damage due to direct infection leaking autoantigens in systemic circulation have been thought to trigger autoimmunity [107].

1.1.7.6. Persistent infection

MV virus often persists and slowly spreads from cell to cell without production of detectable amounts of infectious virus [108]. Some of the characteristic features of persistent infection include accumulation of nucleocapsids in the cytoplasm, decreased virus-induced cytopathic effect, limited expression of viral proteins on the infected cell surface and defects in viral proteins. Persistent MV infections of the CNS (central nervous system) can have early or late occurrence after acute onset of MV.

The MIBE (measles inclusion body encephalitis) occurs 1-9 months after acute infection. The frequency of occurrence is rare. MIBE is exclusively seen in immunocompromised individuals especially those with HIV and patients receiving immunosuppressive drugs [109][110]. It is characterized by giant inclusion bodies in neurons and glia [111]. Although the virus can be directly isolated from brain, MIBE differs from SSPE due to the absence of a strong humoral response.

Subacute sclerosing panencephalitis (SSPE) is a fatally progressive neurological disorder which occurs within months to years after the initial onset of measles [112]. Children below the age of two with acute measles infection are at great risk of developing SSPE later in life [113] [114]. Grey and white matter are affected in SSPE and loss of cognitive functions, motor loss, seizures and eventual organ failure are seen in all affected patients (reviewed in [115]). Severe demyelination and wide spread infection of neurons is observed. Oligodendrocytes, astrocytes and endothelial cells are also infected [116]. Abnormally high titres of neutralizing antibodies in serum and CSF (cerebrospinal fluid) are observed in

SSPE patients [112]. Taken together, MV and its protein along with the host's immune response contribute to MV persistence, though the exact role of each and underlying mechanisms yet remain to be elucidated [117].

1.1.8. Epidemiology

1.1.8.1. Strain variation

MV genomes have exceptional stability, a property that is shared among other members of *Paramyxovirinae*. A stable genome, absence of animal reservoir and absence of latency resulted in maintenance of MV only in susceptible human population. Till date, 8 clades and 24 distinct genotypes A, B1-B3, C1-C3, D1-D11, E, F, G1-G3 and H1-H2 of MV have been reported [118]. Association between MV and SSPE was found only with wild-type stains and not with vaccine strains [119]. Despite a number of genotypes MV has only one serotype which is marked by high genetic constrains on H, F, N and M protein. These constrains contributed to the absence of antigenic drift, one serotype and life-long immunity [10].

1.1.8.2. Vaccines

Measles is a vaccine-preventable disease. Herd immunity through active vaccination reduces MV disease burden. Antibody-mediated neutralization of viral glycoprotein have been shown to be sufficient for passive protection against MV [94]. Adaptation by serial passaging of Edmonston strain in chick embryo and chick embryo cells resulted in Edmonston B strain, a first live attenuated vaccine strain [120]. Various efficacious and successful vaccine stains such as Zagreb, AIK-C, CAM, Leningrad-16, Shanghai 191 were derived in subsequent years [4]. Two - dose vaccination at the age of six months and 12 months has shown more than 95% protection during an outbreak [121].

The lyophilized vaccine is a stable vaccine at lower temperatures but lose potency rapidly within one day after reconstitution [122] thus, hamper availability of effective vaccine in undeveloped regions of the world. To improve the delivery method of current vaccine various vaccination strategies are being developed such as inhalation of aerosols or dry powder form [123][124].

1.1.8.3. Global disease burden

Despite availability of an effective vaccine, MV remains a leading cause of mortality and morbidity in young children. In the pre-vaccine era, the outbreaks were frequent, and more than 90 % of the children acquired measles by age of 15. The absence of animal reservoir and latency results in maintenance of MV in the human population only when the stable supply of susceptible individuals is available. Due to high R_0 (basic reproduction number), a 95% level of herd immunity is required to discontinue measles transmission [125][4]. The introduction of mass vaccination in 1963 has reduced the incidence rate, however, it still remains a significant disease burden in children. In 2016, according to WHO 132,129 cases and 89780 deaths were reported worldwide[126] [127].

MV due to its vaccine preventability was targeted for eradication by World health assembly in 2010 [125]. Although MV is eliminated from the North American continent, the remaining five regions yet have to achieve the eradication target. The current incidence rate of MV worldwide is shown in **Figure 1.9**. More than 95% coverage of vaccination is still an unreached target in many parts of the world. In developing countries, poor infrastructure, lack of cold chain, financial burden and availability of trained medical personnel have hampered the coverage of vaccine [128].

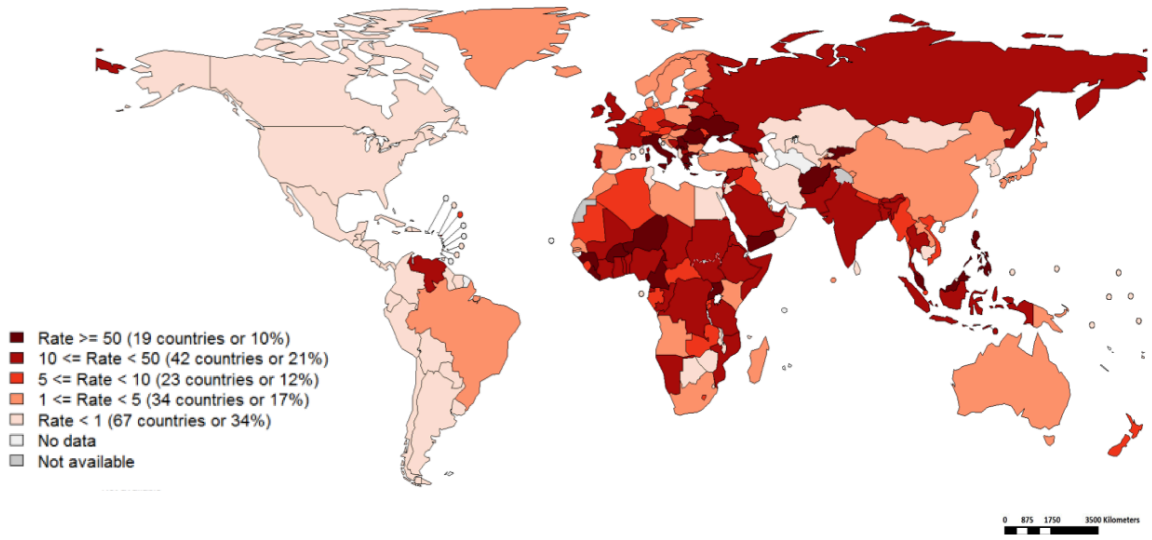

Figure 1.9. Current MV incidence rate worldwide (source WHO 2018)

In developed countries, despite the existing infrastructure and access to the vaccine, hesitancy about vaccination and exemption have led to serious and large outbreaks [129][130]. According to ECDC (European Centre for Disease Prevention and Control) in 2017 Europe itself has seen a fourfold increase in MV incidences [131]. Therefore, sustained efforts and adequate epidemiological surveillance to improve vaccine coverage are required to achieve the goal of global measles elimination.

1.1.9. Treatment

Measles was often reported to re-appear in developed countries when vaccination rates have declined [132]. Currently, there is no specific anti-viral treatment available for measles. An effective therapeutic approach along with broader vaccination coverage could help to promote measles eradication.

Oral supplementation of a high dose of Vitamin A during measles has been observed with a decrease in mortality and morbidity. According to WHO, Vitamin A is recommended for all children with measles [133][134]. IFNα has been used as therapeutics in SSPE patients with partially beneficial and partially relapsing results [135][136]. Treatment with Ribavirin and/or IFNα have shown more promising results than the use of IFNα alone [137][138]. Thus, administration of antivirals after the initial onset of disease might reduce measles complications. Debated reports of MV antiviral efficacy, limitations of IFN and ribavirin and Ig therapies mark requirement of safe, novel and efficacious antiviral against MV [117].

1.2. Innate restriction factors

Recognition of pathogens by several sensing mechanisms and the innate immune response act as the first line of defence. PPRs (Pattern recognition receptors) mediate innate microbial sensing that detects PAMPs (Pathogen - associated molecular patterns). PPRs such as RLRs (RIG-I like receptors), NLRs (NOD-like receptors) are cytoplasmic autonomous viral sensing molecules recognizing viral 5' tri-phosphorylated ss RNA or regions of double-stranded RNA. Whereas TLRs (Toll like receptors) are PPRs that recognize extracellular, endosomal, or membrane-bound structures of pathogens. These different innate sensing mechanisms converge to induce innate and adaptive immune responses [139] [140].

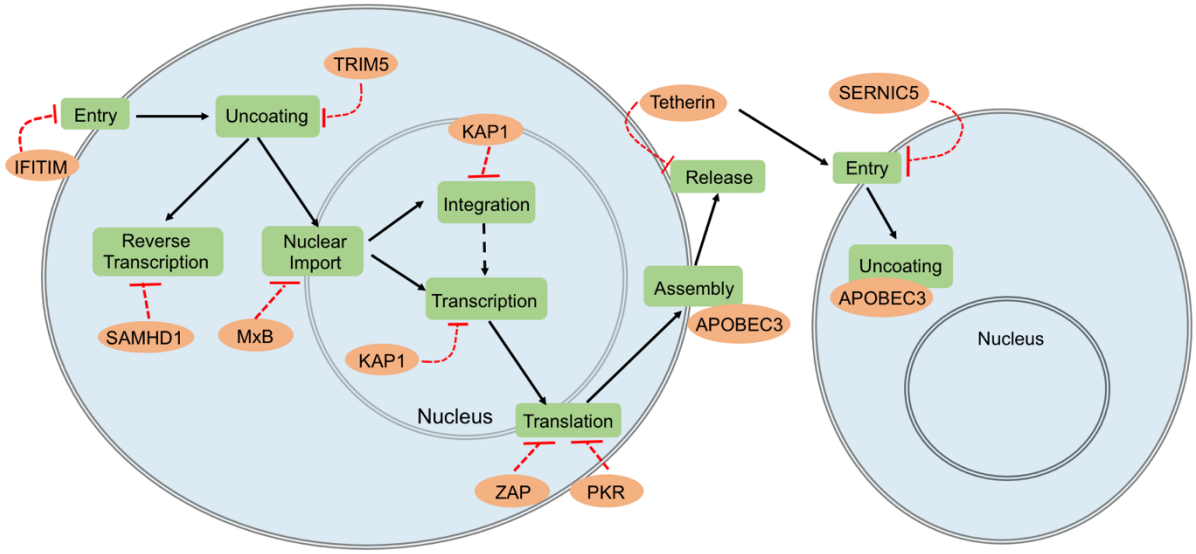

Figure 1.10. Antiviral restriction factors (adapted from [141])
Various restriction factors target various viral components and active against various viral families. Overview above show these restriction factors (in the orange box) target various stages of viral life cycle (in the green box). (IFITIM: interferon-induced transmembrane protein, SAMHD: SAM domain and HD domain-containing protein 1, MxB: myxovirus resistance gene B, TRIM5: tripartite motif-containing protein 5, KAP1: KRAB-associated protein 1, ZAP: zinc-finger antiviral protein, PKR: (ds)RNA-dependent protein kinase R;, APOBEC3: apolipoprotein B mRNA-editing enzyme, catalytic polypeptide-like 3, SERNIC5: serine incorporator; CH25H, cholesterol 25-hydroxylase).

Anti-viral restriction factors are germline encoded proteins that target almost every stage of viral replication **(Figure 1.10)**. Several of these restriction factors are ISGs (interferon-inducible genes) or constitutively present in cells **(Table. 1.3)**. The term 'Restriction Factors' was coined in 1970 by the laboratories working on retroviruses. Although, now it is applicable to a wide range of gene

products targeting different viruses. For qualification of a host gene as a restriction factor, it requires to have certain features such as, antiviral activity, induction by IFN or virus, antagonized by viral proteins and signatures of positive selection. It is also possible that these factors may have unidentified cellular functions. These potent cellular blocks are in a constant evolutionary battle with rapidly mutating antagonizing viral proteins. Thus, have an important role in shaping innate immunity.

Table 1.3: List of various well studied restriction factors (adapted from [140]**)**

Restriction Factor	Target virus	MOA	IFN-inducible
Fv1	Retroviruses	Capsid uncoating	No
TRIM5α	Retroviruses	Capsid uncoating	Yes
APOBEC3 family	Retroviruses, retrotransposons, hepadnaviruses	Reverse transcription	Yes and/or constitutive
SAMHD1	Retroviruses	Reverse transcription	Yes
ZAP	Retroviruses, filoviruses, alphaviruses	Viral protein translation	Yes
Tetherin	Retroviruses, flaviviruses, herpesviruses, rhabdoviruses, paramyxoviruses, arenaviruses	Budding	Yes
Viperin	Orthomyxoviruses, flaviriruses, herpesviruses, alphaviruses, paramyxoviruses	Budding	Yes
MxA and Mx1	Orthomyxoviruses, paramyxoviruses, hepadnaviruses, rhabdoviruses, alphaviruses, bunyaviruses, togaviruses, picornaviruses	Nucleocapsid transport or another early lifecycle step	Yes
IFITM1, IFITM2 and IFITM3	Orthomyxoviruses, flaviviruses, coronaviruses	Endosomal fusion or uncoating	Yes
PKR	Poxviruses	Viral protein translation	Yes

(Fv1: Friend virus susceptibility-1, TRIM5: tripartite motif-containing protein 5, APOBEC3: apolipoprotein B mRNA-editing enzyme, catalytic polypeptide-like 3, SAMHD1: SAM domain and HD domain-containing protein 1, ZAP: zinc-finger antiviral protein, MxA: myxovirus resistance gene A/B, PKR: (ds)RNA-dependent protein kinase R.)

Various viral proteins antagonize these restriction factors by various mechanisms. For example, by targeting restriction factors to cellular protein degradation pathway, down-regulating their expression, mimicking a substrate, or sequestering them. Constant selection pressure on the virus by restriction factors and vice-versa can be seen in the genetic footprint of such proteins. Therefore, the study of these restriction factors is important to enhance our current understanding of immune response against viral infections.

1.3. APOBEC3G

APOBEC3G/A3G (Apolipoprotein B mRNA-editing enzyme catalytic polypeptide-like 3G) belongs to a family of cytidine deaminases and was the first restriction factor identified against HIV-1. HIV-1 Vif (virion infectivity factor)

phosphoprotein deficient virus produced non-infectious virus in “non-permissive” cells such as CD4+ T cells and macrophages whereas, this virus replicated efficiently in lab adapted “permissive” cell line. The non-permissive cells expressed antiviral factor which was antagonized by Vif. In 2002, this factor was identified to be APOBEC3G (A3G) [142].

1.3.1. Evolution

The origin of APOBEC family has been proposed to be in AID (activation-induced cytidine deaminase) ancestral genes found in lymphocytes of jawless fish such as lamprey that lived more than 500 million years ago. These proteins were potent inducers of mutagenesis in various infectious agents of lamprey [143]. Complex gene duplication and positive gene selection in the past have resulted in the generation of current members of the APOBEC family **(Figure 1.11A)** [144]. Currently, the APOBEC family consists of 11 primary gene products that include, AID, APOBEC2 (A2), APOBEC3A (A3A-H) and APOBEC4 (A4) proteins. As shown in **Figure 1.11B** cytidine deaminase motifs are a hallmark of these family [145].

(A) (B)

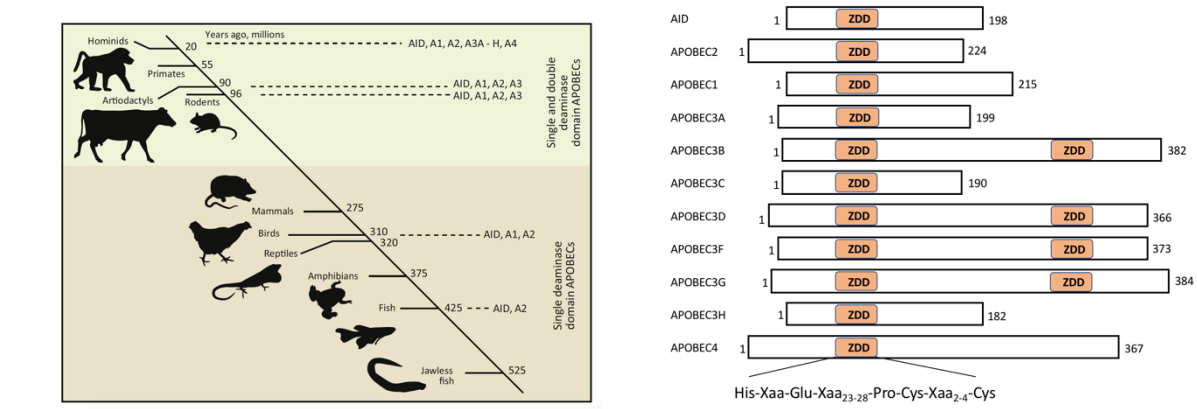

Figure 1.11. A3G evolution and family members
(A) Phylogenetic tree of the evolution of APOBEC family from Jawless fish which contained single deaminase domain to recent single and double deaminase domain containing APOBECs in rodents, primates and human. **(B)** ZDD (Zinc-dependent deaminase domain) organization in each member of APOBEC family is shown schematically. The uniform amino acid sequence is shown below.

AID hyper-mutational activity is responsible for the generation of enormous diversity during V(D)J recombination by three distinct gene diversification processes: class-switching recombination, somatic hypermutation and gene conversion [146]. Along with A3G, other members of APOBEC family such as A3B and A3F have been shown to restrict HIV-1 in absence of Vif [147][148][149]. Not

much information is available about A2 and A4 proteins. Some studies have reported a link of A2 with liver cancer and muscle development (reviewed in [150]). APOBEC proteins of non-human primates have been shown to inhibit HIV-1 which explains the extent of these proteins as restriction factors [151][152].

1.3.2. APOBEC3G structure and function

As mentioned above, APOBEC family members consist of one or two ZDD domains. The C-terminal motif (CD2) is catalytically active, whereas, the N-terminal motif (CD1) is not **(Figure 1.12)**. CD1 mediates RNA binding and encapsidation in HIV virions along with that it is also a target site of Vif. CD2 is responsible for cytidine deaminase activity [153]. The A3G core contains 5 β-sheets and 6 α-helices with loops in their secondary structures which play a significant role in the overall function of this enzyme.

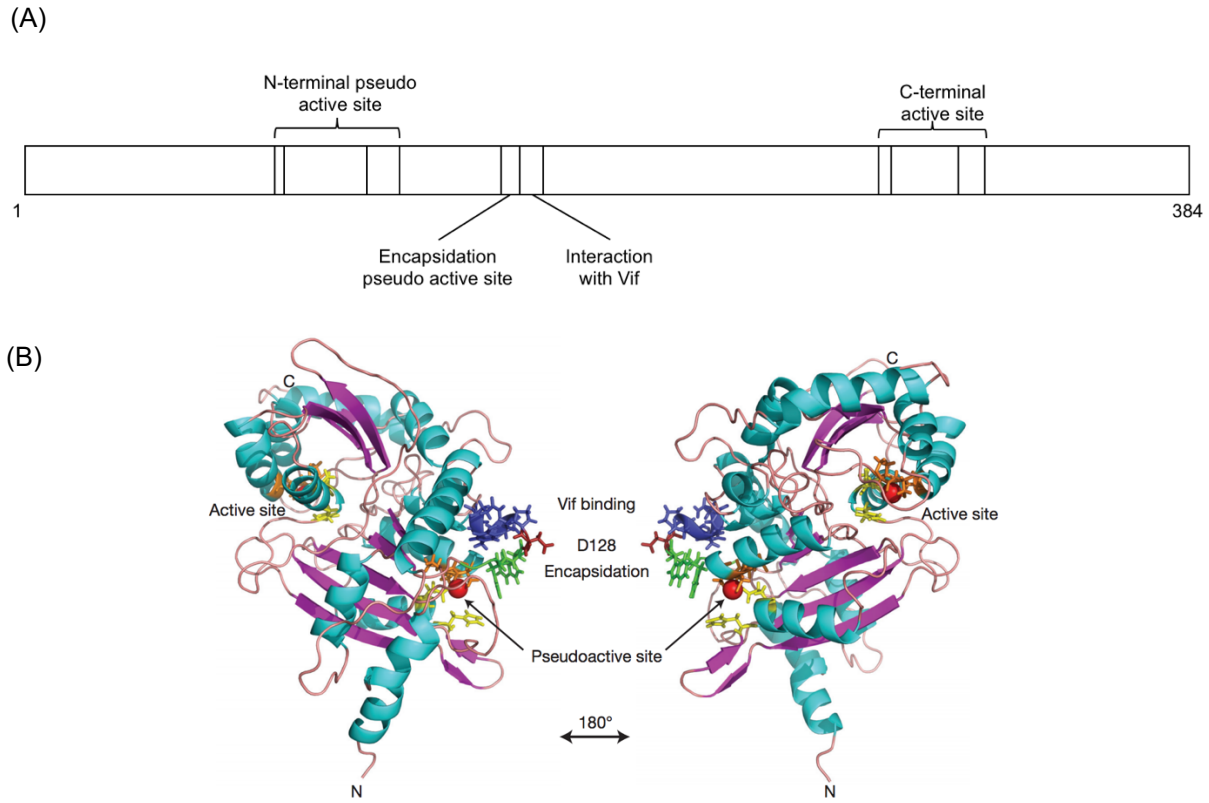

Figure 1.12. Domain structure of A3G
Putative interaction domains of A3G **(A)** Schematic and **(B)** Full-length model of significant domains of A3G (adapted from [154]).

The antiviral activity of A3G is not only attributed to deamination but also to various deaminase independent functions as summarized in **Figure 1.13**. The

deamination by A3G prefers 5'-CCCA-3' sequence and is not a random event. The chemical process **(Figure 1.13B box)** is initiated by hydrolytic deamination at the C4 position of cytosine (C). Briefly, a conserved glutamic acid in the catalytically active domain of A3G deprotonates water, whereas histidine and two cysteine residues coordinate Zn^{2+} ions. The resultant zinc-stabilized and reactive hydroxyl nucleophile attacks the C4 position and replaces the amine group (NH_2) with a carbonyl group (=O) thereby deaminating cytidine (C) to uridine (U) [155][156]. The A3G enzyme preferentially targets viral ssDNA and not retroviral RNA. These mutations are responsible for alterations in the viral open reading frames and erroneous insertions of termination codons. Accumulated dU also results in reduced (-) DNA synthesis [157].

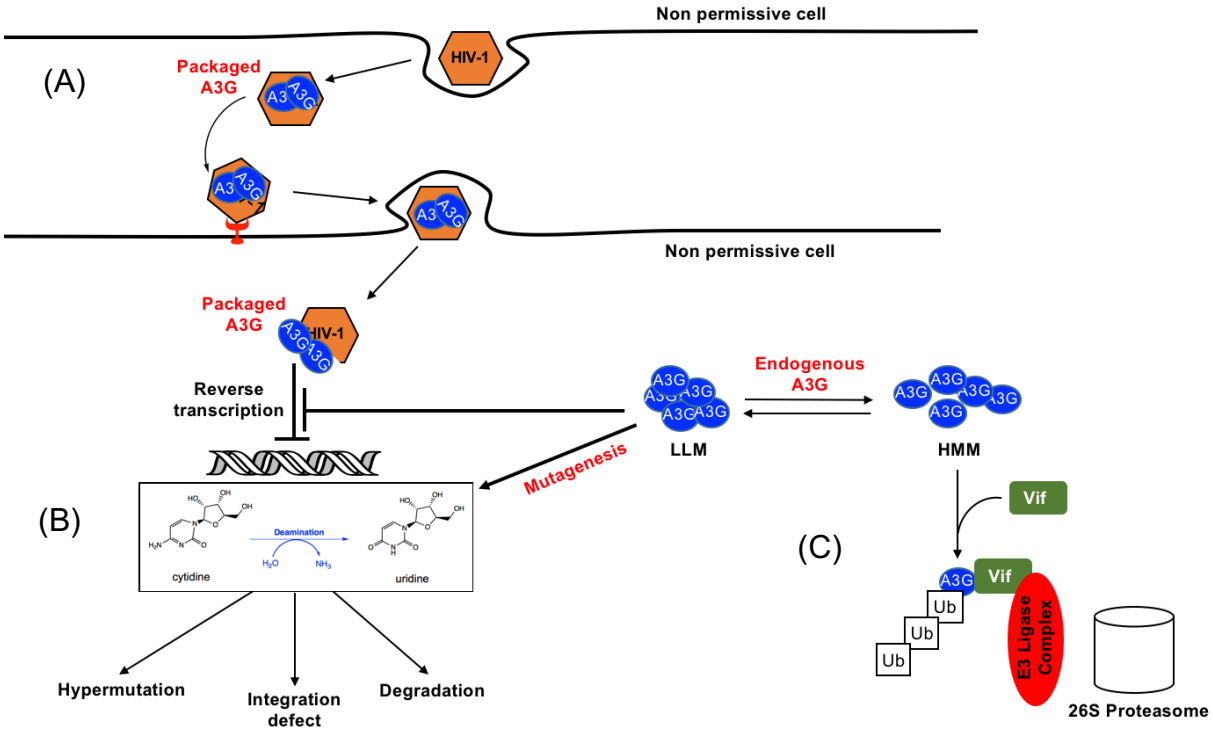

Figure 1.13. HIV-1 restriction by A3G.
(A) Through RNA binding capacity LLM (low molecular mass) complex of A3G interfere with reverse transcription in deaminase independent manner result in post-entry block. **(B)** The post reverse transcription functionally active HMM (high molecular mass) complex of A3G deaminate dC to dU in viral minus strand synthesis and the resultant virus is non-infectious. **(C)** In wild-type HIV-1 viral protein Vif direct A3G to ubiquitin-mediated degradation pathway.

In absence of Vif protein (mode of targeting discussed in **1.3.3**) the mutations are retained in pro-viral RNA and the extent of hypermutation is such that infectious progeny virus is not encoded by this erroneous pro-viral RNA. Mutated dU residues also target viral DNA to cellular DNA repair machinery and eventual degradation.

The catalytic ability of A3G is not its only antiviral activity [158]. A significant amount of HIV-1 restriction by catalytically defective variants was reported by several groups [159][160][161]. These deamination defective mutants of A3G were efficiently packaged into virions and retained antiviral activity. A3G also affects the priming ability of $tRNA^{lys3}$ to initiate reverse transcription (RT) [162]. Along with this mechanism, several other models have been proposed to show the ability of A3G to inhibit RT (reverse transcription) such as first strand and second strand transfer, minus strand stop synthesis, minus strand DNA synthesis, proviral DNA synthesis and integration (reviewed in [163]).

Circulating resting CD4+ T cells are resistant to HIV-1, whereas lymphoid tissue resident resting CD4+ T cells are susceptible. Though, A3G is found in both types of cells, it is present in two distinct forms. The LMM (low molecular mass) A3G is the catalytically active form, whereas HHM (high molecular mass) A3G is catalytically inactive. A3G is found in LMM complexes in circulating resting CD4+ T cells. This enzymatically active complex functions as a potent post-entry restriction factor of HIV-1 [164]. However, in a complex lymphoid environment, the stimulation of resting CD4+ T cells by mitogens and cytokines such as IL-2 and IL-15 renders these cells susceptible to HIV-1 due to the recruitment of A3G into HMM complexes [165].

Taken together these findings suggest that a second, editing-independent antiviral mechanism of A3G exists, which is not yet understood completely.

1.3.3. HIV-1 Vif hinders antiviral activity of APOBEC3G

Vif, a 23 kDa protein, is crucial for HIV-1 infectivity and replication [166] and Vif deleted HIV-1 (Δ*vif*) could not replicate in non-permissive cells such as primary T cells and macrophages [167]. Expression of A3G in permissive cell lines resulted in a non-permissive phenotype for HIV-1 [142].

An N-terminal A3G binding motif of Vif is responsible for its interaction with A3G. The C-terminal domain of Vif binds to ElonginC and the second zinc-binding motif binds to Cullin5. This binding results in the hijacking of an E3 ubiquitin complex containing ElonginB, ElonginC, Cullin5 and Ring box-1. As a result, a suicidal polyubiquitinylation of Vif occurs and subsequent proteasomal

degradation of not only Vif but also of linked A3G is inevitable [168][169]. It has also been reported that Vif interferes with A3G packaging in virions and the antiviral activity of degradation resistant variants of A3G [170].

1.3.4. Cellular expression of APOBEC3G

A3G is located in an anthropoid-specific single cluster on chromosome 22 at q13.2 along with several other members of the APOBEC family [145]. As shown in **Figure 1.14,** A3G RNA is detected in a wide range of tissues. The A3G expression is inducible and stimulation with PHA and IL-2 has been shown to increase expression in PBL [164]. However, it is also present constitutively in some cells. Stimulation of cells with PMA was shown to increase the expression of A3G via activation of the MAPK (mitogen-activated protein kinase) signalling pathway [171]. How exactly A3G expression is induced in cells is still not clear. In some cells such as HepG2.2.15 cells, the A3G expression is induced upon IFN-α treatment [172], whereas in the T lymphocytic cell line H9, A3G expression remains unaffected after treatment with type I and II IFNs [171]. IL-2, IL-15, IL-7 and IFN-γ have been shown to induce A3G expression.

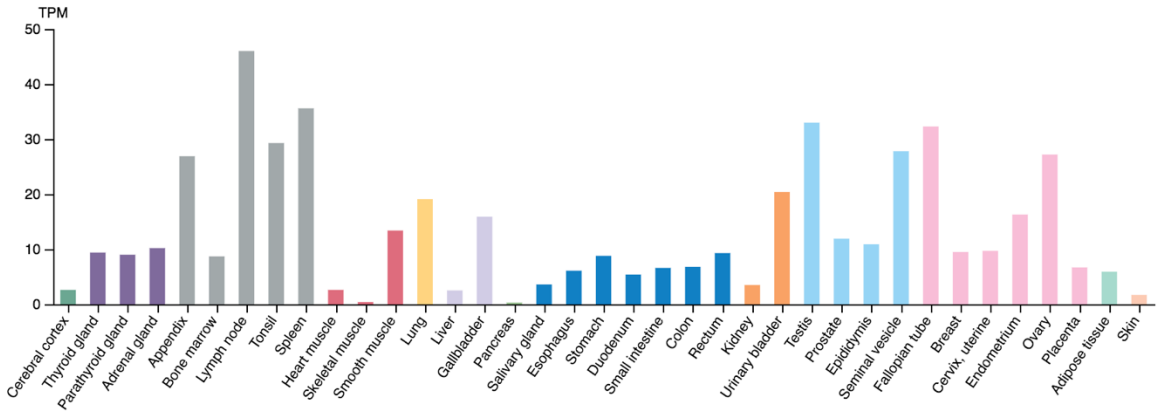

Figure 1.14. RNA signature of A3G in different human organs (adapted from proteinatlas.org)

At the transcriptional level human A3G expression is controlled by a constitutively active promotor with multiple transcription start sites. A GC-box plays an important role in the functioning of this promoter and has binding sites for nuclear transcription factor Sp1 (specificity protein 1) and Sp3 (specificity protein 3) [173]. Recently transcription factor USF1 (upstream regulatory factor 1) has been shown to regulate A3G transcription in human hepatocytes [174].

Similarly, another transcriptional cofactor CBF-β (Core-binding factor subunit beta) has been shown to regulate A3G expression. Interestingly, the lentiviral Vif protein has been evolved to hijack CBF-β to suppress antiviral defence of A3G [175].

Due to the highly editing nature of A3G, it was assumed that this protein is located only in the cytoplasm. However, recently it was shown that A3G is cytoplasmic in resting CD4+ T cells and translocated to the nucleus in activated and proliferating CD4+ T cells [176]. These recent findings indicate that A3G may have a physiological role in cells.

1.3.5. APOBEC3G oligomerization and interaction with RNA

The N-terminal domain (NTD) of A3G is a catalytically inactive domain but possesses the important function of interaction with RNA/DNA and incorporation of A3G into the virion. A3G monomers have been observed to form oligomers [177] [178] [179] and the exact role of this process is yet to be uncovered. However, alterations in NTD have been shown to affect oligomerization and thus hinder packaging of A3G into the budding virion [180].

A road-block model has been proposed to support this critical role of A3G oligomerization [181]. According to this model, A3G quickly deaminates viral ssDNA and then oligomerizes to present a road-block for reverse transcription. This may explain why the low number of A3G as found in virions can efficiently carry out antiviral function on large scale [181].

Apart from oligomerization, A3G was found in cellular ribonucleoprotein complexes (RNPs) containing more than 90 different cellular proteins. Many of these proteins were found to be RNA-interacting proteins having important roles in determining the fate of newly synthesized RNA as well as various other cellular RNA functions such as the Staufen containing RNA granules which are RNP complexes containing cellular RNA translation machinery and decay enzymes [182] [183][184][185]. Furthermore, the established sites of RNA metabolism and storage such as Stress granules and P-bodies contained substantial amounts of A3G [182]. Taken together these dynamic interactions between A3G and the RNA

processing machinery may play a crucial role in the regulation of the antiviral activity of A3G.

1.3.6. Restriction of other viruses by APOBEC3G

As initially believed, HIV-1 is not the only target of APOBEC enzymes. After initial identification of A3G antiviral activity in the majority of research was focused on A3G-retroviral interaction. However, recent evidence suggests that many other viruses are targeted by APOBEC family of proteins especially by non-enzymatic mechanisms.

A3G is a well-known restriction factor of hepatitis B virus (HBV) independent of its cytidine deaminase activity. A3G shown to inhibit HBV DNA production in Huh7 cells [186] and recently HBV X protein has been identified to down-regulate A3G levels in a dose-dependent manner in Huh7 cells [187]. Extensive editing of human T-cell leukaemia virus type 1 genome by A3G, A3B, A3C and A3F was observed [188]. CTD of A3G was shown to directly bind to HCV non-structural protein NS3 and diminish helicase activity to inhibit HCV replication in Huh7.5 cells [189]. Catalytically active A3A effectively inhibited replication of a parvovirus, adeno-associated virus (AAV), and endogenous retroelements [190]. Similarly, A3G has been shown to provide partial protection in mice against mouse mammary tumour virus (MMTV) [191]. In addition, A3G mediated restriction of three RNA viruses, Measles, Mumps and Respiratory syncytial virus (RSV), was reported [192]. Another positive-stranded RNA virus, the human coronavirus, was restricted by A3C, A3F and A3H without causing hypermutations in the viral genome [193].

Taken together, A3G antiviral potency is not just limited to cytidine deaminase activity but also extrapolate to various deaminase independent functions. Apart from protection from viral threat, APOBEC protein may also have pleiotropic effects on cellular functions and may contribute to malignant transformation. Only future research can help to completely understand the activities of this protein.

1.4.REDD1

1.4.1. Structure and function

In our group, we investigated the basis of A3G-mediated inhibition of MV replication. Upon ectopic expression of A3G in Vero cells a significant reduction in MV titre was observed [192]. In these cells, the differential regulation of cellular genes was analysed by microarray. Two of the significantly upregulated genes/gene products were *REDD1* and *KDELR2,* which are introduced below.

REDD1 (Regulated in development and DNA damage response 1) or DDIT4 (DNA-damage inducible transcript 4) or RTP801 or dig2 is a 24 kDa stress response protein. *REDD1* is a highly conserved gene on human chromosome 10. REDD1 structure **(Figure 1.15)** is composed of two-layered sandwiches made of two anti-parallel α helices and mixed β sheet. No oligomerization of REDD1 has been reported in overexpressing cells [194].

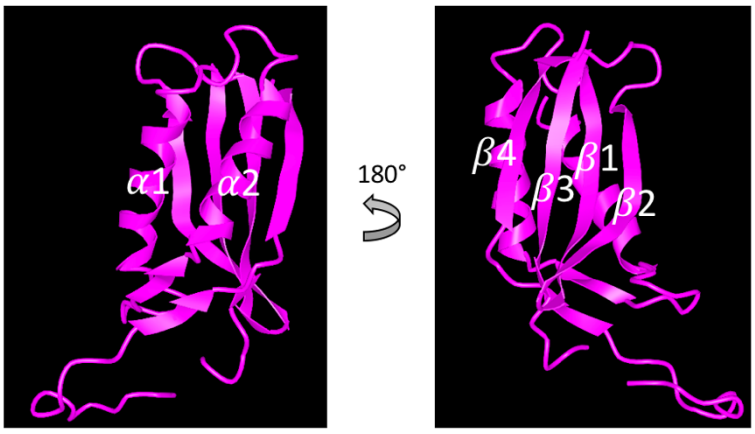

Figure 1.15. Crystal structure of REDD1 [194].
Ribbon model of REDD1 shows the sandwich arrangement of α and β helices.

Ubiquitous expression of REDD1 was detected in many tissues. A diverse range of cellular stress has been shown to induce expression of REDD1 such as hypoxia and DNA damage [195][196], ER stress, serum depletion, energy-related stress and nutrient depletion [197] [198] [199]. Various stress condition related transcription factors such as HIF1 (hypoxia-inducible factor 1), p53, p63, ATF4 (activating transcription factor 4), and Sp1 (specificity protein) control expression of REDD1 [195] [200][201]. The half-life of 5-7 minutes makes REDD1 a highly unstable protein with the tight transcriptional regulation [202].

Functionally, REDD1 is a negative regulator of mTORC1 (mammalian target of Rapamycin 1) specifically during hypoxic and stress condition and this effect is TSC2 (tuberous sclerosis complex) dependent [203] **(Figure 1.16)**. TSC2 is a GTPase-activating protein that targets small Ras-related GTPase Rheb (Ras homolog enriched in brain) [204]. Rheb binds to the mTORC1 complex which results in activation of the TOR kinase via an unknown mechanism [205]. REDD1 releases TSC2 from its growth factor-induced association with the inhibitory 14-3-3 protein and blocks mTOCR1 signalling [206]. REDD1 expression alone results in significant down-regulation of S6K1 (Ribosomal protein S6 kinase beta-1) in a TSC2 dependent manner indicating that REDD1 acts upstream of mTOR1 [203].

1.4.2. REDD1 and mTORC1

Initially, after identification of REDD1, a Drosophila homolog 'Scylla' has been shown to repress TOR (a Drosophila ortholog of human mTORC) by targeting S6 kinase phosphorylation [207]. Later REDD1 was shown to negatively regulate mTOR in mammalian systems [208].

mTOR consist of two distinct protein complexes, mTORC1 and mTORC2. Both complexes target different downstream molecules and therefore regulate different cellular functions. The mammalian target of rapamycin 1 (mTOR1) is the central regulator of cellular anabolic and catabolic processes. mTOR regulated downstream signalling governs the fate of extracellular and intracellular events that regulate cellular metabolism, growth, cytoskeleton rearrangement, transcription, protein synthesis and ribosomal biogenesis **(Figure 1.16)** (reviewed in [209][210]). mTOR has been shown to play a crucial role in determining the outcome of Ag recognition by regulating T cell activation and anergy [211]. In contrast, mTORC2 phosphorylates AKT (Protein kinase B) and PKC (Protein kinase C) to regulate cell survival and cytoskeletal organization [212] [213].

mTOR is a highly conserved large protein of 289 kDa. As shown in **Figure 1.16** mTORC1 complex consist of five major components, mTOR, Raptor (regulatory associated protein of mTOR), PRAS40 (Proline-rich Akt substrate of 40 kDa), Deptor (DEP domain containing mTOR-interacting protein) and mLST8 (mammalian lethal with Sec13 protein 8). Two activating subunits of mTORC1

complex, Raptor assist in cellular localization of mTORC1 and help in substrate recruitment, whereas mLST8 stabilizes the catalytic domain. The two negative regulators PRAS40 and Deptor inhibit substrate binding (reviewed in [214]).

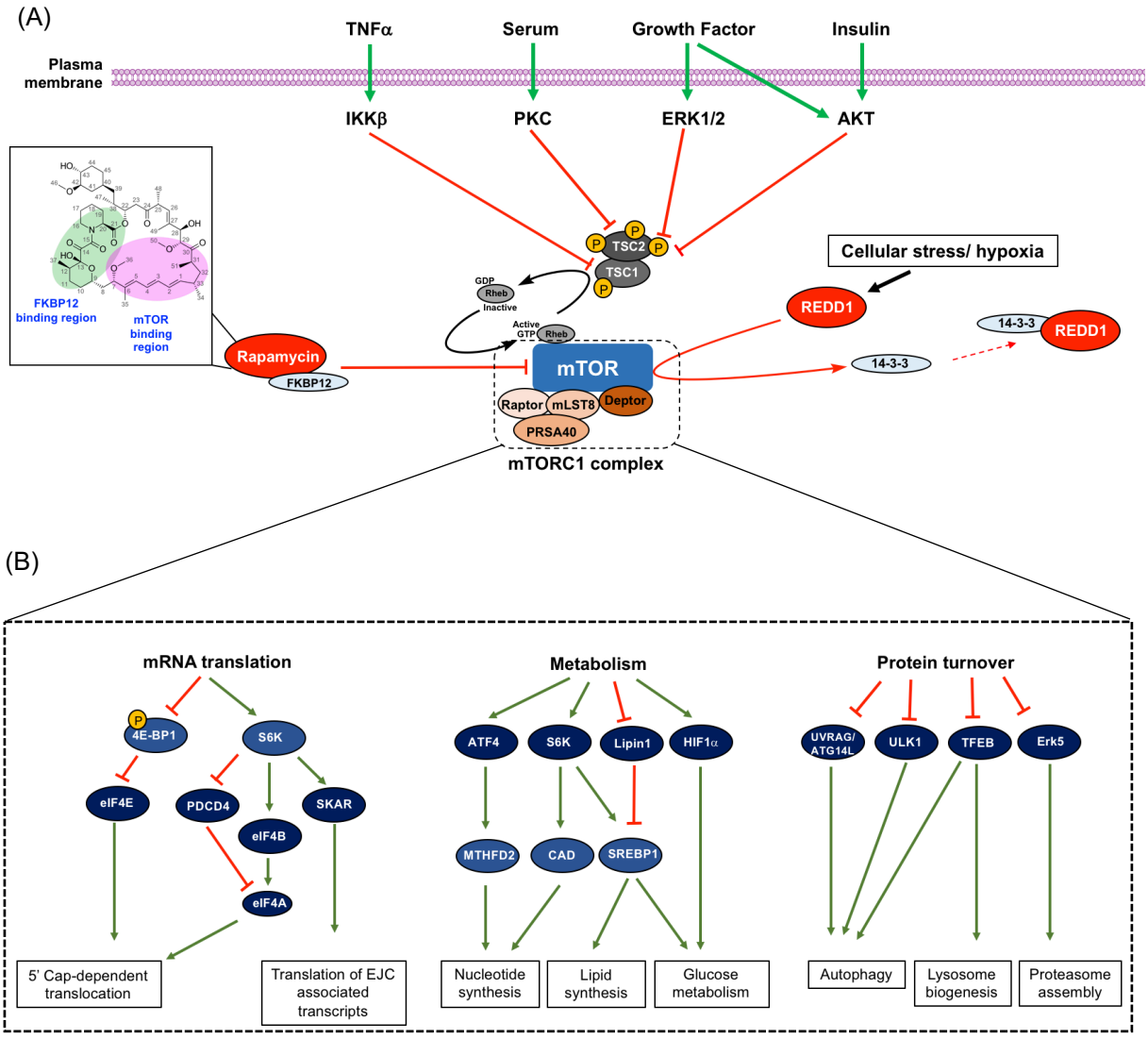

Figure 1.16. mTOR1 signalling: role of REDD1 and Rapamycin
(A) various upstream signalling events regulate the fate of mTORC1 either by activating or inhibiting signalling events. The green line represents positive signalling and red line represent negative signalling. **(B)** significant downstream signalling cascades are depicted here(4E-BP1: eukaryotic initiation factor 4E.binding protein 1, AKT: protein kinase B, Deptor: DEP domain containing mTOR-interacting protein, eEF2: eukaryotic translation elongation factor 2, eEF2K:eEF2 kinase, eIF: eukaryotic translation initiation factor, ERK1/2: extracellular signal-regulated kinase 1/2, FKBP12: FK506 binding protein of 12kDa, IKKβ: IkB kinase-β, mLST8: mammalian lethal with Sec13 protein 8, PKC: Protein kinase, Raptor: regulatory associated protein of mTOR, Rheb: Ras homolog enriched in brain, S6: ribosomal protein S6, S6K1: p70 ribosomal S6 kinase1, SREBP1: sterol regulatory element binding protein 1, TSC: tuberous sclerosis complex) (adapted from [214])

One of the significant downstream signalling events of mTORC1 activation is activation of S6 Kinase. Phosphorylation at Thr389 results in activation of S6K1,

which subsequently activates several downstream targets to promote mRNA translation initiation and ribosome biogenesis [215].

In accordance with the crucial role of REDD1 on mTORC1 signalling, it has a very short life of 5-7 minutes. To restore mTOR signalling during the recovery phase, REDD1 degradation plays a crucial role. CUL4A-DDB1 (Cullin 4A-DNA damage-binding protein1) regulates the ubiquitin-mediated degradation of REDD1 **(Figure 1.17)** [216].

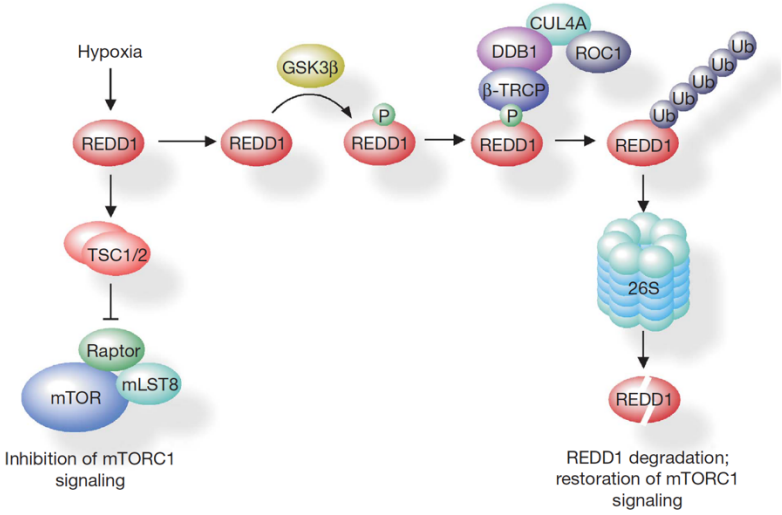

Figure 1.17. Restoration of mTOR functions via degradation of REDD1 [216].
REDD1 induced upon hypoxic condition inhibit mTORC1 signalling and during recovery phase phosphorylation of REDD1 recruit CUL4A E3 ligase-mediated ubiquitination of REDD1 and subsequent proteasomal degradation. (b-TRCP: beta-transducin repeat-containing protein, CUL4A: cullin 4A, DDB1: DNA damage-binding protein 1, GSK3b: glycogen synthase kinase-3b, ROC1: regulator of cullins 1;)

Interestingly, also a mTORC1-REDD1 feedback loop has been reported in which mTORC1 regulates REDD1 expression in a proteasome-dependent manner to exert some control over the inhibitory effects of REDD1 [217].

mTORC1 was defined by its sensitivity to a naturally occurring macrolide antibiotic Rapamycin or Sirolimus. Isolated from bacteria found on South Pacific island of Rapa Nui in 1964. This compound was acknowledged as an anti-fungal, immunosuppressive and anti-tumour agent. Rapamycin has been shown to specifically inhibit pathways involved in cell growth and proliferation by affecting p70S6K signalling [218]. Rapamycin binds to the intracellular receptor FKBP12 (FK506 binding protein of 12kDa) and this complex binds to the FRB (FKBP12-rapamycin binding) domain of the mTOR catalytic region at its C-terminus [219] [220]. This interaction occludes the binding of downstream substrates such as

S6K1 and 4E-BP1. S6K1 levels have been shown to be significantly down-regulated after Rapamycin treatment [203]. Interestingly, mTOR2 is insensitive to Rapamycin treatment [221].

1.4.3. Antiviral activity

As a metabolic regulator of the cell, a variety of factors that contribute to any kind of cellular stress converge to the mTOR pathway. Viral infection is one important mediator of cellular stress. Depending on the type of virus and the subcellular location of viral replication, activating or inhibiting signals for mTOR can be triggered. A number of viruses have been shown to target mTOR signalling for their own benefit (reviewed in [222]). Apart from the role of REDD1 in regulating mTORC1, recently REDD1 has been redefined as a cellular host defence factor and its regulation triggered an antiviral response against Influenza virus [223].

These findings have highlighted a potent antiviral strategy against viruses that require mTOR signalling. Testing of synthetic and natural chemical compounds that can trigger REDD1 expression is certainly worth investigating to find new antivirals.

1.5.KDELR2

The fate of every newly translated protein is decided by its sequence (transmembrane domains, disulphide bonds, localization sequences etc) and post-translational modifications (protein folding, glycosylation, acetylation, phosphorylation etc) which occur in the ER (endoplasmic reticulum). Subsequent membrane transport is a well-coordinated series of events in various cellular organelles to ensure correct delivery of proteins to their functional site. Various ER resident chaperones drive the correct folding of newly translated proteins. KDELR family receptors have been shown to play an important role in the retrieval of these ER-resident chaperones and also by triggering various cellular events.

1.5.1. KDELR2 structure and function

In 1987, several ER-resident chaperones such as GRP78, GRP94 were shown to contain the C-terminal tetra peptide signal sequence KDEL (lys-asp-glu-leu) [224] which is responsible for retention of these chaperones in the ER. The attempt to identify these retention signals first resulted in the identification of two genes *ERD1* and *ERD2* in yeast system [225][226], followed by identification of human homologue *hERD2* (later referred as KDELR1 (ERD2.1)) [227]. Subsequently, the receptors KDELR2 (ERD2.2 or ELP1) and KDELR3 were identified (reviewed in [228]). Although KDEL receptors perform similar functions, the protein-encoding genes are located on different human chromosomes, namely KDELR1 on chromosome 19, KDELR2 on chromosome 7, and KDELR3 on chromosome 22. KDELRs are ubiquitously expressed. KDELR1 was shown to regulate PP1 (protein phosphatase 1) in T cells, a key enzyme that regulates integrated stress response in naive T cells. Specific dysfunction of KDELR1 results in depletion of naive T cell population in mice [229].

Functionally, ER chaperones ensure the maturation of proteins before they are exported out of the ER or direct them for degradation, which is known as ERAD (ER-associated degradation) and thus prevent the excessive aggregation of proteins in the ER-Golgi network. Proteins destined to be exported out of the ER are packaged in COPII coated vesicles and transported to the Golgi via IC (pre-Golgi intermediate compartments). The resultant membrane flow is sufficient to bulge the Golgi complex to a detrimental level making it necessary to have compensatory mechanisms. One of such mechanisms is retrograde transport back to the ER [230]. The ER resident soluble chaperones with KDEL motif (such as calnexin and GRP78) are recognized by KDELRs and then sorted out to COPI vesicles and retrograde transport. Thus, the KDELR family plays a decisive role in ER quality control.

At homeostatic levels, KDELRs are located predominantly in the Golgi but redistributed to the ER upon ligand binding [231] or upon overexpression [232]. KDELR-ligand binding is efficient at acidic pH and at neutral or basic pH binding is weaker [233]. Therefore, the ligand bearing proteins bind to KDELRs in the

acidic environment of the Golgi and after retrieval to ER due to neutral pH the proteins are released in ER [234].

KDELRs contain seven transmembrane domains that span across the membrane. These domains are connected by three cytoplasmic loops and three luminal loops with cytoplasmic C-terminus and luminal N-terminus **(Figure 1.18A)**. KDELR2 has similarity to the family of PQ-loop proteins **(Figure 1.18B)**. These proteins contain at least two conserved PQ-loop (Proline-glutamine) domains of 40-60 amino acids [235].

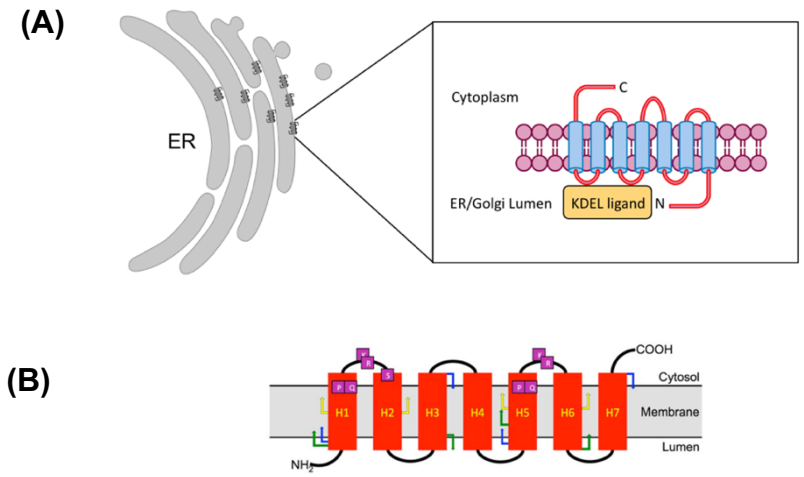

Figure 1.18. Schematic representation of KDELR2 receptor
(A) KDELR2 is membrane protein with cytoplasmic C terminal and luminal N terminal domain. KDEL motif containing peptide bind to KDELR2 to trigger transport of KDEL peptide-containing proteins **(B)** representation of PQ-loop protein topology which contain at least two PQ sequence [235] (ER: endoplasmic reticulum, C: C terminal of protein, N: N terminal of protein, H: Helices, P: Proline, Q: Glutamine)

Interestingly, recent findings showed that KDELR structures are similar to GPCR (G-protein coupled receptors) superfamily proteins **(Figure 1.19)** with significant similarities within the transmembrane region of KDELRs [236]. GPCR family proteins are known to activate various signalling pathways upon binding to its ligands. Interestingly, KDELRs have been shown to bind to Gα proteins and to activate $G\alpha_{q/11}$ which results in activation of Golgi SFKs (Src family kinases) and regulation of the secretory traffic [236]. KDELR-ligand binding also induces p38 MAP kinases which are known not only to regulate cell growth and differentiation but also immune and inflammatory responses [237].

KDELR2 self oligomerizes and interacts with ARF1 (ADP ribosylation factor) and GAP (GTPase-activating proteins) to regulate ARF1-mediated

vesicular transport. KDELR1 and KDELR2 also have been linked to the promotion of ECM (extra cellular matrix) degradation and invadopodia formation and may contribute to cancer cell dissemination [238].

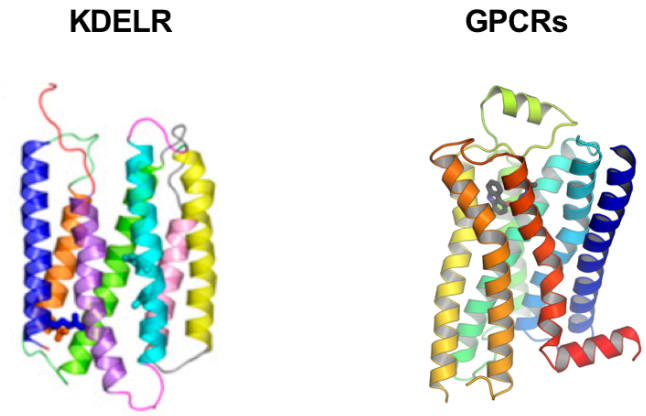

Figure 1.19. Schematic representation of KDELR2 receptor and comparison with GPCR
Structural model of KDELRs showing seven helices with intracellular loops (Left) compared to classical GPCR (G protein coupled receptors) family proteins (right) ([236] [239]).

Although identified in already 1990, KDELR receptor family functions are still poorly understood. Recent finding showed that the KDELR redistribution across the ER-Golgi network mediates signalling events and exerts effects on multiple levels which implies unidentified novel roles played by KDELRs.

1.5.2. Role in viral egress

Viral entry and replication processes occur in close interaction with various cellular proteins. During infection viral proteins must traffic across various cellular compartments to an exit site at the plasma membrane while avoiding transportation to degradative compartments. The ER is one of the crucial cellular organelles to regulate viral protein expression and assembly (reviewed in [240]).

Membrane webs formed in the ER are important for HCV replication and assembly [241], whereas DENV (Dengue virus) form vesicle pockets for a similar purpose [242]. Since KDELR transport across ER to Golgi is pH a dependent process, it can be easily exploited by various viruses. In the case of DENV, excessive production of viral proteins in the ER requires equivalent transport via cellular cargo to the plasma membrane. DENV has been demonstrated to require assistance from KDELR1 and KDELR2 for vesicular transport. The DENV prM protein directly interacts with KDELRs for this process and sequestering of KDELRs in Golgi by depletion of Arf4 (ADP ribosylation factor 4) and Arf5 (ADP

ribosylation factor 5) resulted in the accumulation of DENV proteins in the ER [243].

Interestingly another member of the Flavivirus family JEV (Japanese encephalitis virus) also was shown to be dependent on the KDELR1-mediated ER-Golgi retrieval system for viral particle trafficking [244]. Similarly, KDELRs along with coatomer proteins deliver host cellular membranes to early forms of Vaccinia virus virions [245]. Moreover, FIPV (Feline infectious peritonitis coronavirus) glycoprotein 6b possesses the ER retention signal KTEL (similar to KDEL) for slow release of this protein from the ER [246].

Taken together there is increasing evidence pointing out towards a critical role of KDELRs as host factors assisting viral egress.

1.6. ER chaperones

1.6.1. Calnexin and Calreticulin

ER is the home of several chaperones of a distinct chaperone family. These chaperones are cellular sensors to detect and differentiate between native and non-native protein conformations. They accurately interact with incorrectly folded protein and ensure correct processing or target incorrectly folded proteins for degradative pathways.

Calnexin and Calreticulin (CRT) are unique ER chaperones which coordinate precise folding of newly synthesized monoglucosylated N-linked glycoproteins. Structurally they are type-I integral membrane lectins in the ER. Calnexin is membrane bound, whereas CRT is a luminal soluble protein. The luminal domain of calnexin immediately associates itself with newly synthesized peptides. The primary quality control of folding of glycoproteins is provided by the Calnexin-Calreticulin cycle. Cleavage of nascent protein chains by glucosidases I and II allows interaction of Calnexin/CRT with the polypeptide chain. Upon correct folding, glucosidase II releases these chaperones from the folded proteins so that they can exit ER. Otherwise, proteins are cycled back for re-folding. If they are permanently misfolded, they are targeted to ERAD [247].

1.6.2. GRP78

GRP78 (Glucose-regulated protein 78) or BiP (binding immunoglobulin protein) is a 78 kDa chaperone located in the lumen of ER. GRP 78 is a crucial protein that assists in the maturation of proteins and regulates the UPR (unfolded protein response). In steady state, binding of GRP78 to luminal domains of PERK (Protein kinase RNA-like endoplasmic reticulum kinase) and IRE1 (inositol-requiring protein 1) **(Figure 1.20)** maintains them in a monomeric state thus prevents the UPR signalling cascade [248]. An increased amount of unfolded proteins results in depletion of all available luminal GRP78 molecules and dissociation of these proteins from PERK and IRE1 resulting in their oligomerization and initiation of UPR. Apart from the regulation of UPR, GRP78 was also found at the cell surface playing roles in cell signalling and antigen presentation. Various malignancies, neoplastic conditions and viral infections result in increased surface expression of GRP78 (reviewed in [249]).

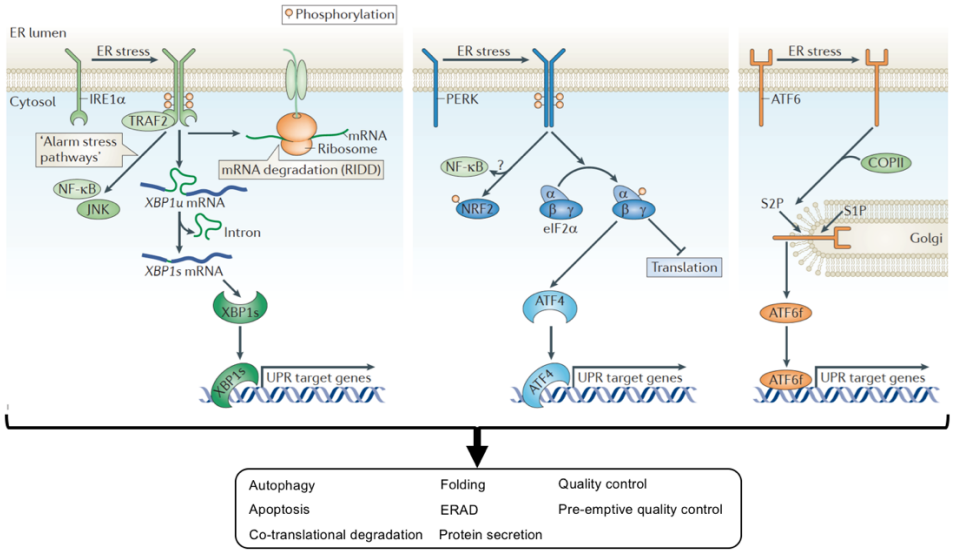

Figure 1.20. The UPR stress sensors and downstream signalling [250]
ER stress sensing molecules initiate downstream signalling from ER to cytosol and then to the nucleus.
(IRE1α: inositol-requiring protein 1α, PERK: protein kinase RNA-like endoplasmic reticulum kinase, ATF6: activating transcription factor, XBP1: X-box binding protein 1, ERAD: ER-associated degradation, RIDD: IRE1 dependent decay, JNK: JUN N-terminal kinase, NF-κB: nuclear factor κB, eIF2α: eukaryotic translation initiator factor 2α, NRF2: nuclear factor erythroid 2-related factor 2, COPII: coat protein II, S1P: site 1 protease, S2P: site 2 protease, TRAF2: TNFR associated factor 2.)

The UPR either results in ER recovery, or inability to handle the stress may lead to apoptosis. During a viral infection, the UPR either tries to control the infection or is used by the virus for its own benefit (reviewed in [251]). In **figure 1.20** the complex signalling network of UPR is summarized.

1.7.Aim of study

It has been reported earlier in our group that measles, mumps and respiratory syncytial virus replication was reduced by more than 90% in A3G expressing Vero cells. A3G is a cytidine deaminase shown to hypermutate the HIV-1 genome. However, no such hyper-mutational signatures were found in the MV genome [192]. Interestingly, it has also been shown that A3G is localized in various cytoplasmic structures such as P-bodies and stress granules. These structures function to regulate the cellular mRNA turnover. Therefore, we decided to investigate if A3G can alter the cellular RNA expression. On this line, preliminary work in our lab was done by analysing cellular gene expression in A3G expressing and non-expressing cells by using a microarray. This study revealed a differential regulation of several genes. The potential hits contained many interesting candidate genes.

Therefore, this thesis aims to characterize the role of two top candidate genes (1) REDD1 and (2) KDELR2 in detail. Understanding the role of these proteins in MV replication will help to understand how these host factors influence and interact with MV to contribute to A3G mediated antiviral effects against MV.

MATERIALS

2. Materials

2.1. Cell lines and Primary cells

Table 2.1: List of Primary and established cell lines

Name	Origin	Source
Vero	Adherent cell line derived from kidney epithelial cells of *Cercopithecus aethiops* (African Green Monkey)	Lab of Dr. Jürgen Schneider-Schaulies (Institute of Virology and Immunobiology)
Vero hSLAM	Vero cells expressing hSLAM (human CD150)	Lab of Dr. Jürgen Schneider-Schaulies (Institute of Virology and Immunobiology)
Vero 023	Vero cells transduced with empty vector as a control	A kind gift from Dr. Rebecca Holmes (King's College London, United Kingdom)
Vero 024-02	Vero cells transduced with human APOBEC3G	A kind gift from Dr. Rebecca Holmes (King's College London, United Kingdom)
HEK 293T	Adherent cell line derived by transforming human embryonic kidney cells with SV40 T-antigen	Lab of Dr. Jürgen Schneider-Schaulies (University of Würzburg, Germany)
CEM-SS pcMS	Human T4-lymphoblastoid cell line transduced with an empty vector as a control	A kind gift from Dr. Michael Malim (King's College London, United Kingdom)
CEM-SS A3G	Human T4-lymphoblastoid cell line transduced with human APOBEC3G	A kind gift from Dr. Michael Malim (King's College London, United Kingdom)
Hep2	Established epidermoid carcinoma of the larynx via HeLa cell contamination	A kind gift from Dr. Benedikt Weissbrichk (Viral Diagnostic, University of Würzburg, Germany)

2.2. Virus

Table 2.2: List of Virus strains used and origin.

Name	Source
rMV^{Edtag}	A kind gift from Dr. Paul Duprex (Boston University, USA)
rMV^{Edtag}eGFP	A kind gift from Dr. Paul Duprex (Boston University, USA)
rMV^{IC323}eGFP	A kind gift from Dr. Yusuke Yanagi (Japan)
HSV-1 GFP	A kind gift from Dr. Beate Sodeik (Hannover Medical School, Germany)
rgRSV GFP	A kind gift from Dr. C Krempl (University of Würzburg, Germany)

2.3. Bacteria

Transformation of ligation reaction and amplification of plasmids was done in XL10-Gold® Ultracompetent cells from Stratagene, USA (200314).

2.4. Plasmids and cDNA clones

Table 2.3: List of plasmids and source.

Name	Source
F6gW-dsRed2	A kind gift from Dr. Marco Herold (University of Würzburg) [252]
pMD.G/VSV	A kind gift from Dr. Marco Herold (University of Würzburg) [252]
pRSV-rev	A kind gift from Dr. Marco Herold (University of Würzburg) [252]
pMDLg/pRRE	A kind gift from Dr. Marco Herold (University of Würzburg) [252]
pcMS28	A kind gift from Dr. Rebecca Holmes (King's College London, United Kingdom)
RC200007	KDELR2 Expression Plasmid, OriGene Technologies (USA)
RC202847	REDD1 Expression Plasmid, OriGene Technologies (USA)

2.5. DNA and Protein standards

To analyse DNA on Agarose gel GeneRuler™ 50 bp DNA Ladder (#SM0371), GeneRuler™ 100 bp DNA Ladder (#SM0241) and GeneRuler™ 1 kb Plus DNA Ladder (#SM1331) standards were used (**Figure 2.1 A, B and C**). To analyse proteins on SDS PAGE PageRuler™ Pre-stained Protein standard was used (**Figure 2.1D**).

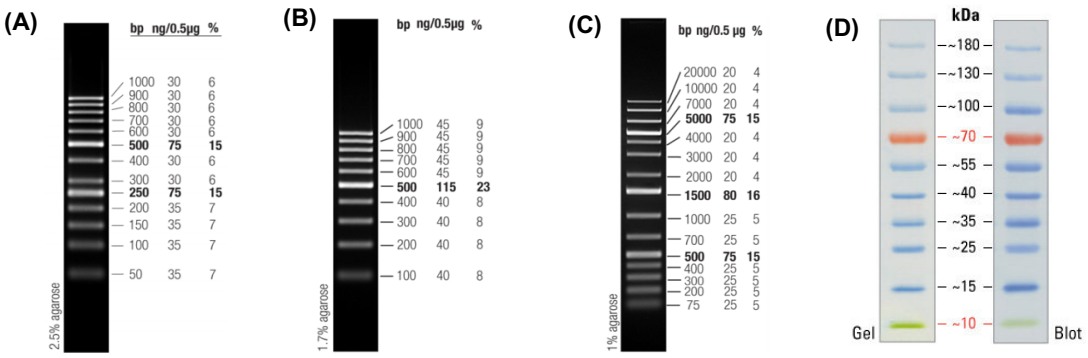

Figure 2.1: DNA and Protein standards pattern on agarose or polyacrylamide gels
(A) GeneRuler™ 50 bp DNA Ladder **(B)** GeneRuler™ 100 bp DNA Ladder **(C)** GeneRuler™ 1 kb Plus DNA Ladder **(D)** PageRuler™ Pre-stained Protein Ladder bands on poly-acrylamide gel and subsequent bands on the blot.

2.6. Primers and Oligonucleotides

2.6.1. Primers

Table 2.4 summarize the list of primers used for cloning of cDNA, Semi-quantitative PCR, Real-time qPCR, PCR, colony PCR and sequencing.

Table 2.4: List of primers. All primers in 5' → 3' direction. F: Forward primer and R: Reverse primer

	Name	Sequence
Cloning	KDEL cloning F	GTCGACTGGATCCGGTACCGA
	KDEL cloning R	GTAGTGAATTCGGCCGGCCGTTTAAACCTT
	REDD1 cloning F	GTCGACTGGATCCGGTACCGA
	REDD1 cloning R	GTAGTGAATTCGGCCGGCCGTTTAAACCT
Semi-Quantitative PCR	KDELR2 F	CTTCCGGCTGACTGGGGACCT
	KDELR2 R	GAGGCCTCCCACAGGGACCAC
	REDD1 F	GGTTTGACCGCTCCACGAGCC
	REDD1 R	CAGCTCTTGCCCTGCTCCACG
Colony PCR	F6gW F	CAGTTTCTTTGGTCGGTTTTATGT
	F6gW R	ACAAAGGCATTAAAGCAGCGTATC
	KDELR2_colonyPCR_new R	CTGGCAAACTGAGCTTCTTTC
	REDD1_colonyPCR_new R	ACCTTATCGTCGTCATCCTTG
Sequencing	F6gW_Seq_F	AGGCGTCAGTTTCTTTGGTCG
	F6gW_REDD1_Seq F	ACTTGTGTGCCAACCTGATGC
	F6gW_KDELR2_Seq F	TCTACCTTGCCTGCTCCTATG
Real-Time qPCR	KDELR2 F	CTCTTCCTCTGCTGCGAAGT
	KDELR2 R	ATGGAAAGCAGCCAAAACTC
	KDELR2 F Exon I	TTCTCTCCTCTTGAGATCCTCTG
	KDELR2 R Exon I	AAACAGCTGCGGAAGGATAG
	KDELR2 F Exon II	ATGAACATTTTCCGGCTGAC
	KDELR2 R Exon II	GGCTTTTCCCAGAAATACCG

2.6.2. shRNA oligonucleotide sequence

Table 2.5: List of shRNA sequences. All oligonucleotides are in 5' → 3' direction. F: Forward and R: Reverse

	Name	Sequence
KDELR2 shRNA 1	KDELR2_sh1_378_F	TGCCACAGTGTACCTGATCTACCGAAGTAGATCAGGTACA CTGTGGCTTTTTTC
	KDELR2_sh1_378_R	TCGAGAAAAAAGCCACAGTGTACCTGATCTACTTCGGTAG ATCAGGTACACTGTGGCA
KDELR2 shRNA 2	KDLER2_sh2_410_F	TGGCAACCTACGATGGAAATCACGAATGATTTCCATCGTA GGTTGCCTTTTTTC
	KDLER2_sh2_410_R	TCGAGAAAAAAGGCAACCTACGATGGAAATCATTCGTGA TTTCCATCGTAGGTTGCCA
KDELR2 shRNA 3	KDELR2_sh3_529_F	TGCTCAGTTTGCCAGCATAAGTCGAAACTTATGCTGGCAA ACTGAGCTTTTTTC
	KDLER2_sh3_529_R	TCGAGAAAAAAGCTCAGTTTGCCAGCATAAGTCGAAACTT ATGCTGGCAAACTGAGCA
REDD1 shRNA 1	REDD1_sh1_F	T GCGGCAGGACGCACTTGTC CTGTGAAGCCACAGATGGG GACAAGTGCGTCCTGCCGC
	REDD1_sh1_R	TCGAGAAAAAA GCGGCAGGACGCACTTGTC CCCATCTGTGGCTTCACAG GACAAGTGCGTCCTGCCGCA
REDD1 shRNA 2	REDD1_sh2_F	TCTCTCCCTTCCTCCCTGGC CTGTGAAGCCACAGATGGG GCCAGGGAGGAAGGGAGAG TTTTTTC
	REDD1_sh2_R	TCGAGAAAAAA CTCTCCCTTCCTCCCTGGC CCCATCTGTGGCTTCACAG GCCAGGGAGGAAGGGAGAG

2.6.3. siRNAs

Table 2.6: List of siRNAs

siRNA	Source	Catalogue no
siA3G	siGENOME Human SMARTpool Human APOBEC3G (60489)	M-013072-00-0005
siREDD1	ON-TARGET plus Human REDD1 (54541) SMARTpool, 5 nmol	L-010855-01-0005
siNT	siGENOME Non-Targeting siRNA pool #1, 5 nmol	D-001206-13-05

2.6.4. Other oligonucleotides, primers and peptides.

Table 2.7: List of other oligonucleotides

Name	Source
dNTP mix (10 mM)	Thermo Scientific (R0191)
Oligo $(dT)_{18}$ primer	Thermo Scientific (SO131)
Random Hexamer Primer	Thermo Scientific (SO142)
Fusion inhibitory peptide (FIP) Z-D-Phe-Phe-Gly-OH	BACHEM (H-9430)

2.7. Antibodies and Antiserum

Table 2.8: List of antibodies

Name	Origin	Source
Anti-ACY1	Rabbit monoclonal (clone EPR8445)	Epitomics 5879-1
Anti-MOSC2 (C-term)	Rabbit polyclonal	Epitomics T3362
Anti REDD1	Rabbit polyclonal	Proteintech 10638-1-AP
Anti-PRDX2	Rabbit polyclonal	Sigma SAB2101878
Anti-TXNIP	Rabbit polyclonal	Sigma SAB2102616
Anti-PRDX1	Rabbit polyclonal	Sigma HPA007730
Anti-KDELR2	Rabbit polyclonal	Sigma SAB1401554
Anti- GAPDH	Rabbit polyclonal (FL-335)	Santacruz sc-25778
Anti-Calnexin	Rabbit polyclonal	Pierce PA1-30197
Anti-GRP78	Rabbit polyclonal	Pierce, PA5-11418
Anti- Calreticulin	Rabbit polyclonal	Pierce PA3-900
Anti-APOBEC3G	Rabbit polyclonal	(a kind gift from Dr. Michael Malim)
Anti MV-H	Rabbit polyclonal (clone H45)	Lab of Dr. Jürgen Schneider-Schaulies
Anti MV-H	Mouse monoclonal IgG_1 (Clone L77)	Lab of Dr. Jürgen Schneider-Schaulies
Anti MV-F	Rabbit polyclonal (clone F42)	Lab of Dr. Jürgen Schneider-Schaulies
Anti MV-F	Mouse monoclonal IgG_1 (Clone A504)	Lab of Dr. Jürgen Schneider-Schaulies
Anti-FLAG	Mouse monoclonal (clone M2)	Sigma, F1804
Anti-flag Alexa 488	Rabbit polyclonal	Cell signaling 5407S
Anti-mouse Alexa 488	Goat monoclonal IgG (H+L)	Life technology A11001
Anti-rabbit Alexa 594	Goat monoclonal IgG (H+L)	Life technology, A11012
Anti- mouse APC	Goat monoclonal IgG (poly4053)	Biolegend 405308
Anti-mouse Alexa 405	Goat monoclonal IgG (H+L)	Life technologies A31553
Anti-mouse Alexa 594	Goat anti-mouse igg (H+L)	Life technologies A11005
Anti-rabbit Alexa 647	Donkey monoclonal IgG (clone poly 4064)	Biolegend, 406414
Anti- mouse HRP	Horse monoclonal IgG (H#ampL)	Cell signaling, #7076S
Anti- rabbit HRP	Goat monoclonal IgG (H#ampL)	Cell Signaling, #7074S
PE anti-human CD3	Mouse IgG1, k (Clone: UCHT1)	Biolegend, 300408
APC anti human CD69	Mouse IgG1, k (Clone: FN50)	Biolegend, 310910

P70 S6 Kinase	Rabbit polyclonal	Cell signaling #9202
Phospho-p70 S6 Kinase	Rabbit polyclonal	Cell signaling #9205
Phospho-AKT	Rabbit polyclonal	Cell signalling #9271
Cell proliferation dye ™670		ebioscience, 65-0840-85

2.8. Enzymes

Table 2.9: List enzymes and source

Name	Detail	Source
CAIP	Calf intestine alkaline phosphate (#EF0341)	Fermentas
M-MLV RT	M-MLV reverse transcriptase (M1701)	Promega
T4 DNA ligase	T4 DNA ligase (EL0011)	Thermo Scientific
T4 PNK	T4 Polynucleotide Kinase (#EK0031)	Thermo Scientific
Taq-Polymerase	*Taq* DNA polymerase (#EP0402)	Thermo Scientific
Xho I	Restriction enzyme (#ER0691)	Thermo Scientific
KspAI	Restriction enzyme (#ER1031)	Thermo Scientific
EcoRI	Restriction enzyme (#ER0271)	Thermo Scientific
BamHI	Restriction enzyme (#ER0051)	Thermo Scientific
Protease inhibitor	Protease inhibitor cocktail (P8340)	Sigma
Phosphatase inhibitor	Phosphatase inhibitor cocktail 2 (P5726)	Sigma
PCR Beads	Illustra PuReTaq Ready-To-GoTM PCR Beads (27-9558-01)	GE Healthcare

2.9. Media and Serum

2.9.1. Media and Serum for Cell culture.

Table 2.10: List of Media and serum and source

Name	Detail	Source
MEM	Minimum Essential Medium	Gibco™ (31095029)
DMEM	DMEM (Dulbecco's Modified Eagle Medium)	Gibco™ (41966029)
RPMI 1640	Roswell Park Memorial Institute (RPMI) 1640	Gibco™ (21875059)

FCS	Fetal Calf Serum (Heat inactivated at 56°C for 30 minutes)	Biochrom (S0115)
BSS	Balanced Salt solution	Institute of Virology and Immunology, Würzburg
BSS + BSA	Balanced Salt solution + 0.1%BSA	Institute of Virology and Immunology, Würzburg

For every 500 ml of MEM/DMEM/RPMI mixture of Penicillin and Streptomycin (100 IU/ml) was added with the required amount of heat-inactivated FCS.

2.9.2. Media for Bacterial culture

LB Medium (1 litre)	
Bacto Tryptone	10 g
Bacto Yeast Extract	5 g
NaCl	10 g
Tris.HCl 1M	10 ml

LB agar (1 litre)	
Bacto Tryptone	10 g
Bacto Yeast Extract	5 g
NaCl	10 g
Tris.HCl 1M	10 ml
Bacto Agar	15 g

Before preparing plates add 100µg/ml of Ampicillin or 30µg/ml of Kanamycin depending upon the antibiotic resistance of plasmid.

2.10. Equipment and Instruments

Table 2.11: List of equipment and instruments

Equipment	Detail	Manufacturer
Acrylamide gel Chamber	NA	Institute of Virology and Immunobiology
Agarose gel chamber	N/A	Institute of Virology and Immunobiology
Agarose gel electrophoresis unit	N/A	Institute of Virology and Immunobiology
Analytical balance	L 610-D	Sartorius
Analytical balance	EW 3000-2M	Kern
Analytical balance	AC210S MC 1	Sartorius
Bacterial shaker incubator	Certomat®H	B Braun

Biofuge	Fresco 75005500	Heraeus (Hanau)
Blotting apparatus	N/A	Institute of Virology and Immunobiology
Cell counter	Neubauer-improved	Superior Marienfeld
Cell sorter	FACS Aria III	Becton Dickinson
Centrifuge	Rotana 460R	Hettich
Confocal Microscope	LSM 780 (Zeiss)	Zeiss
Deep freezer -80°C	NA	Revco
Flow cytometer	FACScan Calibur	Becton Dickinson
Flow cytometer	FACS LSR II	Becton Dickinson
Fluorescence Inverted Microscope	Leica DMi8	Leica
Fluorescence Inverted Microscope	DMIRE2	Leica
Ice machine	AF30	Scotsman
Incubator (Bacterial)	B 60 30	Heraeus (hanau)
Incubator (cell culture)	HERACELL 240i	Thermo Scientific
Inverted Light Microscope	090-135-002	Leica
Magnetic stirrer	NA	Ikamag RCT
Microtitre pipettes	Eppendorf Research®	Eppendorf
Microwave	NA	Panasonic
Milifuge	CT10	Millipore
Nucleofector™	2d device	Amaxa
pH meter	Five Easy	Mettler-Toledo
Photometer	BioPhotometer 6131	Eppendorf
Pipette aid	Accu Jet® Pro	Brand
Power supply (Agarose gel)	E455	Consort
Power supply (PAGE)	EV243	Peqlab
Real-time Thermal cycler	LightCycler 2.0 real time PCR system	Roche
Refrigerator -20°C	Sikafrost Comfort	Siemens
Refrigerator 4°C	Sikafrost Comfort	Siemens
Rocker	WS5	Edmund Bühler
Safety cabinet/Laminar flow	BSB 4A,	Gelaire
Sequencing apparatus	ABI PRISM®310 Gennetic Analyzer	Advanced Biolab Service

Spectrophotometer	Nanodrop	Thermo Scientific
Thermal block	NA	Liebisch
Thermal block	Thermostat 5320	Eppendorf
Thermal Cycler	Eppendorf Gradient Cycler	Eppendorf
Ultracentrifuge	Sorvall® Discovery ™90SE	Hitachi
UV illuminator	Gel Jet Imager	Intas
Vortex	VTX-3000L	A. Hartenstein
Water-bath	NA	Superior Marienfeld

2.11. Lab consumables

Table 2.12: List of lab consumables and their source

Article	Article number	Manufacturer
12 well plate	665180	Greiner
24 well plate	662160	Greiner
48 well plate	MU48	Greiner
6 well plate	657160	Greiner
Cell culture flask 550 ml	660160	Greiner
Cell culture flask 250 ml with filter	658175	Greiner
Cell culture flask 50 ml with filter	690175	Greiner
Cell culture chamber slides 8 well	OTC8	Hartenstein
Cell culture dish 10cm	GK03	Nunc
Cell scraper	ZS23	Hartenstein
Centrifuge tubes 15 ml	188271	Greiner
Centrifuge tubes 50 ml	227261	Greiner
Cryo-vial	122277	Greiner
Cuvettes	Q-vettes Macro	Ratiolab
Dispenser tips 12.5 ml	TD10	Hartenstein
Electroporation Cuvettes 2mm	732-1136	VWR
Eppis Safe lock 1.5 ml	296920086	Eppendorf
FACS tubes (Falcon BD)	FALC352052	Falcon

Corning™ Falcon™ Test Tube with Cell Strainer Snap Cap	352235	Corning™
Histopaque® 1077	10771	Sigma
Filter tips	NA	Hartenstein
Flat filter paper	FF09	Hartenstein
Gel blotting paper	Whatman® 3MM	Whatman
Glass pipettes	NA	Institute of Virology and Immunobiology
Mr. Frosty ™ Freezer	5100-0001	Thermofisher
Nitrocellulose transfer membrane	Amersham™ Protran™ 0.2 µm NC 10600001	GE healthcare
Parafilm	701605	Parafilm
PCR tubes	RT08	PCR tubes
Petri dish GBO (For Bacteria)	633180	Greiner
Pipette tips Kristall (0.5-10µl) long	9260.1	Roth
Pipette tips Yellow (1-200µl)	8156.1	Roth
Pipettes tips Blue (100-1000µl)	732032	Brand
Pipettes tips mikro (0.1-10µl) short	K138.1	Roth
Plastic pipettes 10 ml	607180	Greiner
Plastic pipettes 5 ml	606180	Greiner
Rnase-ExitusPlus™	A7153	Applichem
Stepper	HandyStep®	Brand
Sterile filter 0.22µM	FI02	Sartorius
Sterile filter 0.45 µM	FI04	Sartorius
UV microcuvettes	KUVD	Plastibrand®

2.12. Chemicals

Table 2.13: List of chemicals

Article	Manufacturer
Acetic acid	AppliChem
Acrylamide	AppliChem
Agarose	AppliChem
Albumin Bovine Fraction V	SERVA

Aminohexanoic acid	Sigma-Aldrich
Ammonium persulfate	AppliChem
Ampicillin	AppliChem
Antibiotic Mix (penicillin and streptomycin)	Institute of Virology and Immunobiology
Acetic acid	AppliChem
ATV	Institute of Virology and Immunobiology
BCA (Bicinchoninic Acid)	Sigma-Aldrich
Beta-Mercaptoethanol	Sigma-Aldrich
Bromophenol blue	AppliChem
BSA	AppliChem
$CaCl_2$	AppliChem
$CuSO_4$ solution	Sigma-Aldrich
DAPI	Invitrogen
Di-Sodium EDTA	AppliChem
Distilled water	Institute of Virology and Immunobiology
DMSO	AppliChem
DTT	Sigma-Aldrich
EDTA	AppliChem
Ethanol	AppliChem
Electroporation Solution	Ingenio (MIR 50114)
Fluoromount-G®	Southern Biotech
Gel red (10000X)	Biotium
Glycerin	AppliChem
Glycin	AppliChem
HCl	AppliChem
HEPES	Roth
HPLC water	AppliChem
Isopropanol	AppliChem
KCl	AppliChem
KH_2PO_4	AppliChem
LE agarose	Biozym

$MgCl_2$	Applichem
Methanol	AppliChem
MOPS	
NaCl	AppliChem
NaF	Ferak
$NaHPO_4$	AppliChem
NaOH	AppliChem
Non-fat dry milk powder	Sigma-Aldrich
NP40	Sigma-Aldrich
Paraformaldehyde	Merck
PEI	Polyscience
Phosphatase inhibitor cocktail	Sigma-Aldrich
Phytohemagglutinin (PHA-L)	Roche
Potassium acetate	Applichem
Propidium Iodide	Biolegend
Protease inhibitor cocktail	Sigma-Aldrich
Puromycin	AppliChem
RIPA buffer	Sigma-Aldrich
RNase free water	peqGOLD
Rubidium Chloride	Sigma Aldrich
Rapamycin	Sigma Aldrich
Saccharose	AppliChem
SDS	AppliChem
Sodium azide	AppliChem
Sodium chloride	AppliChem
Sodium deoxycholate	AppliChem
TEMED	Sigma-Aldrich
Tris	AppliChem
Triton® X100	Sigma-Aldrich
Trypan blue	AppliChem
Trypton	Becton Dicknson

Tween® 20	Sigma-Aldrich
Xylene cyanol	Ferak

2.13. Solutions and Reagents

2.13.1. For Molecular Biology methods

Oligo annealing Buffer	
0.5M EDTA	1 mM
1M Tris.Cl pH 7.5	10 mM
1M NaCl	0.1 M
Dissolve in DPEC H_2O	

DNA loading Buffer	
Bromophenol Blue	0.03% (v/v)
Glycerol	60% (v/v)
Na_2EDTA	60 mM
Tris-HCl pH 8	10 mM
Xylen cyanol	0.03 % (v/v)
Dissolve in DPEC H_2O pH 7.6	

Tris-Acetate-EDTA (TAE) buffer	
Tris Ultrapure base	24.2 % (w/v)
Acetic acid	5.71 % (v/v)
EDTA 0.5M pH 8.0	10 % (v/v)
Dissolve in dH_2O pH 8.5	

PBS-T	
PBS	1 litre
Tween 20	0.05%

TE Buffer	
EDTA pH 8	1 mM
HCl	10 mM
Dissolve in dH_2O pH 8	

Agarose gel (1%)	
TAE buffer	100 ml
LE Agarose	1% (w/v)
Gel red	0.005% (v/v)

Transformation Buffer (TFB) I	
Calcium Chloride	10 mM
Glycerol	15% (v/v)
Potassium Acetate	30 mM
Rubidium Chloride	100 mM
Manganese Chloride	50 mM
Adjust pH to 5.8 with 1M acetic acid. Filter sterilizes before use.	

Transformation Buffer (TFB) II	
MOPS	10 mM
Rubidium Chloride	10 mM
CaCl2	75 mM
Glycerol	15% (v/v)
Adjust pH to 6.5 with KOH. Filter sterilizes before use.	

Cathode buffer	
Tris base	0.025 M
Methanol	20% (v/v)
Hexanoic acid	0.04 M
Dissolve in dH_2O, pH 9.4	

Anode buffer 300 mM	
Tris base	0.3 M
Methanol	20% (v/v)
Dissolve in dH_2O, pH 10.4	

Anode buffer 30 mM	
Tris base	0.025 M
Methanol	20% (v/v)
Dissolve in dH_2O, pH 10.4	

Protein gel buffer 10X	
Glycin	1.44 % (w/v)
Tris base	0.303% (w/v)
SDS	0.1% (w/v)
Dissolve in dH_2O pH 6.8	

Stripping buffer	
Tris. HCl, pH 6.8	90 ml
20% SDS	10 ml
Beta-Mercaptoethanol	700 µl
Dissolve in dH_2O, Total volume 100 ml	

Blocking buffer for NC membrane	
Non-fat dry milk powder	5%
Tween 20	0.05%
Dissolve in dH_2O, Total volume 100 ml	

IP lysis buffer	
Tris HCl pH 7.5	50mM
NaCl	150 mM
NaF	50 mM
EDTA	2 mM
Sodium deoxycholate	0.5%
Nonodent-P40 (NP 40)	1%
Protease Inhibitor	1%
Tris HCl pH 7.5	50mM
Dissolve in dH_2O	

Laemmli buffer	
SDS	10%
Tris.HCl pH 8.0	250 mM
Glycerol	50%
Dithiothreitol (DTT)	500 mM
Bromophenol Blue (BPB)	0.25%
Dissolve in dH_2O	

Resolving SDS gel	
1.5 M Tris.Cl pH 8.7	37.5% (v/v)

Stacking SDS gel	
1.5 M Tris.Cl pH 6.7	12.4% (v/v)

4K Bisacrylamid	30% (v/v)
Ammonium per sulphate (APS)	0.2% (v/v)
Sodium dodecyl sulphate (SDS)	1% (w/v)
TEMED	0.25% (v/v)
dH_2O	22.25%(v/v)

4K Bisacrylamid	12.4% (v/v)
Ammonium per sulphate (APS)	0.2% (v/v)
Sodium dodecyl sulphate (SDS)	1% (w/v)
TEMED	0.25% (v/v)
dH_2O	74.95%(v/v)

PBS	
$CaCl_2$	1.5 mM
KCl	2.7 mM
KH_2PO_4	1.4 mM
$MgCl_2$	1 mM
NaCl	137 mM
$NaHPO_4.7H2O$	4.3 mM
Dissolve in dH_2O pH 7.4	

IP lysis buffer	
Tris-HCl pH 7.5	50mM
NaCl	150 mM
NaF	50mM
EDTA	2mM
Sodium deoxycholate	0.5%
Nonodent-P40	1%
Dissolve in dH_2O pH 7.4	

2.13.2. For Immunological methods

Permeabilization buffer	
Triton X-100	0.1% (v/v)
Dissolve in PBS	

Fixation buffer	
Paraformaldehyde	4% (v/v)
Dissolve in PBS	

FACS buffer	
BSA	0.4% (w/v)
Sodium azide	0.02% (w/v)
Dissolve in PBS	

PBS-T	
Tween 20	0.05% (v/v)
Dissolve in PBS	

2.13.3. For Virological methods

10 X NTE buffer	
Tris.HCl	0.1 M
NaCl	1 M
EDTA	0.01 M
Dissolve in dH_2O, pH 7.4	

25% Saccharose solution	
Sucrose	25%
Dissolve in NTE buffer	

2.13.4. For Cell biological methods

ATV	
D-Glucose	5 mM
NaCl	137 mM
Na_2EDTA	200 mg/L
$NaHCO_3$	70 mM
KCl	5.4 mM
Trypsin	500 mg/L
Dissolve in dH_2O	

2.14. Commercial Kits

Table 2.14: List of equipment and instruments

Name	Detail	Source
cDNA synthesis kit	RevertAid™ First-strand cDNA synthesis Kit	Fermentas
Gel extraction kit	QIAquick® Gel Extraction Kit	Qiagen
Plasmid Miniprep	QIAGEN Plasmid Mini Kit	Qiagen
Plasmid Maxiprep	QIAGEN Plasmid Maxi Kit	Qiagen
DNA purification	QIAquick PCR Purification Kit	Qiagen
DNA sequencing	BigDye® Terminator v3.1 Cycle Sequencing Kit	LifeTechnologies
RNA Isolation	GenElute™ Mammalian Total RNA Miniprep Kit	Sigma-Aldrich

NC membrane development	Chemiluminescent Femtomax™ Supersensitive HRP substrate	Rockland
Mycoplasma detection kit	Venor®GeM Classic Mycoplasma Detection Kit	Minerva Biolabs

2.15. Software

Table 2.14: List of software and programmes

Name	Source
Flow cytometry analysis	FlowJo Version 7.6 (Tree Star, USA)
Acquisition of western blot	Image studio (LI-COR)
Quantification of western blots	ImageJ (NIH, USA)
Statistical analysis of data	GraphPad Prism 6 (USA), Microsoft Excel (2013)
Sequence analysis	Snapgene (GSL Biotech)
siRNA sequences	Block-iT RNAi designer (Invitrogen)
Primer designing	Primer Blast (NCBI)
Literature management	EndNote X8
Co-localization analysis	Zen 2012
Electroporation	Amaxa Nucleofector® Device AAD-1001

METHODS

3. Methods

3.1. Cell and Microbiological methods

3.1.1. Cultivation of adherent cell lines

Vero, HEK 293T, Hep 2 and other transduced cells are cultured and maintained in MEM with 10% FCS and antibiotic mix in sterile condition in CO_2 cell culture incubator at 37°C.

Adherent cells are propagated by trypsinization with ATV to detach cells and washed with fresh media before passaging. Cells were passaged every 3-4 days.

For seeding cells in 6/12/24/48 well plates, cells were trypsinized and re-suspended in media. The numbers of viable cells were determined by diluting cells in trypan blue and counting live cells in a Neubauer chamber. Cell density was determined using the following formula,

Cell density (cells/ml) = average cell count x dilution factor x 10^4

Following cell densities were used,

Table 3.1: Cell seeding density used for different cell culture vessels

Cell culture vessel	Seeding density (cells/well)
6 well plate	2×10^5
12 well plate	1×10^5
24 well plate	5×10^4
48 well plate	1×10^4
100 mm dish	8×10^6

3.1.2. Cultivation of suspension cell lines

CEM-SS cells and PBL were cultured and maintained in GIBCO®RPMI 1640 with 10% FCS and antibiotic mix in sterile condition in CO_2 cell culture incubator at 37°C unless otherwise specified. Suspension cells were propagated by centrifugation at 160 × *g* for 5 min at 20°C and then re-suspended in an appropriate volume of culture media. Cells were passaged every 3-4 days.

3.1.3. Revival and stock preparation of cell lines

All adherent and suspension cells were revived from the frozen stock at -140°C deep freezer. Cells were warmed quickly at 37°C and the cell suspension was transferred in a 50 ml falcon tube containing 30 ml of respective cold medium. Cells were then centrifuged at 160 × *g* for 5 min at 4°C. The supernatant was removed, and cells were re-suspended in fresh culture media. These cells were then transferred in appropriate tissue culture flask.

Frozen stock of cells was prepared by harvesting cells in their logarithmic phase of growth. Briefly, cells were trypsinized and/or pelleted down by centrifugation at 160 × *g* for 5 min and re-suspended in the freezing mixture (MEM/RPMI + 10% FCS+10% DMSO). Cells were stored overnight in Mr. Frosty™ freezer at -80°C and then transferred in -140°C deep freezer.

3.1.4. Preparation of competent bacterial cells

A single colony of bacterial cells was inoculated into starter culture of 20 ml LB medium and incubated overnight in 37°C shaker at 220 rpm. 5 ml of this starter culture was inoculated in 500 ml of LB medium. Cells were incubated in 37°C shaker at 220 rpm till OD 600 reaches to 0.4 to 0.6. From this stage onwards, all steps were carried out on ice. Bacterial growth culture was collected and centrifuged at 3000× *g* for 15 minutes at 4°C.

The supernatant was carefully removed, and the bacterial pellet was re-suspended in 150 ml of TFB I. Bacteria were then incubated on ice for 15 minutes followed by centrifugation at 3000× *g* for 15 minutes at 4°C. Pellet was re-suspended in 20 ml of TFB II. Competent bacteria were then aliquoted in pre-chilled Eppendorf caps (Epi) and stored at -80°C.

3.1.5. Transformation of bacteria

Plasmids and ligated clones were amplified using *E.coli* XL10-Gold® ultracompetent cells. 0.1 µg of desired plasmid or 5µl of the ligation reaction was added on 50 µl of bacteria in precooled 1.5 ml Epi. The cells and plasmid were mixed by gentle swirling. The mixture was incubated on ice for 30 minutes followed by heat shock in a water bath for 2 minutes at 42°C. Bacteria were cooled down on ice for 5 minutes. 950 µl of LB medium without antibiotic was added on the

bacterial cells and incubated on a shaker at 200 rpm at 37°C for 1 hr. 200 µl of this bacterial culture was then surface spread on LB agar plate containing 100 µg/ml of Ampicillin or 30 µg/ml of Kanamycin. Plates were incubated at 37°C bacterial incubator for 24-48 hrs. Colonies were selected and further inoculated in LB medium for Miniprep plasmid isolation.

3.1.6. Glycerol stock of transformed bacterial culture

The stock of the selected transformed bacterial cells from a single colony was prepared in Glycerol. Briefly, 850 µl of bacterial culture was mixed gently with 150µl of sterile Glycerol. The mix was then transferred in screw-capped epis and stored at -80°C.

3.1.7. Transient transfection of cells

For the transient expression of the desired plasmid in mammalian cells, PEI (1µg/µl) was used. For transfection, HEK 293T cells were seeded in 6 well plate at the density of 10 x 10^5 cells per well. Cells were incubated in cell culture incubator at 37°C for 24 hrs. 6-8 hrs prior to transfection the media was replaced with MEM 10% FCS without antibiotic. Two separate mixtures were prepared in separate tubes. Mixture A: PEI + NaCl 100 µl (vortex for 1 min) and Mixture B: Plasmids + NaCl 100 µl (for 1 µg of total DNA add 3µl of PEI). Mixture A was added in Mixture B and mixed by gentle pipetting. The tubes were then incubated at room-temperature for 30 minutes to build DNA-PEI complex and then distributed dropwise on the cells and incubated at 37°C. The medium was replaced after 6 hrs of transfection and cells were incubated further for 24-48 hrs for subsequent experiments.

3.1.8. Generation of pseudo-typed Lentiviruses for stable transfection

Long-term over expression or silencing of the target gene in mammalian cells was achieved using Lentiviral vector delivery method. We used 3rd generation packaging plasmids for production of Lentiviruses [253].

HEK 293T cells were seeded in 100 mm tissue culture dish at the density of 5 x 10^6 cells per dish. Cells were incubated in cell culture incubator for 24 hrs. 6-8

hrs prior to transfection the medium was replaced with MEM + 10%FCS without antibiotic. The transfection mixture was prepared as shown in **Table 3.2.**

Table 3.2: Amount of 3rd generation packaging plasmids and PEI used to generate pseudo-typed Lentivirus particles.

Vector	Amount		Size (kb)	
	100 mm dish	**6 well plate**		
Mix I:				
pMDLg/RRE	5 µg	0.8 µg	8.8	HIV-1 gag/pol
pRSV/REV	2.5 µg	0.4 µg	4.2	HIV-1 rev
pVSV-G	2.5 µg	0.4 µg	4.8	VSV glycoprotein
Transfer vector	10 µg	1.5 µg	8-12	
NaCl	200 µl	100 µl		
Mix II:				
PEI (1mg/ml)	60 µl	10 µl		
NaCl (150 mM)	200 µl	100 µl		

Two separate mixtures were prepared in separate tubes. Mixture A: PEI + NaCl (vortex for 1 min) and Mixture B: Plasmids + NaCl. Mixture A was added in Mixture B and mixed by gentle pipetting. The tubes were then incubated at room-temperature for 30 minutes to build DNA-PEI complex and then distributed dropwise on the cells. The medium was replaced after 6-8 hrs of transfection and cells were incubated further for 30-48 hrs. The supernatant containing viral particles was harvested and used directly for transduction of mammalian cells or concentrated.

For concentration of viral particles, the supernatant was transferred in 15 ml Falcon and centrifuged at 160 × *g* for 5 minutes at 4°C. The viral supernatant was transferred in another falcon containing cold PEG-*it* (1 volume of PEG-*it* for 4 volumes of supernatant) and mixed by gently inverting tubes 4-5 times. The tubes were incubated overnight or at least 12 hrs at 4°C. After incubation, the tubes were centrifuged at 1500 × *g* for 30 minutes at 4°C. the supernatant was discarded and

the pellet was re-suspended in 1/100th of the original volume of sterile cold PBS. Aliquots were pipetted in cryo-vials and stored at -80°C till further use.

3.1.9. Transduction of cells

Target cells for transduction were seeded in 48 well plate at the density of 4 x 10^4 cells per well and incubated in cell culture incubator at 37°C for 24 hrs. Cell culture media were removed and cell monolayers were washed once with serum-free MEM. Lentiviral supernatants or concentrated virus (MOI: 2-3) were then added on the cells. To increase the efficiency of transduction and obtain maximum expression of target genes, the plates were centrifuged at 400 *x g* for 2 hrs at 37°C and then incubated at 37°C for 48 hrs. Transduced cells were propagated for 3-4 days to achieve sufficient confluency. These cells were sorted by expression of DsRed2 or transduced again to achieve more than 95% transduction efficiency.

3.1.10. Cell sorting

To achieve the maximum expression of shRNA, cells were sorted in BD FACS Aria III based on the DsRed2 fluorescence. Adherent cells were trypsinized with ATV and washed. Cells were centrifuged at 160 × *g* for 5 min at 18°C and re-suspended in 500 µl of the medium. Cells were then passed through cell strainer tube to prepare a single cell suspension. Cells were then sorted based on the DsRed2 expression. After sorting cells were washed twice and re-suspended in 2 ml of respective media containing double the concentration of antibiotics as in the normal medium. Cells were then transferred into 6 well plates and observed daily for confluency.

3.1.11. Cell proliferation assay

3 x 10^5 adherent or suspension cells were seeded in 6 or 24 well plates respectively. These cells were serum starved overnight. Cells were washed twice with cold BSS w/o BSA to remove any traces of growth factors. 5 µM of eFluor670 was prepared in BSS w/o BSA and added on the cells with gentle agitation every 5 min during the incubation for 15 min at 37°C. Cells were then washed three times with BSS + BSA and further incubated in medium containing serum. 24, 48 and 72 hr later, cells were collected in FACS tubes. Cells were washed once with FACS

buffer and fixed with 4% paraformaldehyde for 20 minutes at 4°C and washed again with FACS buffer. Cells were then acquired in APC channel of FACS LSRII. The percentage of proliferated cells was calculated based on the efluor670 signal at each time point.

3.1.12. Cell viability by Propidium Iodide staining

The viability of cells upon treatment with Rapamycin was determined by staining Rapamycin treated cells with Propidium Iodide (PI). 3 x 10^5 adherent or suspension cells were seeded in 6 or 24 well plates respectively. These cells were treated with increasing concentration of Rapamycin (100, 200, 400, 800, 1000, 2000 nm), and 100 % DMSO treated cells were used as positive control (dead cells), and untreated cells were used as negative control for PI staining. 48 hrs after Rapamycin treatment cells were collected in FACS tubes. All the subsequent steps were carried out on ice. Cells were stained with 2.5 µl of PI per tube and incubated in the dark for 15 minutes. Samples were then acquired immediately in FL-3 channel of FACSCalibur. The percentage of PI-positive cells (dead cells) was determined and the percentage of viable cells was calculated.

3.1.13. Isolation of Peripheral Blood Lymphocytes (PBL)

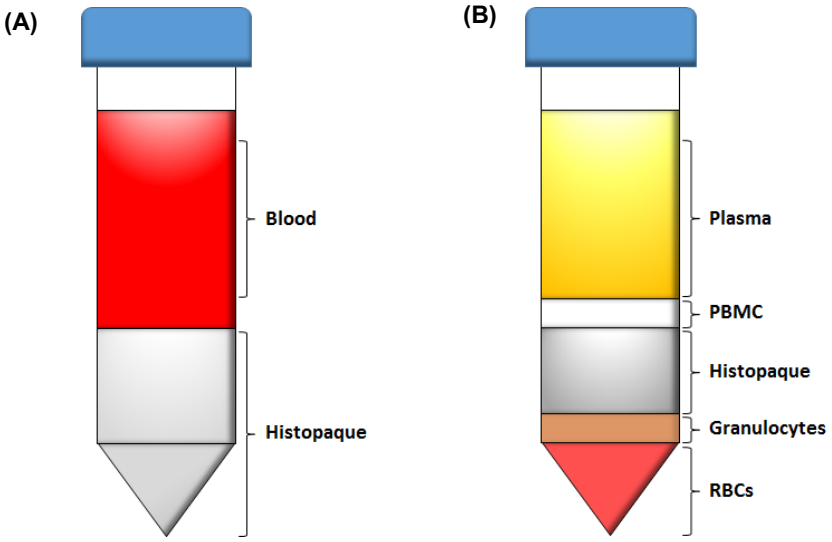

Figure 3.1: Schematic figure of Histopaque density gradient centrifugation. (A) Layers of blood and Histopaque before centrifugation **(B)** layers of blood cells after centrifugation

PBL were obtained with permission of the ethics committee of the medical faculty from leukapheresis filter devices from the department of transfusion

medicine of the Universitätsklinikum Würzburg, kindly provided by Lab group of Dr. Sibylle Schneider-Schaulies. Briefly, peripheral blood mononuclear cells (PBMC) were isolated from fresh blood samples collected from healthy donors by the following procedure: 25 ml of heparinized blood was carefully layered on 9 ml of Histopaque in a 50 ml falcon tube and centrifuged at 160 × *g* without any brakes for 30 minutes at 20°C. the upper layer **(Figure 3.1)** containing serum and platelets was removed carefully and discarded. The buffy coat containing PBMC was carefully removed and transferred in a 50 ml falcon tube. Cells were then washed with sterile PBS thrice by centrifugation at 280 × *g* for 5 minutes at RT. Cells were then re-suspended in 25 ml of RPMI with 10% FCS, plated on 175 cm^2 flask and incubated for 2 hrs at 37°C. Non-adherent cells (PBL) were separated and counted before using.

3.1.14. Stimulation of PBL

To measure the response from isolated PBL, they were stimulated with PHA, IL-2 and IFN-α. For analysing differential gene regulation in stimulated PBL, $1x10^7$ PBL in 3 ml per well were seeded in 12-well plates in RPMI with 10% FCS. Stimulation was done by 2.5µg/ml of PHA, 25ng/ml of Proleukine (human IL-2) and 10^5 units/ml of IFN-α either individually or in combination. 48 hrs post stimulation cells were lysed for western blot analysis.

For stimulation of PBL after electroporation of siRNA **(in 3.2.6.1)** the same concentrations of PHA and IL-2 were used.

3.2. Molecular biology methods

3.2.1. Gene cloning

3.2.1.1. Restriction digestion of Vector plasmids and inserts

Desired DNA fragments from plasmids for cloning were prepared by restriction digestion. These enzymes recognize specific palindromic sequences of 6-8 bases. The selection of enzymes is done on the basis of the desired insert and vector size. All the enzymes used were from Thermo Scientific. The following digestion reaction was set up for Vector and insert. The digested products were analysed on agarose gel for verifying the size of the digested product.

Table 3.3: Restriction digestion reaction of F6gW-dsRed2 plasmid to generate Vector for shRNA cloning

Reagent	For gel extraction
Plasmid	15 µg
XhoI	5 µl
KspAI	5 µl
10x Buffer G	10 µl
Total volume	100 µl

Make desired total volume using DPEC H_2O

Table 3.4: Restriction digestion reaction of F6gW-dsRed2 plasmid and KDELR2/REDD1 cDNA clone to generate Vector and insert fragment

Reagent	For analysis
Plasmid	1µg
EcoRI	1 µl
BamHI	1 µl
10x Buffer R	2 µl
Total volume	25 µl

Reagent	For gel extraction
cDNA clone	15 µg
EcoRI	5 µl
BamHI	5 µl
10x Buffer R	10 µl
Total volume	100 µl

Make desired total volume using DPEC H_2O

3.2.1.2. Gel extraction of nucleic acid

Required DNA fragments were purified from Agarose gel using QIAquick® Gel Extraction Kit according to Manufacturer's instructions. The DNA was eluted in 50µl of elution buffer.

3.2.1.3. De-phosphorylation of Vector

The linearized and purified vectors were de-phosphorylated. De-phosphorylation prevents re-ligation of linearized vectors thus prevents background activity during cloning. The following De-phosphorylation reaction was according to the manufacturer's protocol (**Table 3.5**). The reaction was then incubated for 1 hr at 37°C for de-phosphorylation and 10 min at 72°C to inactivate the enzyme.

Table 3.5: De-phosphorylation of linearized F6gW-dsRed2 plasmid

Reagent	Volume
Plasmid gel purified	2 µg
Calf Intestine alkaline phosphatase (1U/µL)	2 µl
10X buffer R	5 µl
Total volume	50 µl

Make desired total volume using DPEC H_2O

3.2.1.4. Generation of ds DNA-oligos encoding shRNAs

Single-stranded forward and reverse oligonucleotide sequences were designed to silence the desired gene. In order to clone shRNA-expressing vectors, ds DNA-oligos were annealed. The synthesized ss DNA-oligos were dissolved in oligo annealing buffer in stock concentrations of 100µM. Equal amounts of forward and reverse oligos were mixed together to achieve a final concentration of 50µM. The mixture was then heated in a thermal cycler for 5 minutes at 95°C and incubated 5 min at room temperature for cooling. The ds DNA-oligos were stored at -20°C.

3.2.1.5. Phosphorylation of Inserts

The ds DNA-oligos generated by annealing of single-stranded oligonucleotides do not contain 5' phosphate groups. For ligation, it is a pre-requisite to have 5' phosphate groups at least at one end of the insert. The target gene fragments obtained from cDNA clones already have 5' phosphate groups. Therefore, it is not necessary to phosphorylate the inserts obtained from restriction digestion. However, PCR products and oligos will not have 5' phosphate moieties. Hence, it is required to phosphorylate the ds DNA-oligos using T4 polynucleotide kinase. The reaction was incubated at 37°C for 20 minutes for phosphorylation and 72°C for 10 minutes for inactivation of the enzyme.

Table 3.6: phosphorylation of shRNA

Reagent	Volume
ds Oligo (50µM)	15 µl
T4 polynucleotide kinase (10U/µL)	2 µl
T4 ligase buffer	4 µl
Total volume	60 µl

3.2.1.6. Ligation

The two fragments of the digested vector and the insert were joined together by a ligation reaction. DNA ligases catalyse the formation of a phosphodiester bond between the 3'-OH end of one fragment and the 5'-phosphate group of another fragment. Digestion of F6gW-dsRed and cDNA clone with EcoRI and BamHI resulted in sticky ends (3.2.1.1) and prevented relegation of vectors and also insert fragments in a directional manner. The ligation thus results in a circular plasmid containing the target sequence. The following formula was used to calculate the ng of insert required in the ligation reaction.

$$\text{ng of insert required} = \frac{\text{ng of Vector} \times \text{kb size of Insert}}{\text{kb size of vector}} \times \frac{\text{Insert}}{\text{Vector}}$$

Two different amounts of vectors were used, 50 ng and 100 ng, and two different inserts to vector ratios, 3:1 and 5:1, were used. The ligation reaction was incubated overnight at RT.

The ligation mixture was then used for transformation of bacteria (3.1.5).

Table 3.7: Ligation reaction

Reagent	volume
Linear vector DNA	50 ng/100 ng
Insert DNA	As per above calculations
10 X T4 DNA ligase buffer	2 µl
T4 DNA ligase (5 U/µl)	1 µl
Total volume	20 µl

Make desired total volume using DPEC H_2O

3.2.1.7. Colony PCR

In order to confirm if the desired fragment is correctly inserted in the vector, a colony PCR was done using bacterial colonies. The antibiotic-resistant colonies obtained on the LB agar (3.1.5) plate were picked up and dissolved in 20µl of DPEC water. The PCR reaction was set up as follows in a total volume of 25µl in a Thermal cycler. The amplified product was then analysed on agarose gel.

Table 3.8: Colony PCR

Reagent	Volume
PuRe Taq Ready-to-Go PCR bead	1 bead
Forward Primer 10µM	1 µl
Reverse Primer 10µM	1 µl
Dissolved colony	2 µl
HPLC water	21 µl

PCR conditions		
94°C	2 min	
59°C	1 min	
72°C	1 min	
94°C	30 secs	35 cycles
59°C	1 min	
72°C	1 min	
72°C	7 min	
4°C	hold	

3.2.1.8. Plasmid isolation - Miniprep method

Colonies with desired plasmids were used for Miniprep. 10µl of colony suspension or bacterial colony from the LB agar plate was inoculated in 5 ml of LB medium with 100µg/ml of Ampicillin. The culture was then grown in a bacterial shaker at 220 rpm overnight at 37°C.

Plasmid Miniprep isolation was done using "QIAGEN Plasmid Mini Kit" according to manufactures instruction. Plasmids were eluted in 50 µl of TE buffer.

3.2.1.9. Plasmid isolation - Maxiprep method

Colonies with the correct sequence were inoculated for Maxiprep. 10 µl of the bacterial colony was inoculated in 5 ml of LB medium with 100 µg/ml of Ampicillin and incubated in a bacterial shaker at 220 rpm for 4-5 hrs at 37°C. This 5 ml of bacterial culture was then inoculated in 100 ml of LB medium with 100µg/ml of Ampicillin and flasks were incubated in a bacterial shaker at 220 rpm for 4-5 hrs at 37°.

Plasmid isolation was done using "QIAGEN Plasmid Maxi Kit" according to manufactures instruction. The plasmid pellet was then suspended in TE buffer and diluted with DPEC H_2O at the final concentration of 1µg/µl and stored at -20°C.

3.2.1.10. Sequencing of DNA

The sequence of the desired insert in the isolated plasmid was confirmed by sequencing. The sequencing was performed using "BigDye® Terminator v3.1 cycle sequencing kit" from Life Technologies (USA) in a thermal cycler. The following reaction was set up for sequencing:

Table 3.9: Sequencing reaction

Reagent	Volume
Big Dye 3.1 DNA polymerase	1 µl
5x BDT Buffer	1 µl
Primer F or R (5 pmol/µl)	1 µl
Sample DNA (500 ng)	2 µl
Total volume	5 µl

Amplification conditions		
96˚C	30 secs	
50˚C	15 secs	25 cycles
60˚C	4 min	

The amplified product was then sequenced kindly by the Diagnostic department of the Institute of Virology and Immunobiology (Würzburg) in an "ABI PRISM® 310 Genetic Analyzer" Company Advance Biolab Service (Munich). The generated sequence was then analysed and confirmed using Lasergene software.

3.2.2. PCRs

The PCR amplification was carried out using "illustra PuReTaq Ready-To-Go PCR Beads" in a thermal cycler. The following PCR reaction was pipetted in a total volume of 25µl.

Table 3.10: PCR reaction

Reagent	Volume
PuRe Taq Ready-to-Go PCR bead	1 bead
Forward Primer 10µM	1 µl
Reverse Primer 10µM	1 µl
Template DNA (1µg)	2 µl
HPLC water	21 µl

PCR condition		
95°C	5 min	
95°C	1 min	
68°C	1 min	25 cycles
72°C	1 min	
72°C	10 min	
4°C	Hold	

3.2.3. RNA isolation

Two different methods were used for RNA isolation.

3.2.3.1. TRIzol

For RNA isolation using TRIzol method, cells were trypsinised and washed once with cold PBS. 1 x 10^6 cells were centrifuged at 160 × *g* for 5 min at 4°C. The cell pellet was re-suspended in 1 ml TRIzol and transferred in Eppendorf cap. The mixture was then incubated at RT for 5 min. 200 µl of chloroform was then added and mixed for 15 secs followed by incubation at RT for 3 min. The lysate was then centrifuged at 13000 rpm for 15 min at 4°C in a biofuge. The water phase was then carefully transferred into a new Eppendorf cap. Lysates were again treated with chloroform similarly to remove traces of TRIzol. 500 µl isopropanol was added to the water phase and mixed carefully. The mixture was incubated for 10 minutes at RT and then centrifuged at 13000 rpm for 10 min at 4°C. The supernatant was discarded and pelleted RNA was washed with 75% ethanol. RNA was centrifuged at 10000 rpm for 5 min at 4°C. Ethanol was carefully removed and the pellet was air dried for 5 min at RT (avoid over drying of pellet). RNA was then re-suspended in 50µl of DPEC H_2O and incubated for 10 min at 55°C on a heating block to obtain

a better solubility of the RNA. The RNA was once freeze-thawed at -20°C before quantifying with Nano drop.

3.2.3.2. GeneElute Mammalian Total RNA Miniprep Kit

Alternatively, the total cellular RNA was extracted using the GeneElute Mammalian Total RNA kit according to manufacturer's instruction and eluted in 50 µl of elution buffer. The RNA was aliquoted in small volumes and stored at -80°C.

3.2.4. Semi-quantitative PCR

For semi-quantitative PCR, four different amounts of RNA (4, 2, 1, 0.5 µg) were reverse transcribed. The following reaction was setup in a Thermal cycler for generating first strand cDNA in a total volume of 20µl. The cDNA was aliquoted and stored at -20°C till further use. The cDNA was then amplified using gene-specific primers **(Table 2.4)**. The number of PCR cycles (25) was kept constant for all semi-quantitative PCRs and equal amounts from each sample were loaded on agarose gels.

Table 3.11: cDNA synthesis

Reagent	Volume
Template RNA	300 ng
Oligo $(dT)_{12-18}$ primer (0.5 µg/ml)	1 µl
dNTP (10mM)	2 µl
M-MLV Reverse transcriptase (200U/µl)	1 µl
5X reaction buffer	4 µl

cDNA synthesis reaction	
70°C	5 min
4°C	2 min
42°C	2 min
42°C	60 min
70°C	10 min

Table 3.12: Semi quantitative PCR

Reagent	Volume
PuRe Taq Ready-to-Go PCR bead	1 bead
Forward Primer 10µM	1 µl
Reverse Primer 10µM	1 µl
RT product	4 µl
HPLC water	19 µl

PCR conditions		
95°C	5 min	
95°C	1 min	25 cycles
68°C	1 min	
72°C	1 min	
72°C	10 min	
4°C	Hold	

3.2.5. Quantitative RT-PCR

Cellular RNA was isolated from 1 x 10^6 cells by TRIzol ™(3.2.3.1). Isolated RNA was then reverse transcribed to generate cDNA (3.2.4).

Table 3.13: qRT PCR

Reagent	Volume
Template cDNA	2.5µl
Forward primer	1 µl
Reverse primer	1 µl
2X SYBR-Green transcriptase (200U/µl)	5 µl
DPEC water	0.5 µl

qRT-PCR reaction		
95°C	180 secs	
95°C	10 secs	45 cycles
60°C	30 secs	
95°C	10 secs	Melting curve
60°C	60 secs	
95°C	1 sec	
37°C	30 secs	Cooling

Gene-specific primers were used to amplify the target genes. Real-Time PCRs were performed using "2x SYBR Green qPCR Master Mix" from Biomake. The amplification was done in a "LightCycler 2.0 real-time PCR system" from Roche in a total volume of 10µl.

3.2.6. siRNA transfection

3.2.6.1. In PBL

Generally, viral vector-based gene delivery methods are utilized for the expression of shRNAs or genes. However, the use is limited by the time and potential safety issues in primary cells. In addition, human PBL are refractory to

viral DNA/RNA delivery methods. Hence, electroporation is a fast and safe way of delivering target siRNA in stimulated/non-stimulated PBL.

siRNA duplexes were directly purchased from Dharmacon **(Table 2.6)** and dissolved in DPEC water to achieve a stock concentration of 100 µM. A final siRNA concentration of 20 nM in 1 ml was used for transfection of $1x10^7$ PBMCs.

Briefly, the PBL were isolated from human blood as described **(3.1.13)**. Before the electroporation, 12-well plates were filled with RPMI containing 10% FCS and incubated in cell culture incubator at 37°C. The required number of cells was centrifuged in a 15 ml falcon at 160 × *g* for 5 minutes at RT. The supernatant was carefully removed. 100 µl of electroporation buffer was added to the cells and they were re-suspended by gentle pipetting, followed by addition of 20 nM/ml of siRNA dilution and mixed by gentle pipetting. The electroporation mix was then transferred in cuvettes and cells were electroporated in Amaxa Nucleofector® using program U14 for unstimulated cells and U20 for stimulated cells. Cells were then immediately transferred into 3 ml of pre-warmed medium and incubated for 48 hrs. The electroporation procedure was repeated a second time and cells were now incubated for 24 hrs.

Electroporated cells were then stimulated with PHA (2.5 µg/ml) or IL-2 (25 ng/ml) for 24 hrs. To determine the percentage of stimulated cells, 10000 cells were taken in a FACS tube and washed once with FACS buffer. Cells were then stained for surface expression of PE-CD3 for detection of T cells and APC-CD69 for detection of the activation marker CD69 **(3.3.1.1)**. To estimate the siRNA silencing efficiency cells were lysed in RIPA buffer **(3.3.3)**. The protein lysates were then analysed by SDS-PAGE **(3.3.5)** and respective proteins were detected by western blot **(3.3.6)**. 2 x 10^6 cells were infected with rMV^{IC323}eGFP at a MOI of 0.2. The virus was harvested 48 hr post infection by freezing and thawing the complete culture. The virus was titrated on Vero hSLAM cell **(3.4.2)**.

3.2.6.2. In Vero Cells

Same siRNA duplexes were used for transfection of Vero cells as mentioned in **3.2.6.1.** Final siRNA concentration of 50 nM was used for transfection of Vero cells. Briefly, 1 x 10^6 Vero cells were seeded in 6-well plate. A mixture of siRNA and transfection reagent DF2 (Dharmacon) was prepared according to the

manufacturer's instructions. The mix was then incubated at room-temperature for 20 min. The medium was then replaced by the siRNA mix and incubated for 24 hrs. Cells were then infected with rMV eGFP at a MOI of 0.1 and incubated for 48 hrs. The virus was harvested and titrated on Vero hSLAM cells **(3.4.2).** Remaining cells were lysed in RIPA buffer **(3.3.3)**. The protein lysates were then analysed by SDS-PAGE **(3.3.5)** and respective proteins were detected by western blot **(3.3.6)**.

3.3. Immunological methods

3.3.1. Flow Cytometry

Flow cytometry analyzes individual cells in a single stream of fluid. Light scattered based on the size (Forward scatter), granularity (Side scatter) or light emitted from fluorescently labelled antibodies help to distinguish wide array of surface and intracellular molecules of the cell. The measurement of optical and fluorescent characteristics allows quantitative and qualitative analyses of several cell properties simultaneously.

All flow cytometric measurements were performed in BD LSR II or BD FACSCalibur. Experimental data was then analysed by FlowJo Version 7.6 software. Cells were prepared depending on the experimental requirement. All washing steps were done with cold FACS buffer by centrifugation at 200 × *g* for 5 min at 4°C and supernatant was discarded.

3.3.1.1. Surface expression of target molecules

Adherent cells were first detached from flasks using ATV, whereas the required amounts of suspension cells were directly taken into FACS tubes. All subsequent steps were performed on ice. 10000-50000 cells were taken into FACS tube and washed once with cold FACS buffer. Cells were then re-suspended in 100 µl of appropriate primary antibody dilution and incubated at 4°C for 30 min to 1hr. Later, cells were washed once and stained with fluorescent labelled secondary antibody at 4°C for 30 min to 1 hr. Cells were then washed thrice with FACS buffer and acquired in LSR II.

3.3.1.2. Intra-cellular expression of target molecules

To determine the intracellular expression of target molecules, cells were permeabilized to facilitate the entry of antibodies.

10000-50000 cells were taken into FACS tubes and washed once with cold FACS buffer. Cells were then fixed at RT for 15 min with 100 µl of 4% PFA and washed once with FACS buffer. These fixed cells were then permeabilized with 100 µl of 0.1% Triton X 100 at 4°C for 15 minutes and washed once with FACS buffer. Cells were then blocked with FACS buffer containing 10% FCS followed by antibody staining protocol **(3.3.1.1)**. Cells were washed thrice with FACS buffer and acquired in LSR II.

3.3.1.3. GFP/Ds-Red2 expression in infected/transduced cells

For the infection experiments, eGFP expressing measles virus was used. Whereas, for expression of shRNA, fluorescent DsRed2 labelled plasmids were used. Therefore, the percentage of virus-infected, or shRNA transduced cells was determined by directly measuring the expression of eGFP or DsRed2 by FACS.
Measles virus is known to form syncytia. This results in multinucleated giant cells which are difficult to analyse by FACS. Hence to facilitate single cell analysis of infected GFP positive cells, the fusion inhibitory peptide (FIP) was used. This peptide was added to the cells at the final concentration of 200µM 2hrs after the infection. This prevents subsequent fusion of cells and the spread of virus without affecting replication of the virus in single cells.

For FACS analysis 10000-50000 cells were taken into FACS tubes and fixed with 100 µl of 4% PFA at RT for 20 min. Cells were then washed and acquired by a flow cytometer or stained with antibodies depending on the experiment **(3.3.1.2)** and then acquired.

3.3.2. Immunofluorescence staining

Immunofluorescence microscopy combines light microscopy with fluorescence allowing visualization of dynamic processes of cells.

Briefly, 10000 cells were seeded in 8-well chamber slides and incubated overnight. Depending on the experiment, cells were infected with MV (Edmonston strain) with a MOI of 1, and 2 hrs post infection the viral inoculum was removed

and eventually replaced with medium containing 200 µM of FIP. Cells were incubated for different times (8, 16, 18, 24 hrs) and then fixed for microscopy.

Cells were washed gently with cold PBS and fixed with 4% PFA for 20 min at RT. Cells were washed thrice and then permeabilized with 0.1% Triton X 100 for 10 min at 4°C. Blocking of non-specific antigens was done with 10% BSA (albumin fraction V) at 4°C overnight. Next day, cells were washed thrice with cold PBS and stained with 1:100 dilution of primary antibody in PBS with 1% BSA at 4°C overnight. After washing thrice with PBS, 1:400 dilution of secondary antibody in PBS with 1% BSA was added and incubated at RT for 1 hr. Nuclear staining was done by adding 300 nM of DAPI. Cells were finally washed with PBS and the chambers were removed from the slide. Slides were briefly dried before adding 200 µl of Fluoromount-G and carefully a coverslip was placed on the slides. Samples were then analysed by Zeiss LSM 780 confocal microscope.

3.3.3. Protein lysate preparation

In order to analyse specific proteins from cells, SDS-PAGE and western blotting is used to separate and identify proteins. There are different methods of protein extraction and one of the method is lysis of cells using radio-immunoprecipitation assay (RIPA) buffer.

All the steps were carried out on ice. Adherent cells were detached from plates using ATV before lysis, whereas suspension cells were used directly for lysis preparation. Cells were washed twice with ice cold PBS to remove any traces of proteins from growth media. The cell pellets of 1 x 10^6 adherent cells and 1 x 10^7 PBL were then re-suspended in 80-100 µl of RIPA buffer containing 1:100 dilution of protease inhibitor cocktail II and 1µM DTT. The cells were lysed on a shaker for 1hr at 4°C. The lysates were clarified by centrifugation at 10000 rpm for 5 min at 4°C in a Biofuge. Supernatants were carefully removed and transferred in pre-cooled Eppendorf caps. The protein concentration in these lysates was quantified using BCA **(3.3.4)** and samples were stored at -20°C till further use.

For the detection of phosphorylated proteins cell lysates were prepared by a different method to avoid any loss or degradation of phospho-proteins. All the steps were carried out on ice. Cells were washed once with ice cold PBS and then directly lysed in 2X Laemmeli buffer. Samples were mixed in Laemmeli buffer and

incubated at -80°C for 1-2 hrs. Samples were then immediately boiled at 95°C for 10 min. These samples were used for SDS-PAGE analysis or stored at -20°C till further use.

3.3.4. Quantification of proteins by BCA

To determine the effects of various experimental procedures on the expression of proteins, equal amounts of proteins are required to be loaded for separation. Either equal numbers of cells were lysed in equal amounts of lysis buffer and equal volumes were loaded on the gel, or the protein concentrations were determined using the BCA protein quantification method.

Peptide bonds in proteins reduce Cu^{2+} ions from $CuSO_4$. The highly alkaline solution of Bicinchoninic acid (BCA) chelates Cu^{+} ions to form a purple colour complex at higher temperatures (60°C). The intensity of the colour complex is directly proportional to the protein concentration of the sample. This purple complex is then quantified using absorbance at 562 nm in a photometer.

To determine the protein concentration, 1ml of BCA was aliquoted in Eppendorf caps followed by addition of 20µl of $CuSO_4$ and 5 µl of protein sample/DPEC H_2O/standard. Solutions were mixed by gentle vortexing and then heated at 60°C for 15 min. Samples were then transferred into cuvettes for measurement of the absorbance. The colorimetric readings were acquired in an Eppendorf Photometer using manufacturer's instructions.

3.3.5. SDS-PAGE

Sodium dodecyl sulphate polyacrylamide gel electrophoresis (SDS-PAGE) is used to separate proteins based on their molecular mass in the electric field. In discontinues PAGE two gels are used to separate proteins. Proteins first migrate in the stacking gel with neutral pH. This helps to collect and concentrate samples before the actual separation starts in the resolving gel at pH 8.7. This pH gradient gives a stacking effect resulting in sharper and narrower protein bands.

All the gels used contained 10 or 12% polyacrylamide. 20-50 µg of protein lysates were mixed with 5X Laemmeli buffer and heated at 95°C for 5 min for denaturation. These samples then were used immediately or stored at -20°C.
SDS-PAGE was carried out in the following steps:

1. Assembly and preparation of the gel for electrophoresis:

Two glass plates were assembled in a gel apparatus separated by spacers. The assembly was checked for any leakage and the resolving gel was prepared **(2.13.1)**. The components were poured immediately between the glass plates. The gel was layered with 1 ml of iso-propanol untill the gel was polymerised. The iso-propanol was removed before the stacking gel was poured on top and a comb was inserted in the stacking gel.

2. Electrophoresis:

The electrophoresis unit was then filled with protein gel running buffer. The comb was removed carefully from stacking gel and the wells were gently flushed with protein gel running buffer to remove gel residues. Samples and pre-stained protein marker (2-3µl) were then loaded in the wells and separated at 80V (10 cm gels) for 3-4 hrs or till the samples resolved completely.

3. Electrophoretic transfer:

To detect target proteins, they were immobilized by electrotransfer from the gels to a solid membrane support. For all experiments, nitrocellulose (NC) membranes were used. After soaking in the appropriate buffers **(Fig. 3.2)** the NC membrane and the gel were placed together with Whatman filter paper between two electrodes **(Fig 3.2).**

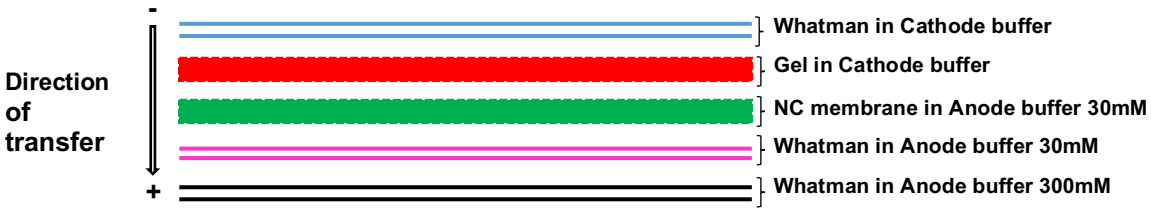

Figure 3.2: Western blot transfer setup
Gel and NC membranes were placed between layers of Whatman filter paper soaked in Anode and Cathode buffer.

The transfer set up was carefully placed in transfer assembly and any air bubbles were removed by gentle rolling. The transfer was carried out at 125 mA for 75 minutes for gels of approximately 10x12 cm. Due to the electrophoretic field generated between the electrodes, the proteins were transferred from the gel onto the NC membrane. The transfer was checked by successful transfer of all bands of the protein marker. The membranes were then probed with specific antibodies as described in **(3.3.6).**

3.3.6. Detection of proteins on nitrocellulose membrane

Following the transfer of protein on NC membrane, the unoccupied binding sites on the membrane have to be blocked to avoid non-specific binding of antibodies.

The membranes were blocked at room temperature for 30 minutes in 5% non-fat dry milk or BSA in PBS-T. The blocked membranes were then probed with specific primary antibodies (1:500 – 1:2000) in 5% milk or BSA in PBS-T overnight at 4°C with gentle shaking. Membranes were then washed thrice for 5 minutes each with PBS-T and incubated with HRP or fluorescent labelled secondary antibodies (1:10000- 1:15000) in 5% milk for 1 hr at room temperature with gentle shaking. The membranes were then washed thrice with PBS-T. Images were acquired in a Li-cor Odyssey® Fc Imaging system. For HRP labelled secondary antibodies, Chemiluminescent FemtoMax™ Super Sensitive HRP Substrate (Rockland) was added on membranes before Imaging and acquired in Chemi channel whereas, fluorescent labelled secondary antibodies were imaged in 700 or 800 channels directly depending on the fluorescent antibody used.

3.3.7. Stripping of nitrocellulose membrane

To remove primary and secondary antibodies bound on the membrane, the NC membranes were incubated in stripping buffer **(2.13.1)** for 30 minutes at 50 °C (stripping buffer was always prepared fresh). Membranes were then washed 5 times thoroughly in PBS-T for 10 minutes each. The membranes were blocked with 5% milk or BSA at room temperature for 20-30 minutes and then probed with another primary antibody **(3.3.6)**.

3.3.8. Co-immunoprecipitation

Co-immunoprecipitation helps to determine whether two proteins interact in non-denaturing physiological conditions in-vitro. Interacting partners (prey protein) of labelled proteins (bait) are precipitated using a specific antibody and/or beads against the bait protein and detected using western blotting.

Immunoprecipitation of FLAG (DYKDDDDK) tagged fusion proteins was done using ANTI-FLAG® M2 affinity gel. It is a purified murine IgG1 monoclonal antibody covalently attached to agarose beads by hydrazide linkage.

Vero-023 and Vero-KDELR2 cells were seeded in 60mm dish at a density of 8 x 10^5 cells. Cells were incubated overnight at 37°C. Cells were then infected with MV eGFP virus at MOI of 0.1 and incubated at 37°C. 2 hrs post infection virus inoculum was removed and replaced with 5 ml MEM containing 2% of FCS. Cell lysates were prepared 48 hrs post infection.

The cell monolayer was carefully washed with cold PBS. Cells were scraped gently in PBS and pelleted down by centrifugation at 13000 rpm at 4°C for 5 minutes in a Biofuge. Cells were re-suspended in IP lysis buffer. Cells were then incubated on a shaker for 1 hrs at 4°C. Protein lysates were collected by centrifugation at 8000rpm at 4°C for 5 minutes.

All the steps were performed on ice. One-third volume of the lysates was used as input control. This input samples were mixed with 5x Laemmeli buffer and boiled at 95°C for minutes and stored at -20°C till further use.

For immunoprecipitation 10µl of ANTI-FLAG® M2 affinity gel was aliquoted in Eppendorf caps per sample. The beads were washed thrice with IP buffer (without SDS) and then lysates were added to the beads. Samples were then incubated using an orbital rotor at 4°C. Lysates were then washed thrice with IP buffer (without SDS) and once with cold PBS. Anti-flag beads were pelleted down by centrifugation at 13000 rpm at 4°C for 5 minutes. The beads were then re-suspended in 70-100 µl of 2x Lammeli buffer and boiled at 95°C for 5 minutes. These samples were then analysed by western blotting or stored at -20°C till further use.

3.4. Virological methods

3.4.1. Measles virus stock preparation

The attenuated vaccine strain MV-Edmonston, the Edmonston based recombinant rMV^{Edtag}eGFP and recombinant wildtype rMV^{IC323}eGFP were used. Required stocks of these viruses were prepared in Vero-hSLAM cells. These cells were cultured in 175cm^2 flask at the 60-70% confluency. Cells were washed once with serum-free MEM and replaced with 3 ml required dilution of virus (MOI: 0.01). Cells incubated for 2hrs at 37°C and then virus inoculum was replaced with fresh 20 ml of MEM with 2% of FCS. Infected flasks were incubated for 2-3 days

depending on cytopathic effect. Media from infected flask were reduced to 5 ml and the flasks were frozen at -80°C for at least 24hrs.

The flasks were then thawed at 37°C and all the subsequent steps were carried on ice. The cells were scraped using cell scraper and virus suspension was collected in a precooled homogenizer. Cells were homogenized 10-15 times to release the intercellular virus and centrifuged at 280 × *g* for 15 minutes at 4°C. The viral supernatants were aliquoted in cryo-tubes and stored at -80°C.

3.4.2. Titration of Measles virus

For the titration of MV virus preparations **(3.4.1.1)** or from other experimental procedures, Vero or Vero-hSLAM cells were used depending on the virus. Cells were seeded in a 48 well plate (1 x 10^4 per well) and incubated at 37°C overnight. Virus dilutions from 10^{-1} to 10^{-6} were prepared in MEM with 2% FCS. Media from cells were replaced with 200 µl of virus dilutions in triplicates and plates were incubated for 72 hrs at 37°C. Infection-induced syncytia (plaques) were counted microscopically. The PFU/ml of the titrated virus preparation was determined by the following formula:

PFU/ml = (mean number of plaques x dilution factor)/ volume of inoculum (ml)

RESULTS

4. Results

4.1. APOBEC3G differentially regulated cellular gene expression upon overexpression in Vero cells

4.1.1. Differential gene regulation at the mRNA level

Our group previously reported that A3G expression in Vero cells significantly reduced transcription and expression of MV proteins in infected cells. However, the underlying mechanism is poorly understood [192]. In the scope of this thesis, we investigated the basis of the A3G mediated anti-viral activity against MV.

The microarray analysis of gene expression in control and A3G expressing cells revealed a differential gene regulation in Vero cells. A3G expression significantly up-regulated 844 transcripts and down-regulated 598 transcripts in Vero cells. We selected the A3G up-regulated genes *REDD1* and *KDELR2* as possible candidate host factors affecting MV replication as discussed in the introduction.

KDELR2 mRNA levels in Vero-A3G cells were confirmed using PCR. For Semi-quantitative PCR, the total cellular RNA was reverse transcribed, and cDNA was amplified by conventional PCR **(Figure 4.1A).** The mRNA expression was also validated by real-time qPCR **(Figure 4.1B)**. The primers used for semi-quantitative PCR and real-time PCR are summarized in Table 2.4. *KDELR2* mRNA levels were found to be increases by 1.5-2-fold in Vero-A3G cells as compared to Vero-023 (empty vector control) **(Figure 4.1A and B)**.

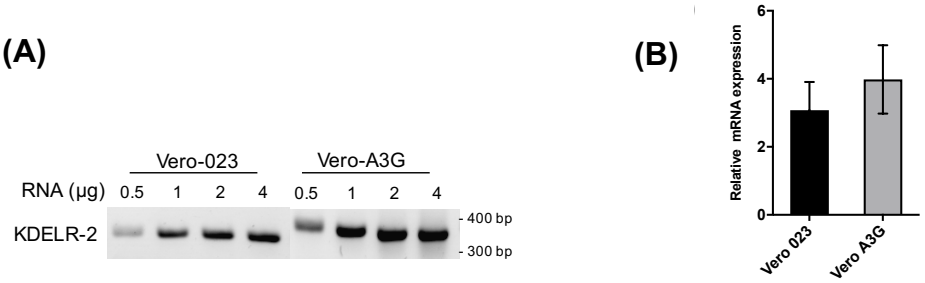

Figure 4.1. A3G expression increased *KDELR2* mRNA levels in Vero cells.
(A) Four different concentrations of cellular RNA (0.5, 1, 2, 4 µg) were reverse transcribed to cDNA. 4µl of cDNA from each sample was amplified by conventional PCR. The PCR products analysed on 1% Agarose gel. **(B)** The relative *KDELR2* mRNA levels were quantified by SYBR-Green Real-Time qPCR. (n=2).

4.1.2. Differential gene regulation at the protein level

The differential regulation in A3G expressing cells was validated at the protein level by western blot. Equal amounts of protein lysates from control and A3G expressing cells were separated on denaturing SDS-PAGE, transferred on nitrocellulose membrane (NC) and probed with respective antibodies. The protein band densities were quantified using ImageJ software. The densities of each target protein were normalized to the densities of the respective loading control GAPDH. The relative fold increase/decrease for the protein of interest in Vero A3G cells was calculated and are depicted below each blot.

Depending on the genes of interest and availability of antibodies, the following genes were selected to validate differential gene regulation at the protein level: A3G up-regulated genes *REDD1* and *KDELR2* and A3G down-regulated genes *MOSC2, ACY1, TXNIP* and *PRDX2*. The protein levels of REDD1 and KDELR2 were found to be increased by 3.3 and 1.3-fold respectively in A3G expressing Vero cells (**Figure 2A**). Whereas, the expression of MOSC2 and ACY1 was decreased by 0.5 and 0.2-fold respectively (**Figure 2B**). Thus, validating the data of the microarray analysis. However, PRDX2 expression was not decreased, and TXNIP was not detected using available antibody (data not shown). Therefore, we investigated the possible antiviral role of the REDD1 and KDELR2 proteins in detail in this thesis.

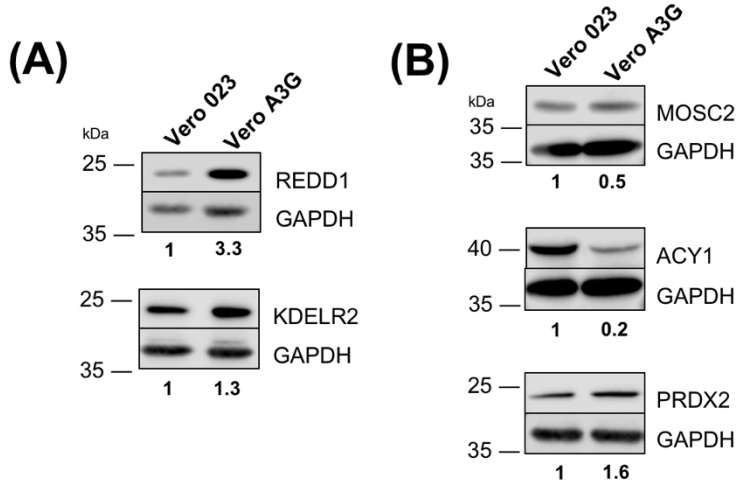

Figure 4.2: Differential gene regulation at the protein level.
Protein lysate from Vero 023 and Vero A3G was analysed by western blot. Expression of each protein was compared with internal loading control GAPDH. The relative fold change is depicted in numbers below each blot. Protein levels of **(A)** A3G up-regulated genes and **(B)** A3G down-regulated genes.

4.2. Overexpression of A3G-regulated genes *REDD1* and *KDELR2* in Vero cells

4.2.1. Stable expression of REDD1-Flag and KDELR2-Flag in Vero cells

To evaluate the differential effects of the *A3G* regulated proteins *REDD1* and *KDELR2*, the corresponding genes were individually overexpressed in Vero cells. Vero cell lines stably overexpressing REDD1 and KDELR2 were prepared using 3rd generation lentiviral packaging system. REDD1 (RC202847) and KDELR2 (RC200007) cDNA clones were purchased from "ORIGENE". REDD1 expressing F6gW-REDD1-Flag plasmids and Vero REDD1 2X cells were prepared by Sabine Kendle.

To determine the effect of overexpression of these target proteins on the replication of MV, first it was important to determine the levels of a target proteins in transformed cells. Therefore, Vero-REDD1 cells were stained for the REDD1 protein which is Flag-tagged and analysed by FACS. Uniform expression of target protein would result in a sharp peak. REDD1 cells transduced twice (2X) showed a shift in the peak of fluorescence intensities as compared to the cells transduced once (1X) **(Figure 4.3A)**.

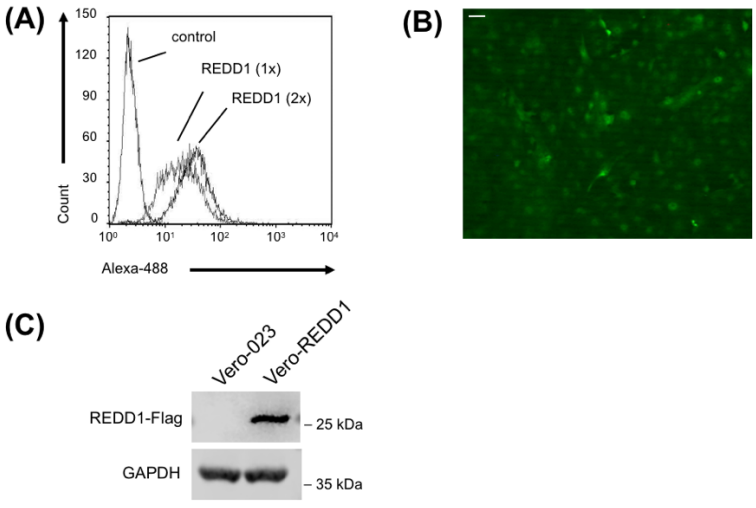

Figure 4.3: Overexpression of REDD1 in Vero cells

Transduced Vero cells were analysed for expression of the REDD1-Flag protein. **(A)** 1x 10^5 cells were fixed, permeabilized and blocked. The cells were stained with primary mouse anti-Flag antibody and secondary anti-mouse Alexa-488. Histograms depict total expression of REDD1-Flag in cells transduced once (1x) or twice (2x) **(B)** Immunofluorescence staining with primary mouse anti-Flag antibody and secondary anti-mouse Alexa-488 for REDD1-Flag protein in REDD1 (2x) cells (100 x magnification; size bar = 100 µm). **(C)** Lysates from transduced and control cells were separated on 10% SDS PAGE. Transferred proteins on nitrocellulose membranes were probed with anti-Flag and anti-GAPDH antibodies. (*Data (A) contributed by Sabine Kendle*.)

The REDD1 protein is a cytoplasmic protein. Therefore, subcellular localization of this protein was confirmed by immunofluorescence staining. The staining for REDD1-Flag protein showed a cytoplasmic distribution of fluorescence intensities **(Figure 4.3B)**. Also, the lysates of REDD1 expressing cells separated on a denaturing gel showed a band of ~ 24 kDa REDD1-Flag protein when probed with mouse anti-Flag antibody **(Figure 4.3C)**.

For the preparation of F6gW-KDELR2 expressing plasmids, the cDNA fragment encoding KDELR2-Myc-DKK tag was enzymatically cleaved using EcoRI and BamHI **(Figure 4.4A)**. This digestion resulted in a fragment of KDELR2-Flag insert of size 779bp **(Figure 4.4B)**. Similarly, F6gW-dsRed2 plasmid was also enzymatically cleaved using EcoRI and BamHI to remove the dsRed2 fragment and to generate a vector backbone of 9527 bp **(Figure 4.4B)**. The digested products of insert and vector were separated on a 1% agarose gel and purified using "QIA quick® Gel Extraction Kit".

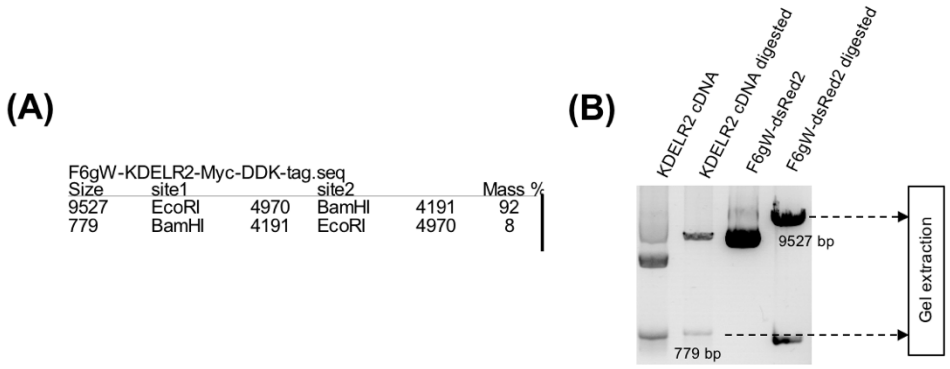

Figure 4.4: Preparation of KDELR2 cDNA insert and F6gW vector.
(A) Predicated size of F6gW backbone plasmid and KDELR2 insert using ApE1 software **(B)** EcoRI and BamHI digested KDELR2 cDNA clone and F6gW-dsRed2 plasmids were separated on 1% Agarose gel and then purified for subsequent use.

Dephosphorylated vector F6gW and KDELR2-Flag cDNA insert were ligated to generate circular transfer plasmids. XL10-Gold ultracompetent cells were transformed with plasmids. Bacterial colonies were selected by addition of marker antibiotic. Selected colonies were then used for Maxiprep plasmid isolation and the isolated F6gW-KDELR2-Flag plasmids were sequenced.

Cells stably expressing KDELR2 were prepared by transducing cells with F6gW-KDELR2-Flag Lentivirus particles. Transduced cells were then analysed for the expression of KDELR2-Flag. FACS analysis of KDELR2-Flag protein using mouse anti-Flag antibody showed 97.4% Flag positive cells in the FACS dot-plot. Also, the sharp peak in the histogram indicated a uniform expression of KDELR2

in Vero cells **(Figure 4.5A)**. In western blot analysis, the KDELR2-Flag protein migrated as ~ 25 kDa **(Figure 4.5B)**. As reported earlier in literature, Vero-KDELR2 cells showed a strong expression of KDELR2-Flag in the ER **(Figure 4.5C)**.

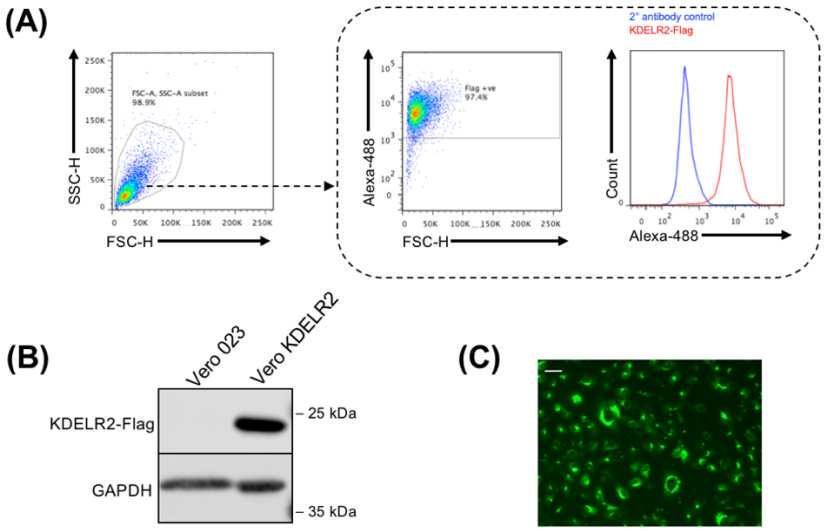

Figure 4.5: Overexpression of KDELR2 in Vero cell-line
Transduced Vero cells were analysed for expression of KDELR2-Flag protein. **(A)** 1x 10^5 cells were fixed, permeabilized and blocked. The cells were stained with primary mouse anti-Flag antibody and secondary anti-mouse Alexa-488. The dot plots indicate % Flag positive cells and Histograms depicts a uniform expression of KDELR2-Flag in the population **(B)** Lysates from transduced and control cells were separated on 10% SDS PAGE. Transferred proteins on nitrocellulose membranes were probed with anti-Flag and anti-GAPDH antibodies. **(C)** Immunofluorescence staining with primary mouse anti-Flag antibody and secondary anti-mouse Alexa 488 for KDELR2-Flag protein showed characteristic localization of KDELR2-Flag protein in ER-Golgi area around the nucleus (100 x magnification; size bar = 100 µm).

4.2.2. Effect of overexpression of *A3G, REDD1* and *KDELR2* on Vero cell proliferation

It is known that; cell proliferation influences the replication of viruses in tissue culture. Therefore, it was important to determine the effect of overexpression of *A3G, REDD1* and *KDELR2 on* the cell proliferation before evaluating its role on viral replication. To quantify cell proliferation, the cell lines were stained with the cell proliferation dye eFluor™ 670. This dye binds to cellular proteins containing primary amines. Upon cell division, this dye is equally distributed in progeny cells resulting in decreased fluorescent intensity. Serum-starved cells were stained with eFluor and incubated in MEM containing 5% FCS. Cells were then fixed and analysed after 24, 48 and 72 hrs. The decrease in fluorescent intensities at the different time point as cells divided are shown in

histograms **(Figure 4.6A)**. The percentages of proliferated cells were calculated for each cell line. As compared to control cells, Vero-A3G cells (blue line) showed decreased proliferation up to 70% after 24 hrs **(Figure 4.6B)**. Whereas 80% of REDD1 expressing cells (green line) proliferated, the proliferation rate of Vero-KDELR2 cells (red line) was almost equal to control cells. At later time points, the decrease in the efluor signal was almost equal in all cell lines. **(Figure 4.6B)** indicating no significant impact on the proliferative capacity of Vero cells after the stable transgene expression.

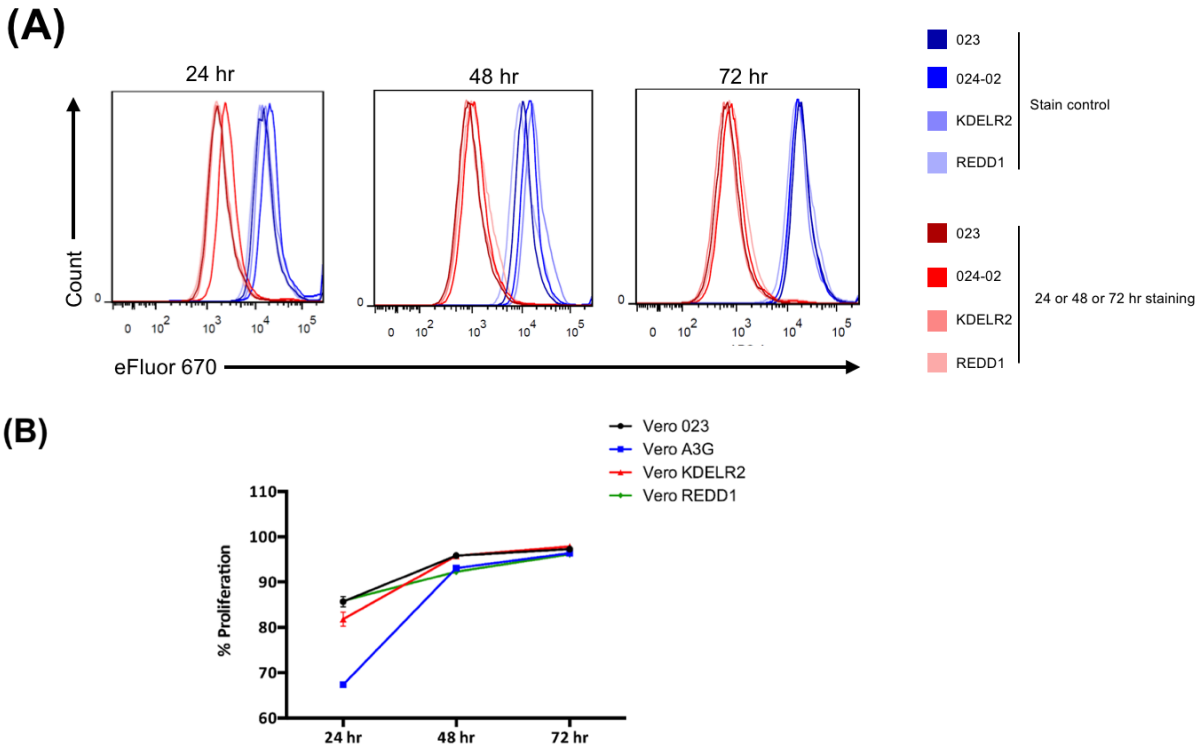

Figure 4.6: Vero cell proliferation after overexpression of A3G, KDELR2 and REDD1.
Individual cell division capacity in transduced Vero cell-line was compared by staining cells with eFluor670. The eFluor670 signal decrease upon cell division **(A)** Cells (3 x 10^5 Cells) stained with eFluor670 were collected at the different time point and analysed by FACS. The histograms show decreased efluor670 intensities as cells divided. **(B)** % proliferation in all transduced Vero cell. Data are shown as mean ± SEM of three independent experiments.

4.2.3. Stable expression of KDELR2 shRNAs in Vero cells

Breakthrough discovery of RNA interference (RNAi) to study gene functions was successfully extrapolated for the introduction of shRNA into cells. Retroviral vectors allowed stable integration and long-term knockdown of the target gene. Using this method, we prepared Vero cells stably expressing KDELR2 shRNA

resulting in long-term knockdown of the gene. This helped us to verify the role of this gene in MV replication.

The target sequence of shRNA for knockdown of *KDELR2* was designed by BLOCK-iT™ RNAi Designer. The KDELR2 NCBI Reference Sequence: NM_006854.3 was used to design the shRNAs. Three best shRNA sequences were selected **(Table 2.5)** and double-stranded shRNA oligos were generated.

For the preparation of F6gW-KDELR2-shRNA expressing plasmids, the F6gW-dsRed2 plasmid was enzymatically cleaved using XhoI and KspAI (HpaI) **(Figure 4.7)**. This digestion resulted in the opening of shRNA cloning site. The digested product of F6gW-dsRed2 plasmids was separated on a 1% agarose gel and purified using "QIA quick® Gel Extraction Kit".

F6gW-DsRed.seq

Size	site1		site2		Mass %
10229	XhoI	2929	HpaI	2912	100
17	HpaI	2912	XhoI	2929	1

Figure 4.7: Predicated size of XhoI and HpaI digested F6gW-dsRed2 plasmid

The dephosphorylated vector F6gW-dsRed2 and the phosphorylated DNA fragments coding for KDELR2-shRNAs were ligated to generate circular transfer plasmids. Selected bacterial colonies were used for Maxiprep plasmid isolation and F6gW-dsRed2-KDELR2-shRNA plasmids were sequenced. Lentiviral particles containing the corresponding sequences as RNA-genomes were generated as described (3.1.8).

The cells stably expressing F6gW-DsRed2-KDELR2-shRNAs were prepared by transducing cells with the corresponding Lentivirus particles. Transduced cells were then FACS sorted based on the expression of DsRed2. The black dots in **(Figure 4.8A)** represent the population selected for sorting. FACS analysis of KDELR2-shRNA using DsRed2 expression showed 84-96% DsRed2 positive cells in FACS dot-plot **(Figure 4.8B)**. Microscopic observation of cells showed strong dsRed2 expression in KDELR2-shRNA2 expressing cells (**Figure 4.8C**). Silencing of the KDELR2 gene at mRNA level was confirmed by semi-quantitative PCR. Total cellular RNA was reverse transcribed, and cDNA was then amplified by conventional PCR **(Figure 4.8D)** and real-time qPCR **(Figure 4.8E)**. The KDELR2 expression in Vero-KDELR2 cells was used as a control. In all three shRNA expressing cells, the KDELR2 expression was significantly reduced.

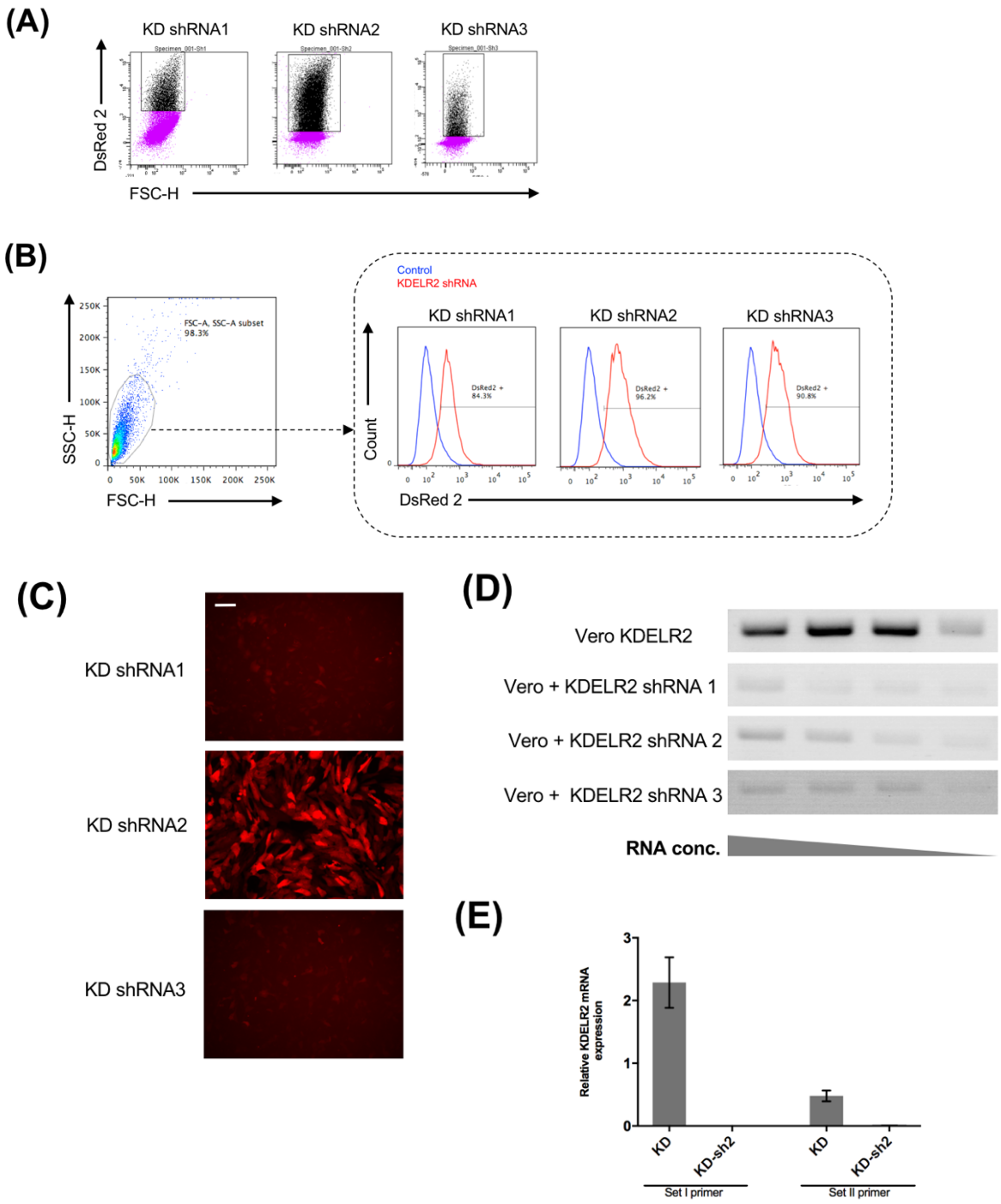

Figure 4.8: shRNA mediated knockdown of *KDELR2* in Vero cells.
Vero cells were transduced with three different shRNAs to knockdown the expression of *KDELR2*. **(A)** Transduced cells were FACS sorted based on the DsRed2 fluorescence. The dot-plots shows the population selected for sorting. **(B)** 1x 10^5 cells were fixed and analysed for dsRed2 expression by FACS. Histograms depict uniform expression of dsRed2 expression in the sorted population. **(C)** dsRed2 expression in sorted cells was analysed by microscopy (100 x magnification; size bar = 100 µm). **(D)** The shRNA mediated knockdown at mRNA level was confirmed by semi-quantitative PCR. Four concentrations of RNA (4, 2, 1, 0.5 µg) were reverse transcribed. The cDNA product was amplified by PCR and analysed on 1% Agarose gel. **(E)** The relative *KDELR2* mRNA levels in KDELR2 shRNA2 expressing Vero cells were quantified by SYBR-Green Real-Time qPCR using two different set of primers. (n=3).

4.3. Overexpression of *REDD1* and *KDELR2* in CEMSS T cells

4.3.1. Stable expression of REDD1-Flag and KDELR2-Flag in CEMSS T cell line

To demonstrate that the effects of *REDD1* and *KDELR2* are cell type independent, and because *in vivo* MV replicates in lymphocytes, CEMSS cells, a T lymphoblast cell line, were stably transduced to overexpress these genes.

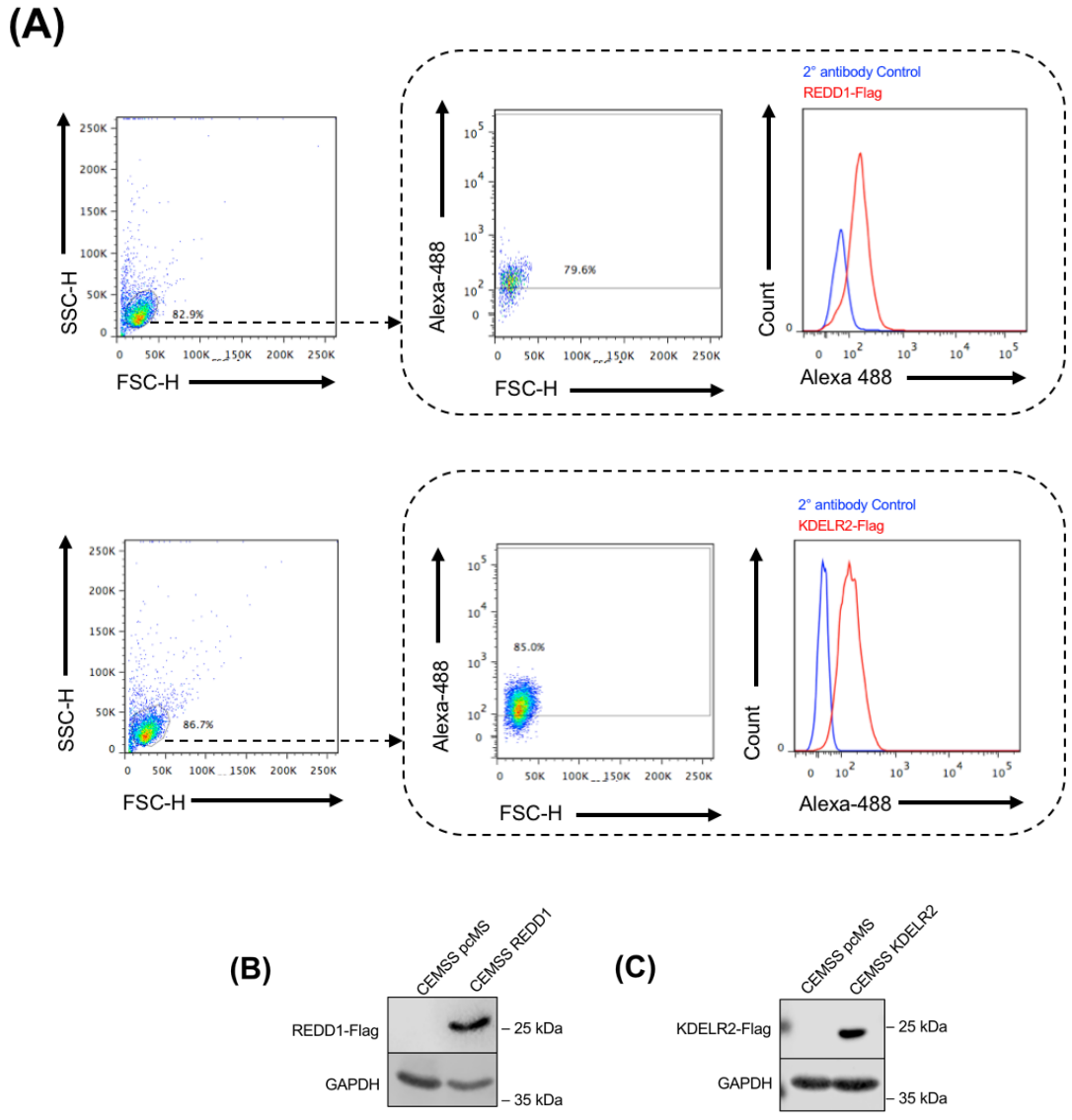

Figure 4.9: Overexpression of REDD1 and KDELR2 in CEMSS T cells.
Transduced CEMSS cells were analysed for the expression of REDD1-Flag and KDELR2-Flag proteins. 1x 10^5 cells were fixed, permeabilized and blocked. The cells were stained with primary mouse anti-Flag antibody and secondary anti-mouse Alexa-488. The dot-plots indicate % of Flag positive cells and Histograms depicts uniform expression of REDD1-Flag and KDELR2-Flag in the population **(A)** Upper panel: FACS analysis of CEMSS- REDD1 cells and Lower panel: FACS analysis of CEMSS-KDELR2 cells. **(B)** and **(C)** Transduced and control cells were separated on 10% SDS PAGE. Transferred proteins on nitrocellulose membranes were probed with anti-Flag and anti-GAPDH antibodies. Flag expression in CEMSS-REDD1 cells (B) and Flag expression in CEMSS-KDELR2 cells (C).

REDD1 and *KDELR2* expressing lentiviral plasmids were prepared as described **(4.2.1).** CEM-SS pcMS cells stably expressing *REDD1* and *KDELR2* were prepared by transducing these cells with respective lentivirus particles. Transduced cells were then analysed for the expression of REDD1-Flag and KDELR2-Flag. FACS analysis of REDD1-Flag and KDELR2-Flag protein using mouse anti-Flag antibody showed 79% (upper panel) and 85% (lower panel) Flag positive cells in FACS dot-plot **(Figure 4.9A)**. Also, the sharp peak in the histogram indicated uniform expression in cells. Western blot analysis confirmed REDD1-Flag **(Figure 4.9B)** and KDELR2-Flag **(Figure 4.9C)** expression as the Flag-tagged protein migrated as ~ 25 kDa band.

4.3.2. Effect of overexpression of *A3G, REDD1* and *KDELR2* on CEM-SS cell proliferation

The effect of overexpression of *REDD1* and *KDELR2* on CEM-SS cells was evaluated by staining cells with cell proliferation dye eFluor™ 670 (similar to **7.2.2**). As shown in **(Figure 4.10A)** serum-starved cells were stained with eFluor, fixed and analysed after 24, 48 and 72 hrs same as above **(4.2.2)**. The histograms show decreased fluorescent intensities at the different time points as the cells divided. The decrease in the efluor signal was almost equal in all cell lines. The percentages of proliferated cells were calculated for each cell line **(Figure 4.10B)**. CEM-pcMS (empty vector control), CEM-A3G, CEM-REDD1 and CEM-KDELR2 overexpressing cells proliferated equally after 48 and 72 hrs of incubation indicating no significant effect on the proliferative capacity of CEM-SS cells after the transgene expression.

(A)

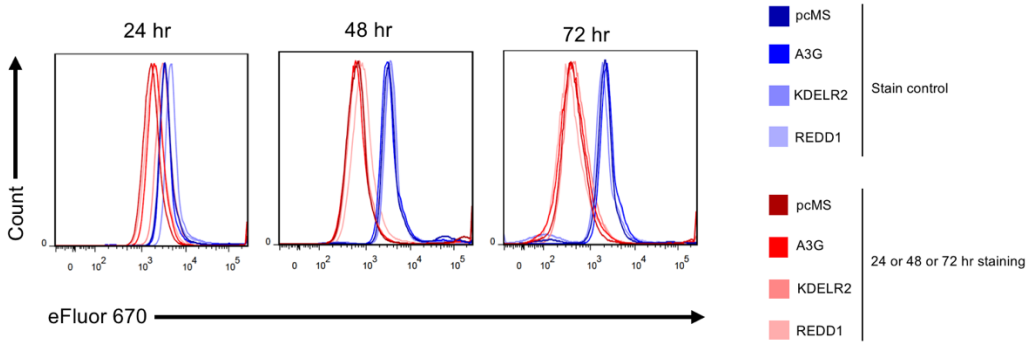

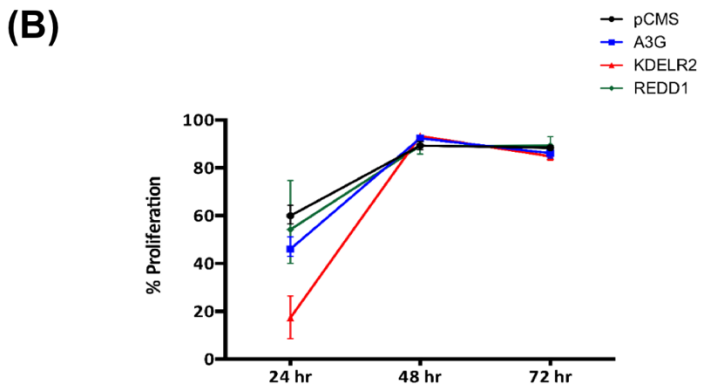

Figure 4.10. CEMSS T cell proliferation after over-expression of A3G, KDELR2 and REDD1
Individual cell division capacity in transduced CEMSS cell-line was compared by staining cells with eFluor670. The eFluor670 signal decreased upon cell division **(A)** Cells (3 x 10^5 Cells) stained with eFluor670 were collected at the different time point and analysed by FACS. The histograms show decreased efluor670 intensities as cells divided. The decrease in the signal was almost equal in all the cells. **(B)** % proliferation in all transduced CEMSS cell lines. Data are shown as mean ± SEM of three independent experiments.

4.4. REDD1 expression inhibited MV infection as efficiently as A3G in Vero cells

REDD1 protein, a negative regulator of mTORC1, has been shown to affect replication of Influenza and VSV [223]. As a next step, the antiviral activity of REDD1 on MV laboratory-adapted strain of rMV^{Edtag}eGFP was evaluated **(Figure 4.11A)**. The cells transduced with empty vector (Vero-023) served as control cells (negative-control) and Vero-A3G cells were used as a positive-control in subsequent experiments.

The viral syncytia were observed daily under the fluorescent microscope and the 48 hr post-infection (hpi) time point was selected as the maximum infection rate was attained at this time point in control cells. The apparent size of GFP positive syncytia in Vero REDD1 was significantly reduced as compared to control Vero-023 cells. Indeed, the size of syncytia was similar to that observed in Vero-A3G cells **(Figure 4.11B).** The total virus synthesised in the cells was collected by scraping the cells 48 hr post-infection and the titre was determined on Vero cells. The virus titre was reduced by 90% in Vero-REDD1 cells, whereas the reduction was more than 95% in Vero-A3G. These findings demonstrated that the individual expression of REDD1 efficiently inhibited MV in Vero cells.

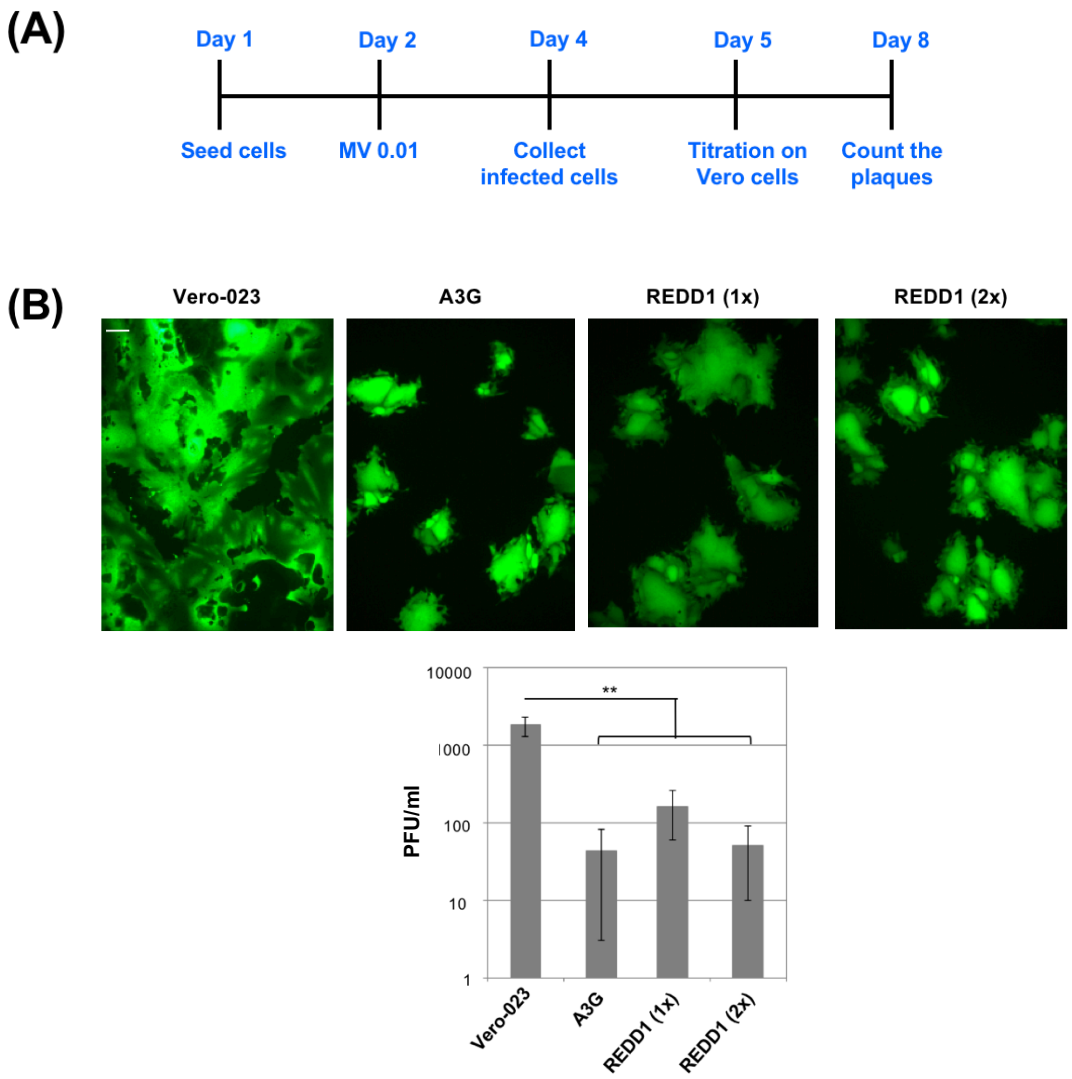

Figure 4.11: REDD1 expression reduced MV titre in Vero cells
Transduced Vero cells were infected with rMV ^{Edtag} eGFP with MOI of 0.1. **(A)** Scheme of infection and titration **(B)** Representative micrographs of eGFP expressing syncytium formation in control and transduced cells were taken 48 hpi (100 x magnification; size bar = 100 µm) **(C)** Titre of newly synthesized virus from transduced cells was determined 48 hrs post infection on Vero cells. Each titration was done in triplicate and data are shown as mean ± SEM of three independent experiments. ** p<0.01 (Unpaired Student's t-test). Data contributed by Sabine Kendle.

4.5. KDELR2 expression reduced MV infection in Vero cells

KDELR2 is ER-Golgi resident cargo receptor with known function in retrograde and anterograde transport of protein in ER and Golgi. Recent evidence suggested a crucial role of this protein in viral egress. We assessed the antiviral activity of this protein on MV laboratory-adapted strain rMV^{Edtag}eGFP using a similar experimental strategy as mentioned in **4.4**. Vero-023 cells served as empty vector control and Vero-A3G cells used as a positive control. MV induced syncytium formation was significantly reduced in KDELR2 overexpressing cells, however, not as efficient as seen with REDD1 **(Figure 4.12A: upper panel).** The total virus

synthesised in the cells was collected by scraping cells 48 hrs post infection and the titre was determined on Vero cells. The virus titre was reduced by 85% in Vero-KDELR2 cells **(Figure 4.12B)**. To validate the role of KDELR2 in MV replication, KDELR2 was knocked down in Vero cells using shRNA mediated silencing. We therefore, tested MV-induced syncytium formation in KDELR2 knock-down cells using three different shRNAs. Interestingly, all three KDELR2 knock-down cell significantly increased MV syncytium formation **(Figure 4.12A: lower panel)** and restored the virus titre equal to control cells **(Figure 4.12B)**. These experiments indicated that individual expression of KDELR2 restricted MV replication in Vero cells.

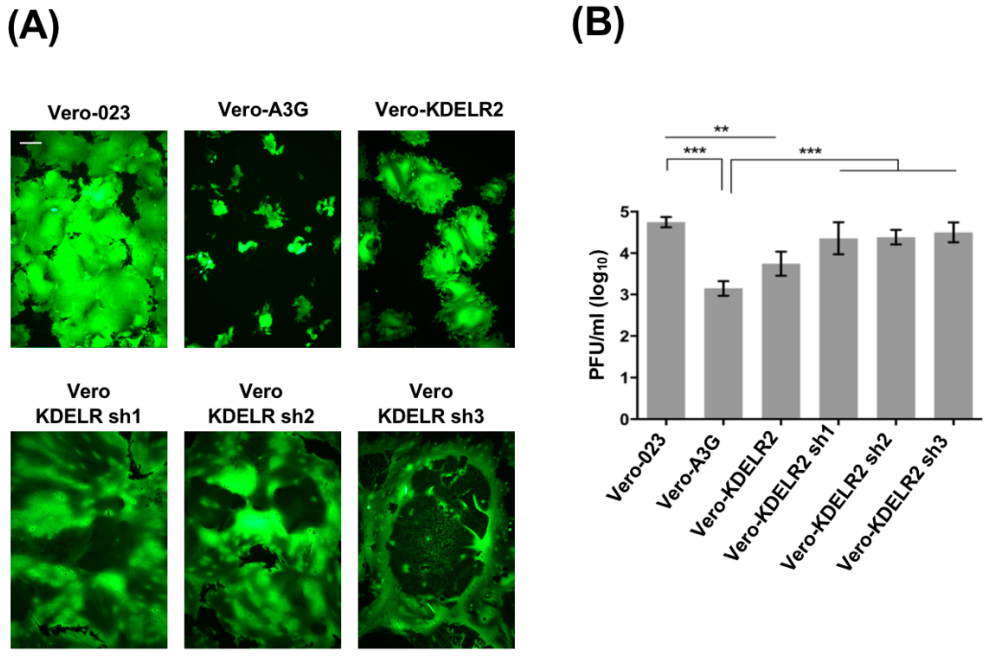

Figure 4.12: KDELR2 expression reduced MV titre in Vero cells.
KDELR2 overexpressing and KDELR2 knockdown Vero cells (3 x 10^5 cells) were infected with rMV ^{Edtag} eGFP with MOI of 0.1 **(A)** Representative micrographs of eGFP expressing syncytium formation in control and transduced cells were taken 48 hpi (100 x magnification; size bar = 100 µm) **(B)** Titre of newly synthesized virus from transduced cells was determined 48 hrs post infection on Vero cells. Data shows mean value ± SEM of three independent experiments and statistical significance was calculated by Unpaired Student's *t*-test (*p< 0.05, **p < 0.01, ***p<0.001).

4.6. REDD1 and KDELR2 reduced MV titre in CEMSS T cells

The MV restriction by REDD1 and KDELR2 so far was tested in Vero cells. Vero cells are kidney epithelial cells of primate origin and deficient in mounting interferon response. Because naturally MV replicates in human lymphocytes, we assessed the ability of REDD1 and KDELR2 mediated MV inhibition in the human T cell line CEM-SS. CEM-SS are human lymphosarcoma T cells that are highly

permissive to HIV-1 infection. CEM-SS A3G and CEM-SS pcMS (empty vector control) cells were a kind gift from Prof. Michael Malim (Kings College London).

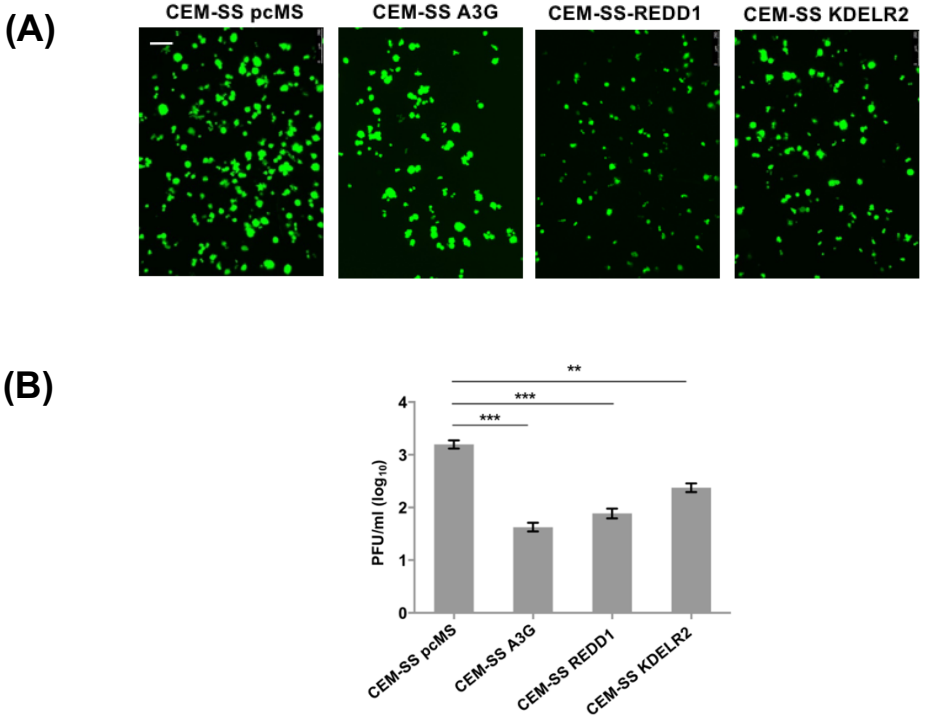

Figure 4.13: REDD1 and KDELR2 expression reduced MV titre in CEMSS T cells.
REDD1 and KDELR2 overexpressing CEMSS cells (2 x 10^5 cells) were infected with rMV ^{Edtag} eGFP with MOI of 0.1 **(A)** Representative micrographs of eGFP expressing syncytium formation in control and transduced cells were taken 48 hpi (100x magnification; size bar = 100 µm) **(B)** Titre of newly synthesized virus from transduced cells was determined 48 hpi on Vero cells. Histograms shows mean value ± SEM of three independent experiments and statistical significance was calculated by unpaired Student's *t*-test (*p<0.05, **p<0.01, ***p<0.001).

Viral syncytium formation was significantly reduced in A3G expressing cells as demonstrated earlier [192]. The total virus synthesised in these cells was titrated on Vero cells 48 hr post infection. Interestingly, REDD1 and KDELR2 expressing cells also reduced viral syncytium formation in CEMSS cells **(Figure 4.13A).** The virus titre was reduced by 95% in CEM-SS REDD1 cells and by 84% in CEM-SS KDELR2 cells **(Figure 4.13B)**.

4.7. Silencing of REDD1 and KDELR2 in A3G expressing cells abrogated the antiviral effect exerted by A3G

As demonstrated above **(Figure 4.11-13)** the individual expression of REDD1 and KDELR2 significantly affected MV replication independent of cell type. As a next step, it was important to confirm the role of REDD1 and KDELR2 in A3G mediated inhibition of MV replication. Therefore, we depleted these two factors

individually or together in Vero cells using shRNAs. Vero cells stably expressing A3G were transduced using lentiviruses expressing shRNAs targeting REDD1 and/or KDELR2 and FACS sorted based on dsRed2 expression **(Figure 4.14A).**

FACS analysis of dsRed2 expression showed 99%, 70% and 92% dsRed2 positive cells in Vero A3G-shREDD1, Vero A3G-shKDELR2 and Vero A3G-shREDD1+shKDELR2 respectively **(Figure 4.14B).** All three cell lines showed a strong dsRed2 expression microscopically **(Figure 4.14C).** Silencing of the respective gene was confirmed by western blotting. Cell lysates were separated on SDS-PAGE and probed with respective antibodies. REDD1 and KDELR2 were not detected in the cells transduced with respective shRNAs **(Figure 4.14D)**.

(A)

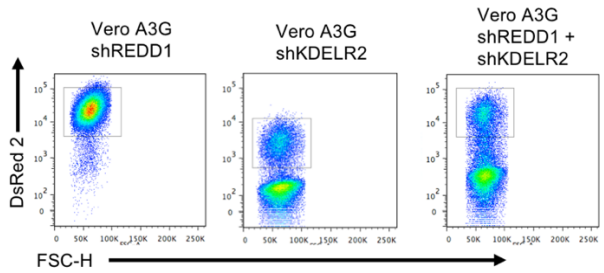

(B)

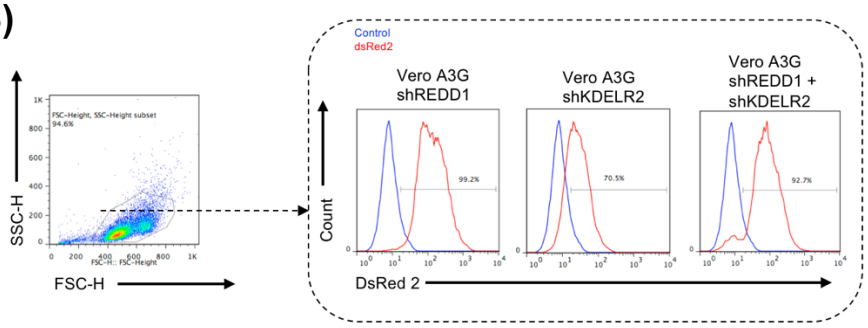

(C)

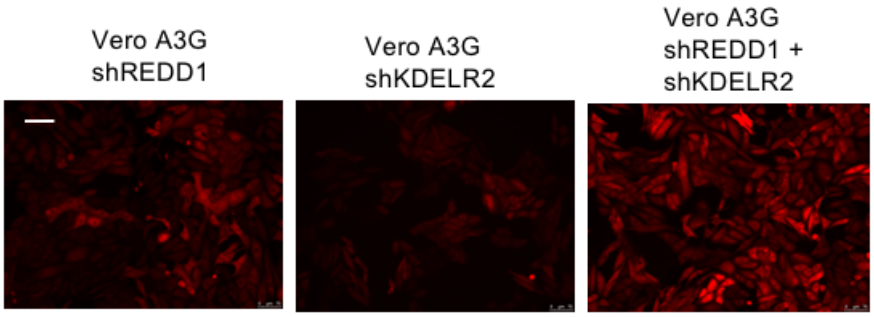

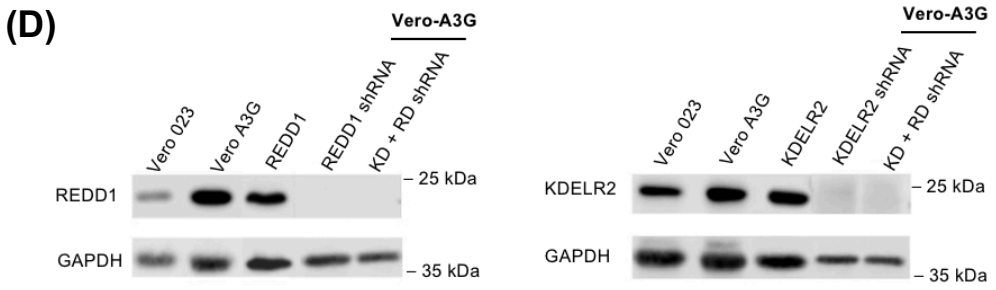

Figure 4.14: Silencing of REDD1 and KDELR2 in A3G expressing Vero cells.
Vero A3G expressing cells were transduced with shRNAs to knockdown the expression of REDD1 and/or KDELR2. **(A)** Transduced cells were FACS sorted based on the dsRed2 fluorescence. The dot-plots shows the population selected for sorting. **(B)** 1x 10^5 cells were fixed and analysed for dsRed2 expression by FACS. Histograms depict a uniform expression of dsRed2 expression in the sorted population. **(C)** dsRed2 expression in sorted cells was analysed by microscopy (100 x magnification; size bar = 100 µm). **(D)** Protein expression in cells was analysed by western blot. 20 µg lysates of Vero-023, Vero-A3G, Vero-REDD1, Vero-KDELR2, REDD1 and/or KDELR2 shRNA transduced Vero A3G cells were separated on 10% SDS PAGE. Transferred proteins on nitrocellulose membrane Were probed with respective primary and HRP antibodies, followed by visualization with ECL.

Now, Vero-A3G cells in which REDD1 and KDELR2 expression were knocked down were used to assess the effects on replication of rMV^{Edtag}eGFP. Vero-023 cells transduced with scrambled shRNA were used as a control. MV induced syncytium formation in knock-down cells was comparable to that in Vero-023 and 023 scrambled shRNA expressing cells **(Figure 4.15A).** The silencing of REDD1 and/or KDELR2 significantly increased the viral titres as compared to parental Vero A3G cells abrogating the antiviral effect exerted by A3G **(Figure 4.15B).**

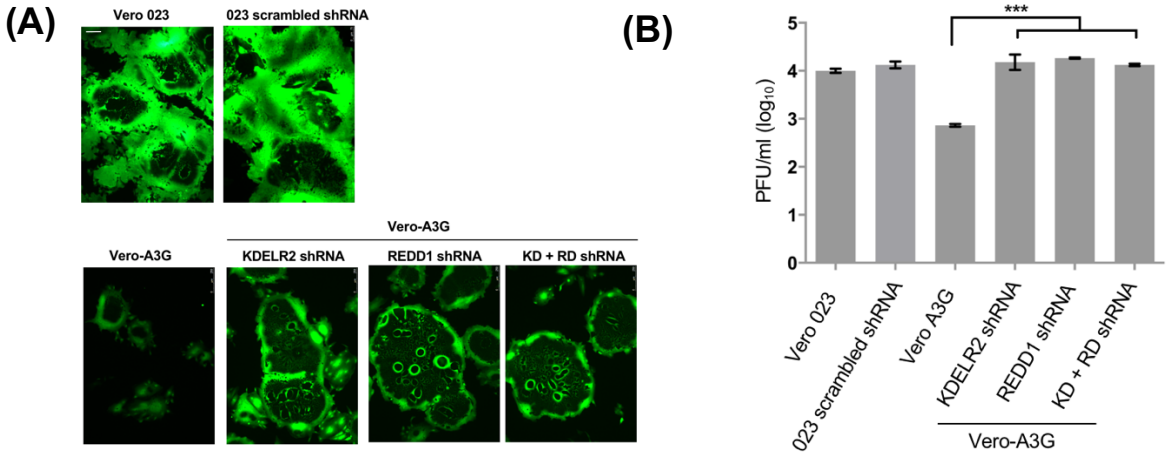

Figure 4.15: Silencing of KDELR2 and REDD1 in A3G expressing Vero cells abrogated the antiviral effect exerted by A3G
REDD1 and KDELR2 were knocked down by shRNA mediated gene silencing in A3G expressing Vero cells. **(A)** 3 x 10^5 cells were infected with rMV ^{Edtag} eGFP with MOI of 0.1. Representative micrographs of eGFP expressing syncytium formation in control and transduced cells were taken 48 hpi (100 x magnification; size bar = 100 µm) **(B)** Titre of newly synthesized virus from infected cells were determined 48 hrs post infection on Vero cells. Histograms shows mean value ± SEM of three independent experiments and statistical significance was calculated by Unpaired Student's *t*-test (*p< 0.05, **p < 0.01, ***p<0.001).

4.8. REDD1 exerts antiviral effect via inhibition of mTORC1

4.8.1. Viability of cells upon Rapamycin treatment

REDD1 is a stress response protein and plays a vital role in the regulation of mammalian target of rapamycin complex 1 (mTORC1) signalling. Therefore, we investigated if REDD1 mediated inhibition of mTORC1 is responsible for the antiviral effect, and if the same effect can be achieved by the known inhibitor of mTORC1, rapamycin. To test this hypothesis, we first determined the range of rapamycin concentration in Vero and CEM-SS cells which does not result in cytotoxicity. As described in the literature [254][255], we tested 0.1 to 2µM of rapamycin concentrations.

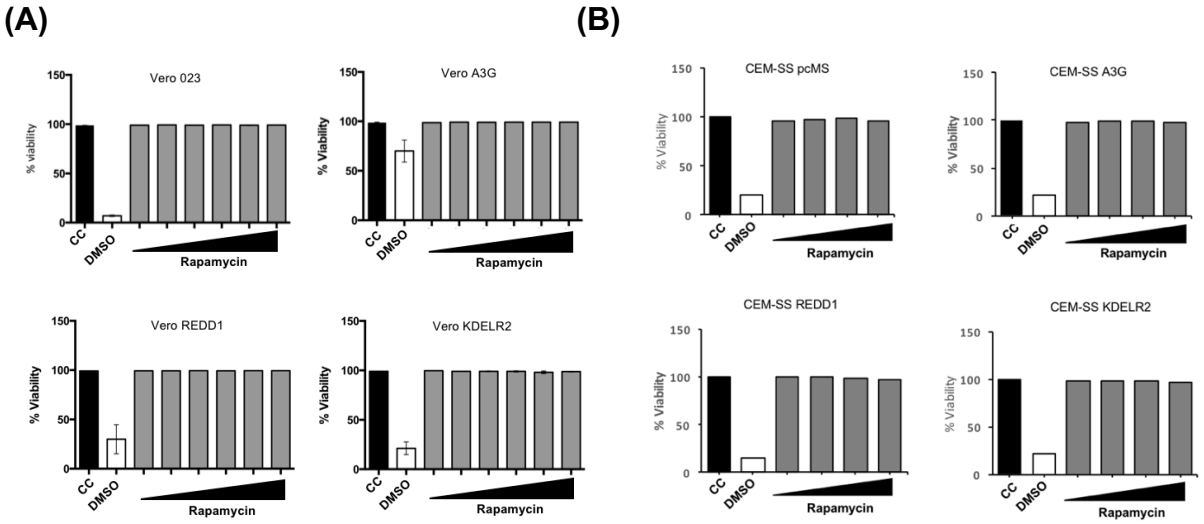

Figure 4.16: Viability of Vero and CEMSS cell line upon Rapamycin Treatment
Control, A3G, KDELR2 and REDD1 expressing cells (3 x 10^5 cells) were treated with different concentrations of Rapamycin and 48 hrs later cell viability was determined by staining cells with Propidium iodide. **(A)** Vero cells were treated with increasing concentration of Rapamycin (100, 200, 400, 800, 1000, 2000 nm). % Viability in the control group was set to 100% and relative viability was determined in treated groups. Histograms shows mean value ± SEM of three independent experiments. **(B)** CEMSS cells (1 x 10^6 cells) were treated with increasing concentration of Rapamycin (100, 200, 500, 1000 nm). Viability in the control group was set to 100% and relative viability was determined in treated groups.

Vero 023, A3G, REDD1 and KDELR2 overexpressing cells were treated with an increasing concentration of rapamycin for 48 hrs and the % of living cells was calculated by staining cells with propidium iodide. The viability of control, overexpressing Vero **(Figure 4.16A)** and CEM-SS cell lines **(Figure 4.16B)** was found to be not affected upon rapamycin treatment for all concentration we tested.

4.8.2. Pharmacological inhibition of mTORC1 by Rapamycin reduced replication of the laboratory-adapted MV strain in both Vero cells and CEM-SS cells

After determination of the suitable concentration of rapamycin for our experiments, we tested if the observed REDD1 effect was mediated by inhibition of mTOR1 signalling. Vero-023, Vero-KDELR2 and Vero-REDD1 expressing cells were infected with rMV^{Edtag}eGFP and treated with increasing concentrations of Rapamycin throughout the incubation period. Rapamycin treatment showed a dose-dependent decrease in MV syncytium formation in Vero-023, Vero-KDELR2 and Vero-REDD1 cells. No increased (or additive) effect on the syncytium formation was seen in Vero-REDD1 cells after rapamycin treatment **(Figure 4.17A)**. Similarly, rapamycin exerted a significant dose-dependent decrease of virus titres in Vero-023 and Vero-KDELR2 cells, but not in Vero-REDD1 cells **(Figure 4.17B)**.

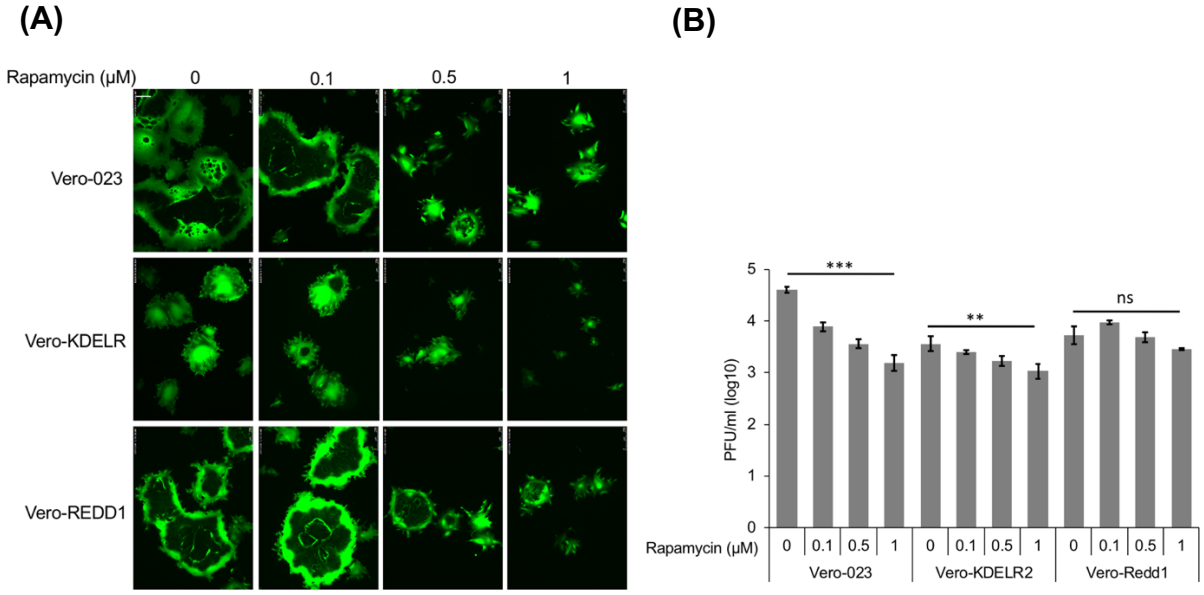

Figure 4.17: Rapamycin treatment significantly reduced MV replication in Vero cells
Control, KDELR2 and REDD1 expressing Vero cells (3 x 10^5 cells) were infected with rMV ^{Edtag} eGFP with MOI of 0.1 for two hrs and then treated with Rapamycin (0, 0.1, 0.5, 1 μM) for 48 hrs. **(A)** Representative micrographs of eGFP expressing syncytium formation in control and Rapamycin treated cells were taken 48 hpi (100x magnification; size bar = 100 μm) **(B)** Titre of newly synthesized virus from infected cells were determined 48 hrs post infection on Vero cells. Data shows mean value ± SEM of three independent experiments and statistical significance was calculated for each cell line by one-way ANOVA test (n.s – non-significant, **p < 0.01, ***p<0.001).

We also performed a similar experiment in CEM-SS cells. Control CEMSS pcMS cells, CEMSS KDELR2, and CEMSS REDD1 expressing cells were infected with rMV^{Edtag}eGFP and then treated with rapamycin. Interestingly, CEMSS-pcMS and CEMSS-KDELR2 cells did not show a rapamycin dose-dependent decrease in virus-induced syncytium formation **(Figure 4.18A)** and in virus titre **(Figure**

4.18B), whereas CEM-SS-REDD1 cells showed dose-dependent decrease in syncytium formation and virus titre.

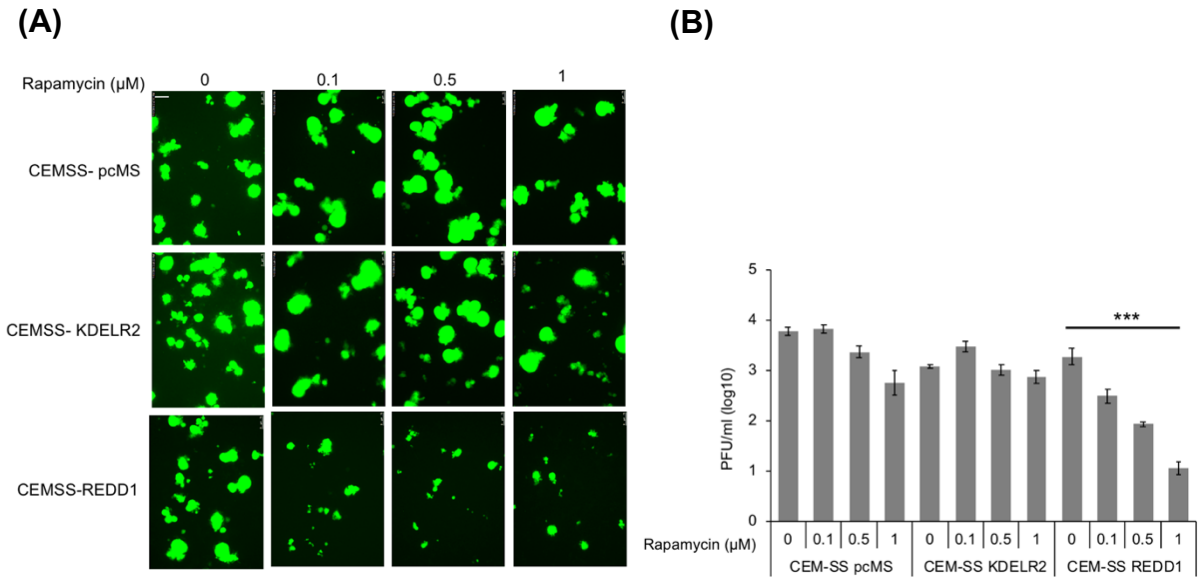

Figure 4.18: Syncytium formation and viral titres in rapamycin-treated CEM-SS cells
Control, KDELR2 and REDD1 expressing cells (3 x 10^5 cells) were infected with rMV ^{Edtag} eGFP with MOI of 0.1 for two hrs and then treated with Rapamycin (0, 0.1, 0.5, 1 μM) for 48 hrs. **(A)** Representative micrographs of eGFP expressing syncytium formation in control and Rapamycin treated cells were taken 48 hpi (100 x magnification; size bar = 100 μm) **(B)** Titre of newly synthesized virus from infected CEMSS cells were determined 48 hrs post infection on Vero cells. Data shows mean value ± SEM of three independent experiments and statistical significance was calculated for each cell line by one-way ANOVA test (***p<0.001).

4.8.3. REDD1 expressing cells showed decreased p70S6K phosphorylation

To further assess the effect on mTORC1 signalling, we decided to quantify the phosphorylation levels of the ribosomal protein S6 kinase 1 (S6K1). mTORC1 signalling regulates mRNA translation via phosphorylation of S6K1. The phosphorylation activates it and leads to the phosphorylation of various substrates involved in cellular translation. S6K1 phosphorylation sites have been shown to be highly sensitive to rapamycin [256]. Therefore, we quantified and compared phospho-P70S6K1 levels in the presence and absence of rapamycin. Vero-023, Vero-A3G, VERO-KDELR2 and VERO-REDD1 cells were treated with 1μM rapamycin, or with 0.1% DMSO or serum starved and then treated with EGF as a positive control. P70S6K phosphorylation at Thr^{389} position was then detected by western blotting **(Figure 4.19A)**.

Indeed, untreated A3G and REDD1 expressing Vero cells showed a significant decrease in phosphorylation of p70S6K by 50% and 80%, respectively, and rapamycin treatment reduced these levels significantly. Interestingly,

untreated KDELR2 expressing cells did not show any significant impact on the levels of phospho-p70S6K. **(Figure 4.19B)**, whereas rapamycin further reduced the levels of phospho-p70S6K to undetectable levels in Vero-KDELR2 cells. In REDD1 expressing cells, rapamycin reduced the phosphorylation of p70S6K also to undetectable levels, however, the difference to untreated REDD1 cells was not significant indicating that both act in the same pathway **(Figure 4.19B)**. These results showed that the ectopic expression of A3G and REDD1 resulted in a substantial decrease in mTORC1 signalling.

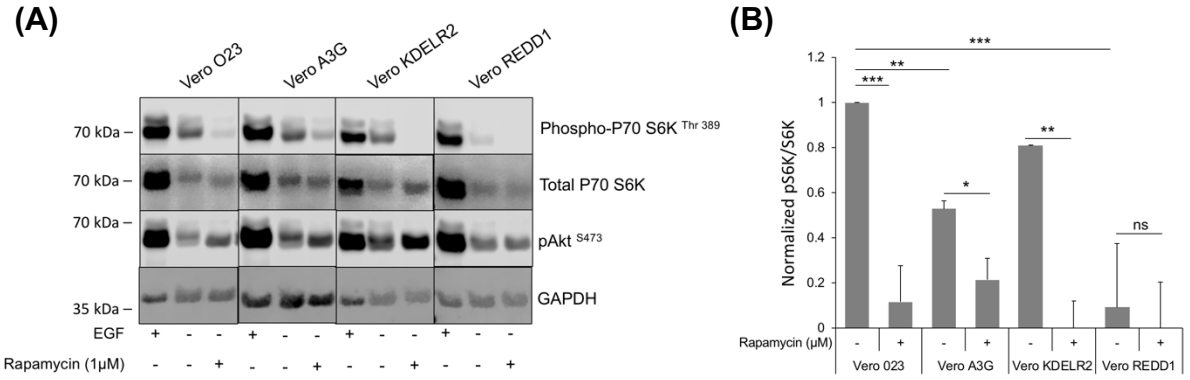

Figure 4.19: REDD1 and A3G expressing Vero cells showed decreased p70S6K phosphorylation
Control, A3G, KDELR2 and REDD1 expressing Vero cells (3 x 10^5 cells) were treated with 1μM of Rapamycin or 0.01% DMSO for 24hrs. For positive control, cells were serum starved overnight and then treated with 50ng/ml of EGF for 15 minutes. Cells were directly lysed in the 2X lammeli buffer. Transferred proteins on nitrocellulose membrane were probed with respective primary and HRP conjugated antibodies, followed by visualization with ECL. **(A)** Representative NC membrane from Immunoblot analysis against the depicted proteins **(B)** Total S6K and p70S6K levels in each lane were normalized with GAPDH loading control in the same lane. Ratio of normalized p70S6K and Total S6K were used for analysis. Data shows mean value ± SEM of densitometric analysis of three independent experiments and statistical significance was calculated by Unpaired Student's *t*-test (*p< 0.05, **p < 0.01, ***p<0.001, ns: not significant).

4.8.4. A3G, REDD1 and KDELR2 were found to be increased in stimulated human Peripheral blood lymphocytes

A3G and REDD1 levels have been studied independently in stimulated PBL [164][257], however, there is no evidence about the levels of KDELR2 in stimulated PBL. Therefore, we determined A3G, REDD1 and KDELR2 protein levels in unstimulated and stimulated PBL. Freshly isolated human PBL were stimulated with 2.5 μg/ml of PHA or with 25 ng/ml of human IL-2. 48 hrs after stimulation protein levels were determined by western blotting.

Upon stimulation with PHA and IL-2, A3G levels were increased by 2-3 folds. However, due to the high variation between each individual donor the

increase was not statistically significant. Interestingly levels of REDD1 and KDELR2 were also found to be simultaneously increased in stimulated PBL **(Figure 4.20A)**. Next, we compared levels of A3G in stimulated PBL to Vero-A3G cells. Since stimulation with IL-2 resulted in higher A3G expression, we used IL-2 stimulated cells as a control. We found comparable levels of A3G in Vero cells ectopically expressing A3G to that of IL-2 stimulated PBL **(Figure 4.20B)**. Thus, the A3G over-expression in Vero A3G cells was found to be within in the range of physiological conditions and therefore, ruling out the possibility that massive overexpression would have contributed to the MV restriction.

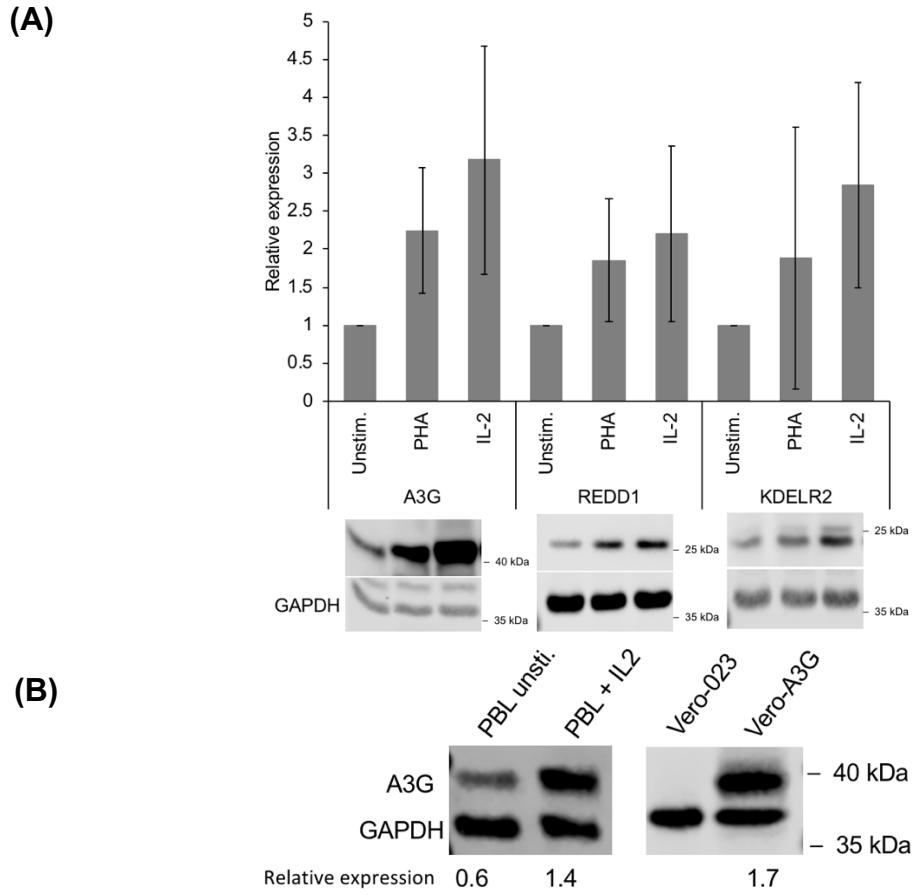

Figure 4.20: A3G, REDD1 and KDELR2 levels were increased in stimulated PBL
(A) 1 x 10^6 primary human PBL were stimulated with 2.5 µg/ml of PHA or 25 ng/ml of human IL-2 for 48 hrs. cells were lysed and separated on 10% SDS PAGE. Transferred proteins were probed with respective primary and HRP labelled secondary antibodies, followed by visualization with ECL. Levels of A3G, REDD1 and KDELR2 in each lane were normalized with GAPDH loading control in the same lane. Ratio of relative protein expression normalised to the values of unstimulated PBL were used for quantification. Data shows mean value ± SEM of densitometric analysis of three donors (above). Representative NC membrane from Immunoblot analysis against the depicted proteins (below) **(B)** Comparison of A3G expression in primary human PBL (left panel) and Vero-A3G cells (right panel).

4.8.5. Rapamycin treatment inhibited replication of wildtype MV strain in activated PBL

The rapamycin treatment of Vero cells resulted in a reduced titre of the laboratory-adapted MV strain as well as reduced downstream signalling events in Vero cells **(Figure 4.17 and 4.19)**. This finding led to the important question of whether pharmacological inhibition of mTORC1 activity by rapamycin would inhibit the replication of wildtype MV in primary human PBL. For this study, we used PHA stimulated human PBL and infected them with wildtype rMV^{IC323}eGFP. These MV-infected cells were then further incubated without and with rapamycin throughout the incubation period.

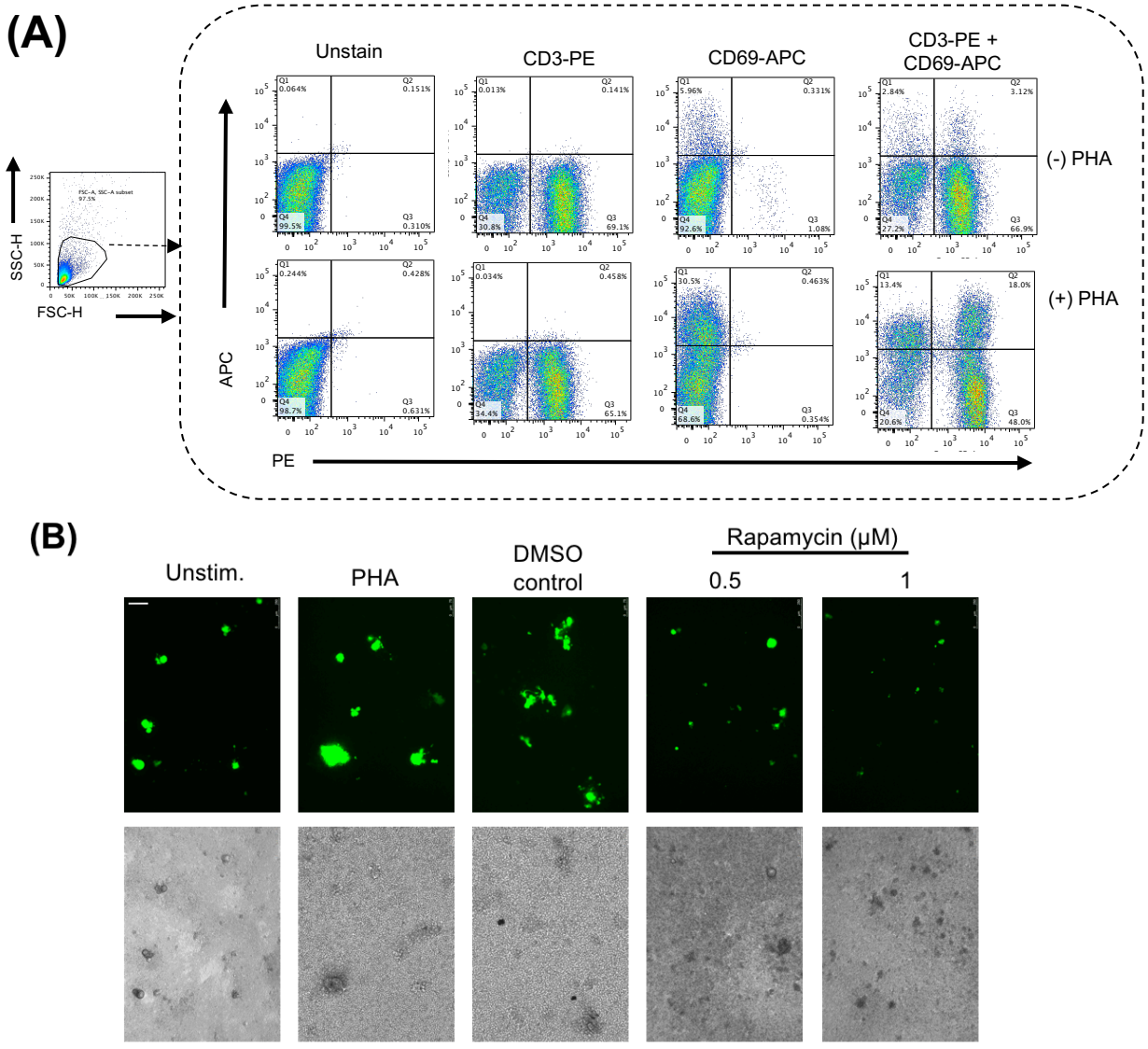

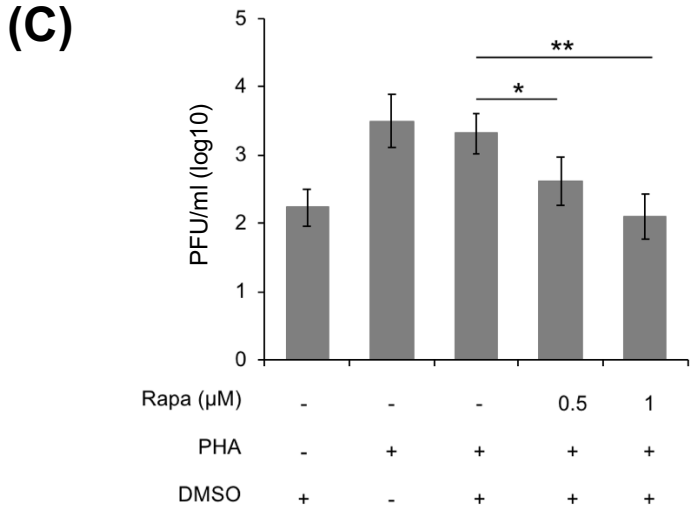

Figure 4.21: Pharmacological inhibition of mTORC1 reduced wildtype MV titres in stimulated human PBL. 1 x 10^6 unstimulated and 24 hr. stimulated PBL were infected with MV^{IC323}eGFP with MOI of 0.1 for two hours and then treated with Rapamycin (0.5, 1 μM) for 48 hrs. **(A)** stimulation of PBL was controlled by detecting the expression of stimulation marker CD69 by FACS. 1x 10^5 cells were stained with CD3-PE and /or CD69-APC. The representative dot plots indicate % CD3 and or CD69 positive cells **(B)** Representative micrographs of eGFP expressing syncytium formation in control and Rapamycin treated cells were taken 48 hpi (100 x magnification; size bar = 100 μm) **(C)** Titre of newly synthesized virus from infected PBL were determined 48 hrs post infection on Vero hSLAM cells. Data shows mean value ± SEM of three donors and statistical significance was by one-way ANOVA test (**p < 0.01).

The stimulation of the PBL of each donor was controlled by staining of the early activation marker CD69 before infection **(Figure 4.21A)**. As shown in **Figure 4.21B** inhibition of mTOCRC1 by rapamycin reduced the virus-induced syncytium formation significantly. Similarly, the titre of newly synthesised virus was reduced by 1 log **(Figure 4.21C)**.

Taken together, findings in Figure 17,19 and 21 demonstrate that mTORC1 activity plays an important role in enhancing MV replication not only in Vero cells but also in human PBL.

4.8.6. Antiviral role of A3G on MV replication in primary human PBL

As described, we found a simultaneous increase of the A3G and REDD1 expression upon stimulation of human PBL **(Figure 4.20)**. Now, we aimed to investigate the possible role of A3G in MV replication in stimulated PBL by siRNA mediated depletion of A3G. PBL were nucleofected with A3G targeted or with non-targeted siRNA. The newly synthesised viruses in PHA or IL-2 stimulated cells were titrated on Vero-hSLAM cells. Stimulation in each donor was controlled by FACS staining for early activation marker CD69 **(Figure 4.22A)**. A3G depletion

resulted in visually better viral syncytium formation **(Figure 4.22B)** and significantly improved MV titre in PHA stimulated PBL as compared to non-targeted siRNA control **(Figure 4.22C)**. IL-2 stimulated PBL showed a similar tendency, however, the difference was not significant due to the high variation between blood donors. The A3G expression in transfected PBL was controlled by western blot for each donor **(Figure 4.22D upper panel)**. Interestingly, quantification of REDD1 expression in cells transfected with siA3G revealed that REDD1 expression was also affected by A3G-specific siRNA **(Figure 4.22D lower panel)**. Quantification of the relative expression clearly showed that increased REDD1 levels were associated with increased A3G expression and deletion of A3G resulted in decreased REDD1 expression **(Figure 4.22D)**.

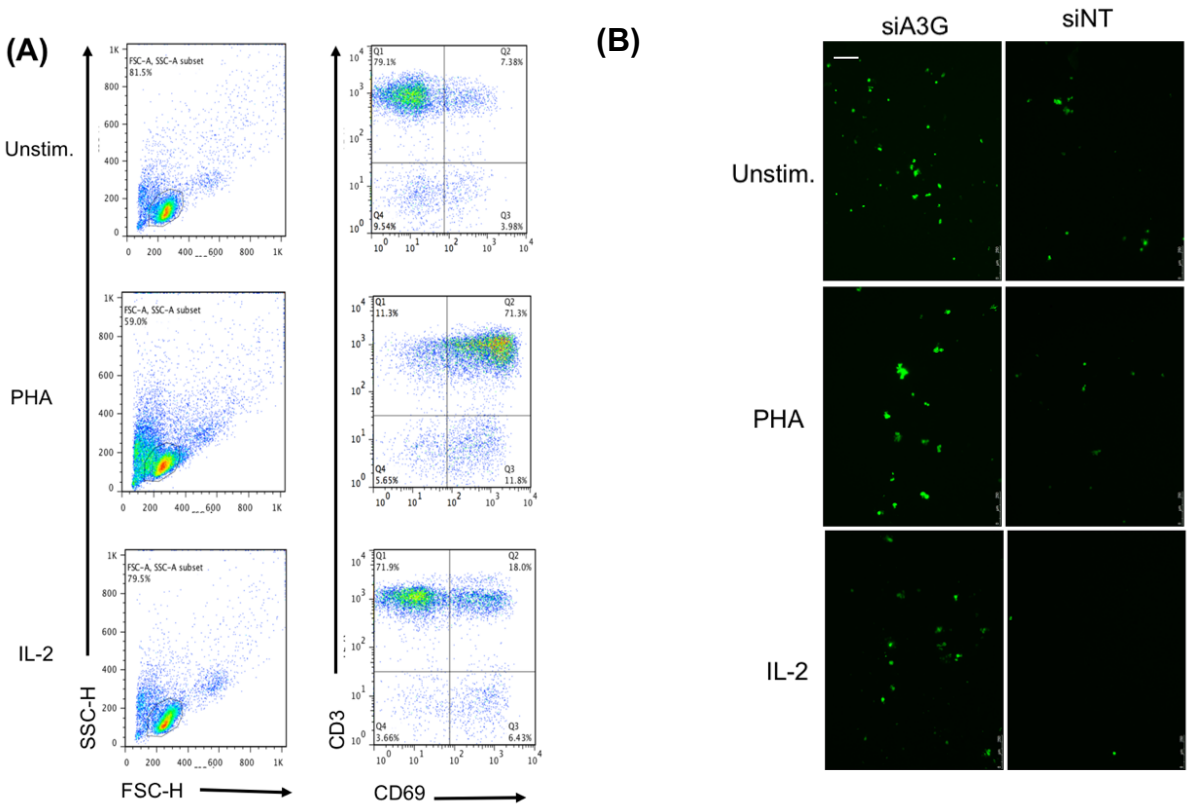

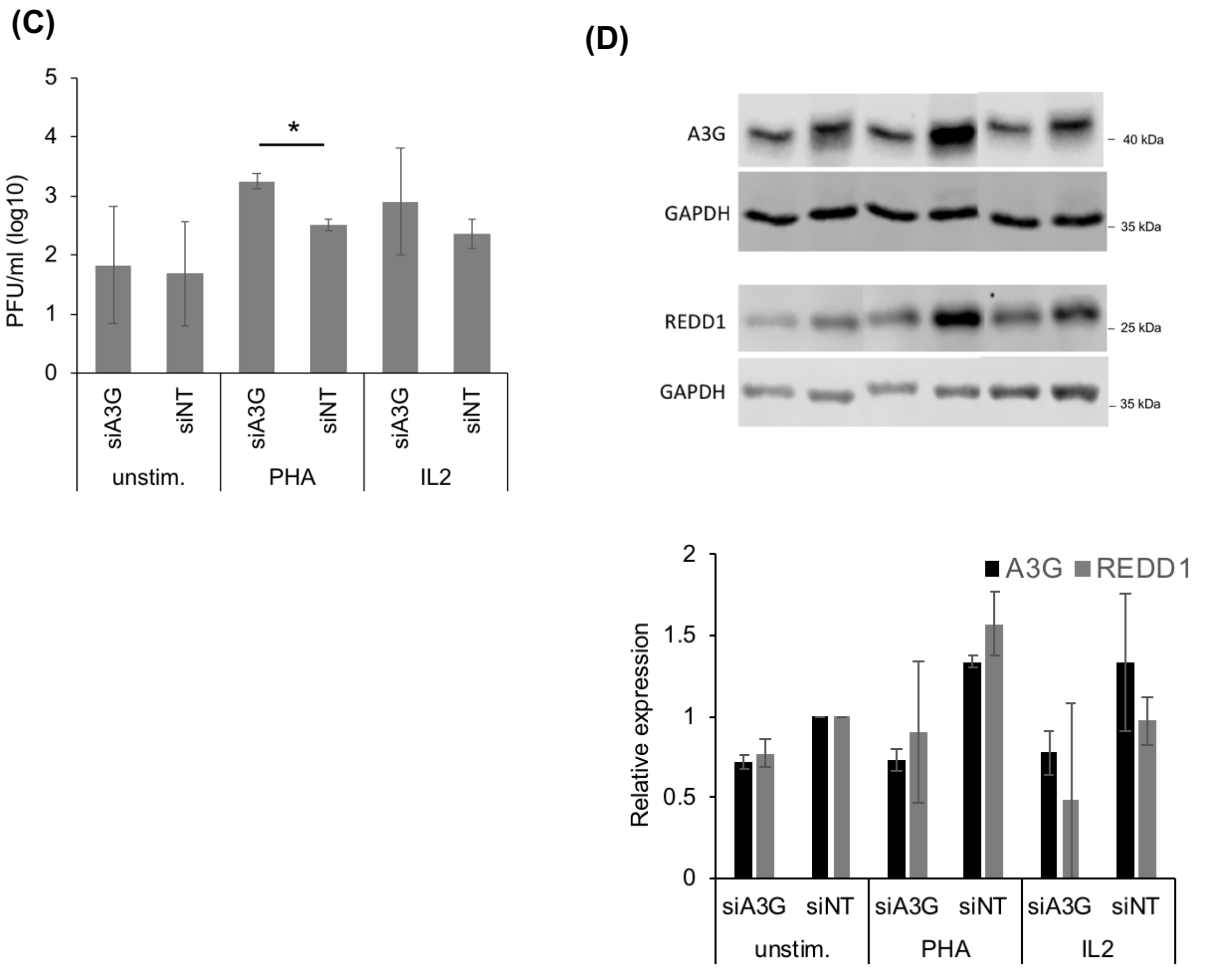

Figure 4.22: Depletion of A3G in stimulated PBL resulted in improved MV replication
10 x 10^6 of freshly isolated primary human PBL were nucleofected with 400 nM of A3G targeted or non-targeted siRNA. Cells were stimulated with 2.5 µg/ml of PHA or 25ng/ml of human IL-2. 24hr after stimulation cells were infected with MV^{IC323}eGFP at MOI 0.1 for 48 hrs. **(A)** stimulation of PBL was controlled detecting expression of stimulation marker CD69 by FACS. 1x 10^5 cells were stained with CD3-PE and /or CD69-APC. The representative dot plots indicate % CD3 and or CD69 positive cells **(B)** Representative micrographs of eGFP expressing syncytium formation in control and siA3G transfected cells were taken 48 hpi (100 x magnification; size bar = 100 µm) **(C)** Titre of the newly synthesized virus was determined on Vero hSLAM cells. Data shows mean value ± SEM of three donors and statistical significance was calculated by Unpaired Student's *t*-test (*p< 0.05) **(D)** 48 hrs after transfection with siRNA cell lysates were prepared and an equal amount (30µg) of proteins were separated on 12 % SDS-PAGE. Proteins were transferred on NC membrane and probed with specific primary and HRP conjugated secondary antibodies. The protein bands were then visualized by ECL (upper panel). A3G and REDD1 levels in each lane were quantified using ImageJ and normalized with respective GAPDH loading control. Data shows quantification of relative expression of A3G and REDD1 from PBL of three independent donors (lower panel).

To sum up, this study showed that in primary PBL, A3G was induced upon stimulation and resulted in up-regulation of REDD1 as observed in Vero cells **(Figure 4.2A).** This indicates a clear association between the expression of A3G and REDD1 which requires further investigation.

4.8.7. Antiviral role of REDD1 on MV replication in primary human PBL

We earlier showed that depletion of A3G in stimulated PBL resulted in improved MV replication and also effected REDD1 expression **(Figure 4.22).** Furthermore, depletion of REDD1 in Vero-A3G cells led to higher MV titres which

indicated that anti-MV activity is majorly attributed to REDD1 **(Figure 4.14-4.15)**. Therefore, we now investigated the potential anti-viral role of REDD1 in human PBL. PBL were transfected with siREDD1 or non-targeted siRNA. 24 hr PHA stimulated cells were infected with MV and titre of newly synthesised virus was determined on Vero-hSLAM cells. Stimulation in each donor was controlled by FACS staining **(Figure 4.23A)**. REDD1 depletion resulted in comparatively bigger syncytium formation **(Figure 4.23B)** and significantly higher viral titre **(Figure 4.23 C; upper panel)**. The REDD1 expression for each donor was controlled by western blotting **(Figure 4.23C; lower panel)**.

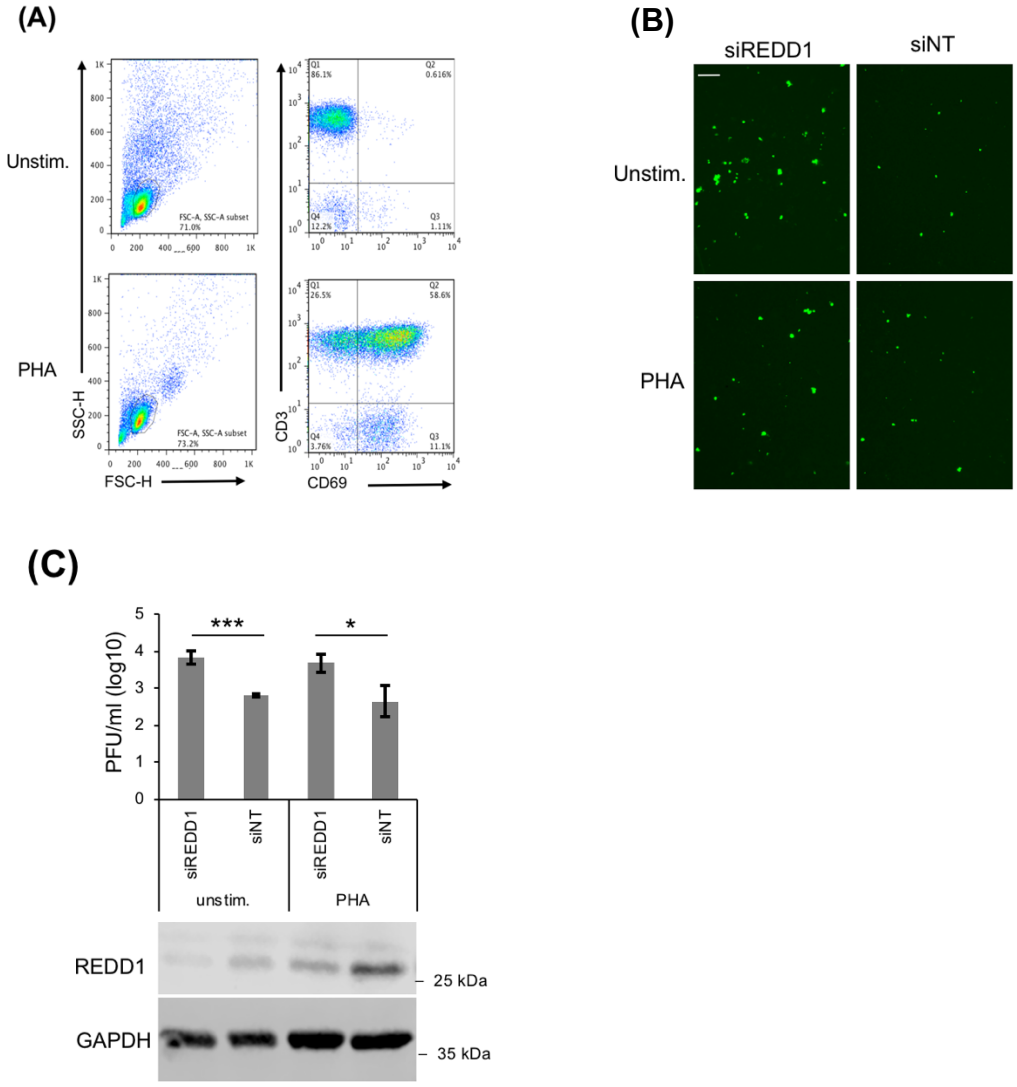

Figure 4.23: Depletion of REDD1 in stimulated PBL resulted in increased MV replication
10 x 10^6 of freshly isolated primary human PBL were nucleofected with 400 nM of REDD1 targeted or non-targeted siRNA. Cells were stimulated with 2.5 µg/ml of PHA. 24hr after stimulation cells were infected with MV^{IC323}eGFP at MOI 0.1 for 48 hrs. **(A)** Stimulation of PBL was controlled detecting expression of stimulation marker CD69 by FACS. 1x 10^5 cells were stained with CD3-PE and /or CD69-APC. The representative dot plots indicate % CD3 and or CD69 positive cells **(B)** Representative micrographs of eGFP expressing syncytium formation in control and siREDD1 transfected PBL were taken 48 hpi (100 x magnification; size bar = 100 µm) **(C)** (upper panel) Titre of newly synthesized virus was determined on Vero-hSLAM cells. Data shows mean value ± SEM of three independent donors and statistical significance was calculated by Unpaired Student's *t*-test (***p<0.0005, *p< 0.05). 48 hrs after

transfection with siRNA cell lysates were prepared and an equal amount (30µg) of proteins were separated on 12 % SDS-PAGE. Proteins were transferred on NC membrane and probed with specific primary and HRP conjugated secondary antibodies. The protein bands were then visualized by ECL. A representative WB is shown here (lower panel).

Taken together, our findings demonstrated that treatment with rapamycin resulted in a reduction of the MV titre **(Figure 4.21)** and depletion of REDD1 improved MV titre in human PBL **(Figure 4.23)**, thus highlighted an important role of mTORC1 in enhancing MV replication in human PBL.

4.9. KDELR2 expression affects MV spread indirectly

The KDELR2 receptor is known to play a crucial role in the retrieval of ER resident chaperones. Recent findings have suggested its role in flaviviral egress [258]. We have found that A3G expression resulted in up-regulation of KDELR2 **(Figure 4.2)** and ectopic expression of KDELR2 in Vero and CEM-SS cells significantly reduced MV titres **(Figure 4.12-15)**. Interestingly, MV glycoproteins undergo post-translational modifications in the ER [259]. Therefore, we investigated the role of KDELR2 in MV assembly and egress.

4.9.1. KDELR2 expression reduced the MV-H surface expression

The MV glycoproteins H and F are expressed on the surface of infected cells [259][260]. Therefore, in this study, we measured the cell surface expression of MV-H and -F in KDELR2 expressing cells. To prevent the MV-induced syncytium formation without affecting MV viral protein synthesis, we added the so-called fusion inhibitory peptide (FIP) after the entry of the virus into cells [261][262](Experimental setup **Figure 4.24A**). This facilitated single cell surface expression analysis of MV-H and -F by FACS. The mean fluorescence intensity (MFI) of surface and total expression of MV-H and -F was determined in MV-GFP expressing cells **(Figure 4.24B).**

Interestingly, the surface expression of MV-H was significantly reduced in Vero KDELR2 expressing cells by 31% as well as in Vero A3G by 35%, whereas the levels remained unaffected in Vero-REDD1 cells. In contrast, the surface expression of MV-F was not altered significantly in A3G and KDELR2 expressing cells **(Figure 4.24 C and D).** Hence, KDELR2 and A3G expression abated MV-H transport to the cell surface. However, the total expression of MV-H in Vero-

KDELR2 was significantly higher, whereas the Vero-A3G cells showed an analogues reduction in total MV-H expression **(Figure 4.24C: lower panel)**. These findings suggested that A3G expression completely inhibited MV replication, therefore the decrease was also reflected in total GFP expression, whereas, in Vero-KDELR2 cells, only the surface transport of glycoprotein H was affected and therefore, the total GFP expression was not reduced.

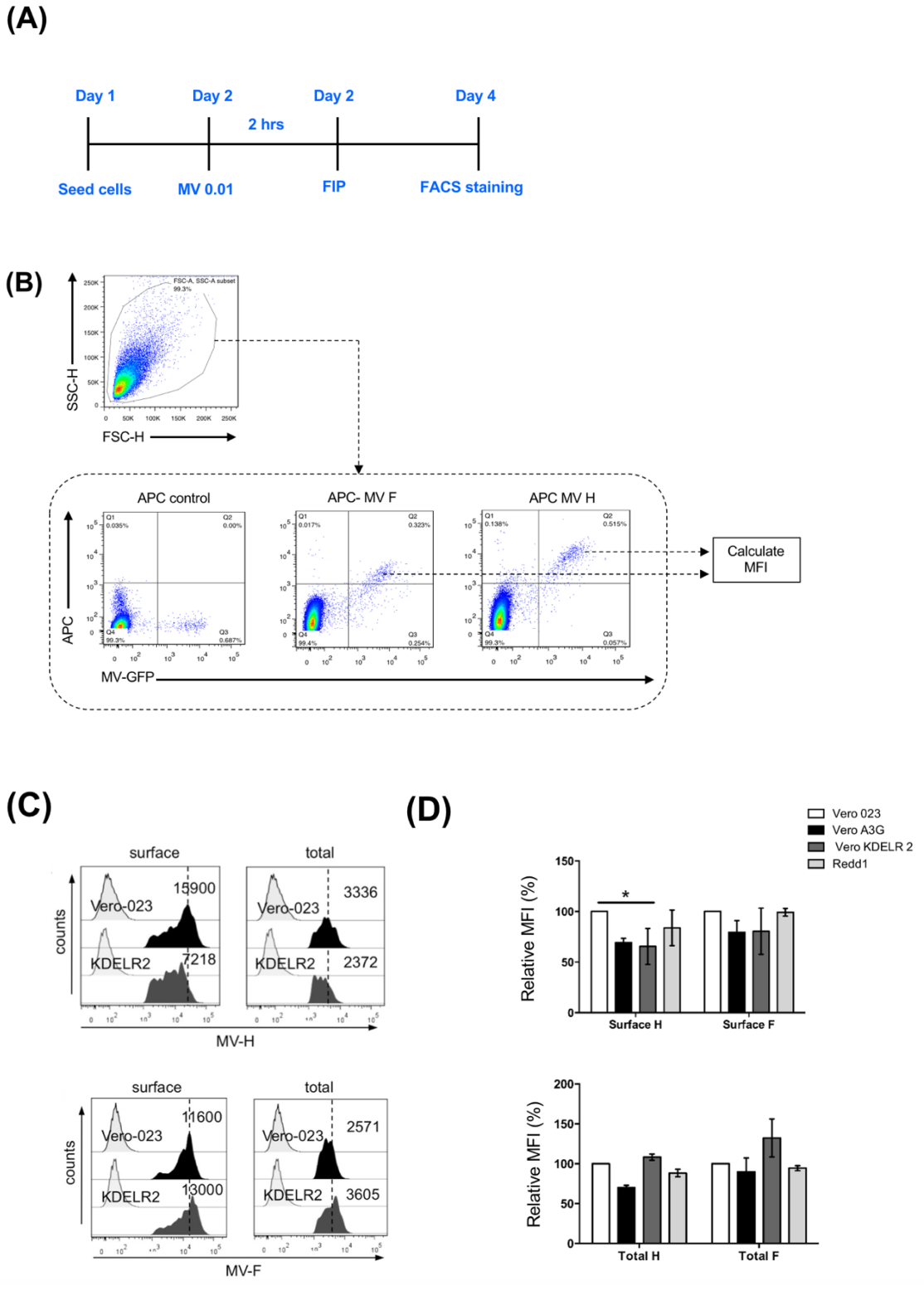

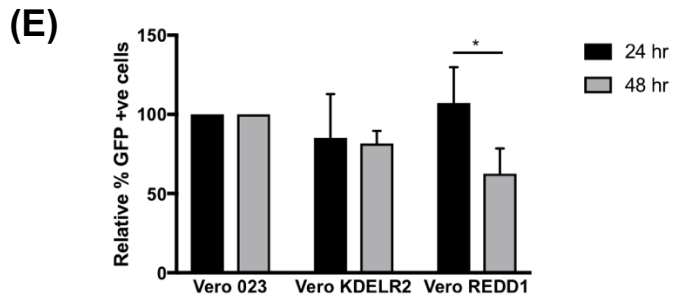

Figure 4.24: Surface expression of MV-H was reduced in KDELR2 expressing cells
Vero 023, Vero A3G, Vero KDELR2 and Vero REDD1 expressing cells (3 x 10^5 cells) were infected with rMV ^{Edtag} eGFP with MOI of 0.1 for 48 hrs. For single cell analysis of infected cells fusion inhibitory peptide (FIP) 200 µM was added. Cells were stained with respective antibodies and then fixed for surface expression or fixed, permeabilized and stained for total expression. Cells were then analysed by FACS. **(A)** Scheme of infection and FACS analysis. **(B)** Dot-plots shows MV GFP positive cells and surface/total expression of MV-H/F (APC labelled) proteins. The double positive population was used to calculate MFI. **(C)** The representative histogram shows MV-H (upper panel) and MV-F (lower panel) mean fluorescent intensities of in infected Vero 023 and Vero KDELR2 cells. **(D)** Data shows mean fluorescence intensities (MFI) ± SEM were presented as percent of control normalized to values of Vero-023 cells of three independent experiments. Statistical significance was calculated using the Student's t-test. (*p< 0.05). **(E)** Vero 023, Vero KDELR2 and Vero REDD1 expressing cells (3 x 10^5 cells) were infected with rMV ^{Edtag} eGFP with MOI of 0.1 and 2hrs post infection 200µm of FIP was added. Cell were fixed 24 and 48 hpi and analysed by FACS. The figure shows % GFP positive cells at each time point relative to the values of control Vero-023 cells. Data shows mean value ± SEM of three independent experiments.

We also confirmed above findings by comparing % GFP positive cells in Vero-KDELR2 cells and compared it with Vero-REDD1 cells. Since Vero-REDD1 cells have earlier been shown to inhibit MV replication they would serve as an appropriate control. The quantification of the percentage of GFP positive cells revealed that in KDELR2 expressing cells the % of MV GFP positive cell was not affected, while as expected the % of GFP positive cells was reduced in Vero-REDD1 cells **(Figure 4.24 E)**.

Taken together, these experiments have shown that, upon ectopic expression of KDELR2, MV-H surface expression was reduced **(Figure 4.24 D)**, whereas there is no significant impact on viral replication in the cell **(Figure 4.24 E)** indicating MV spread is affected upon KDELR2 expression.

4.9.2. MV spread, but not viral replication, was affected by KDELR2 overexpression

FACS analysis of total expression of MV-H in Vero-KDELR2 cells showed high accumulation of MV-H in infected cells **(Figure 4.24).** In contrary, we have found earlier that ectopic expression of KDELR2 resulted in a significant decrease in MV titre **(Figure 4.12D; lower panel).** To address this conflicting finding, we

compared MV-H protein expression in cells where viral spread was restricted by addition of FIP after the infection of the cells **(Figure 4.25A)**.

Corroborating with our previous finding, MV-H protein expression was reduced by 50% in the Vero-KDELR2 cells when virus spread was unrestricted (in absence of FIP) and significantly higher MV-H expression was seen in KDELR2 depleted cells **(Figure 4.25B: left panel).** Interestingly, the restriction of MV spread by addition of FIP resulted in the accumulation of MV-H in the cells **(Figure 4.25B: right panel)**. These findings and the reduction of the size of syncytia by KDELR2 overexpression (**Figure 4.12A)** indicated that the ectopic expression of KDELR2 only affected syncytium formation and viral spread without affecting viral replication, thus explains the reduction in MV titre as observed in **(Figure 4.12B).**

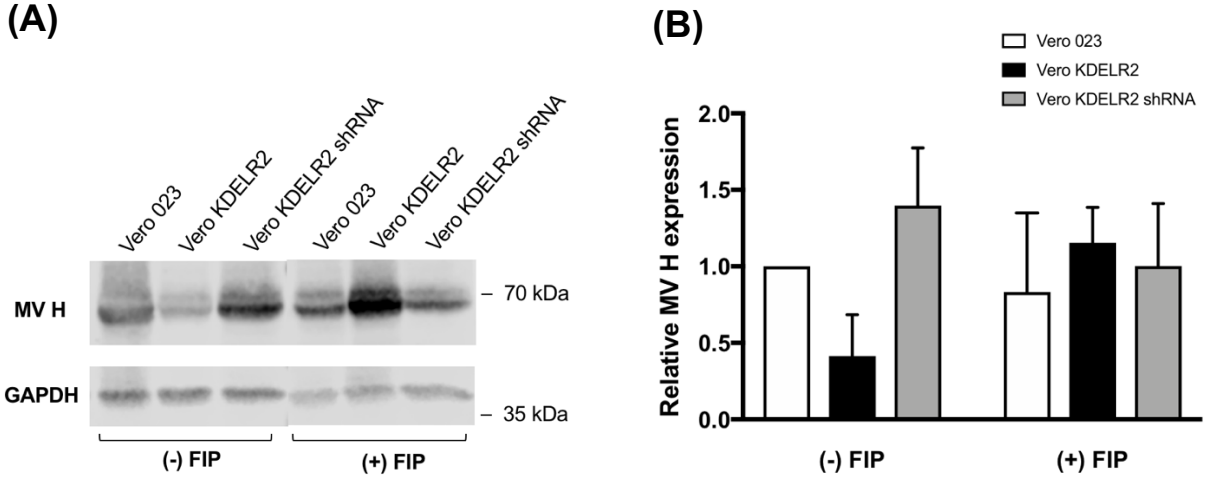

Figure 4.25: Total MV-H expression is affected by KDELR2 overexpression when syncytium formation is allowed (in absence of FIP)
Vero 023, Vero KDELR2 and Vero KDELR2 shRNA expressing cells (3 x 10^5 cells) were infected with rMV ^{Edtag} eGFP with MOI of 0.1 for 2hrs. Cells were then incubated for 48 hrs in presence or absence of 200µm fusion inhibitory peptide (FIP). Cell lysates were separated on 10%SDS PAGE and probed with respective primary and HRP labelled secondary antibodies. **(A)** Representative NC membrane from Immunoblot analysis against the depicted proteins **(B)** MV-H levels in each lane was normalized with GAPDH loading control in the same lane. The ratio of relative MV-H expression normalized to the values of Vero-023 was used for analysis. Data shows mean value ± SEM of densitometric analysis of three independent experiments.

4.9.3. No direct interaction was seen between KDELR2 and MV-H protein

Our experiments illustrated that upon expression of KDELR2 in Vero cells MV spread was affected **(Figure 4.12)**. It has been previously reported that MV-H and -F glycoproteins associate in the ER and that the addition of retention sequences has a significant impact on MV particle assembly [259]. Interestingly, Dengue virus prM protein directly interacts with KDELRs, which plays a crucial

role in viral egress [243]. Therefore, we investigated by microscopy and co-immunoprecipitation if there might be an interaction between KDELR2 and the MV-H glycoprotein.

The KDELR2 and MV-H proteins did not show any co-localization at different time points post infection. Both signals were clearly separated from each other. Rather at late time points, MV-H signals were found to be accumulated inside the cell **(Figure 4.26 A)**. GRP-78, a known interacting chaperone of KDELR 2 [263] was immune precipitated with KDELR2-Flag whereas no immunoprecipitation of MV-H was seen with KDELR2-Flag. Thus, indicating no direct interaction between KDELR2 and MV-H.

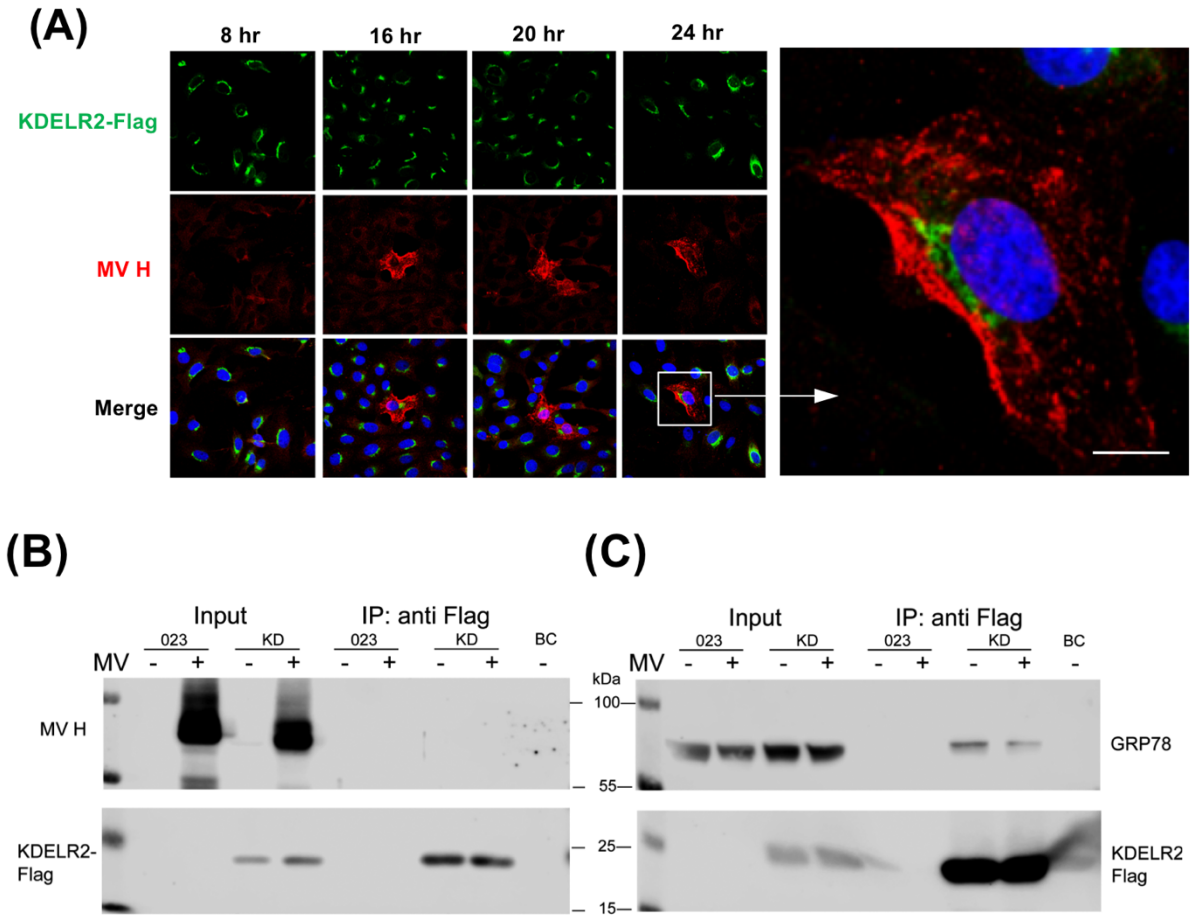

Figure 4.26: No interaction was observed between KDELR2 and MV-H but KDELR2 interacted with GRP78
(A) KDELR2 over-expressing Vero cells (1 x 10^4 cells) were seeded overnight in chamber slides. Cells were then infected with rMV^{Edtag} at MOI of 1. Cells were fixed at depicted time points and stained with antibodies (mouse anti-Flag and anti-mouse Alexa-488, Rabbit MV-H and anti-rabbit Alexa-594) and DAPI for nuclear staining. Confocal images were taken for co-localization analysis (400x magnification; size bar = 20µm). **(B)** The interaction was also confirmed by co-immunoprecipitation analysis. Lysates of MV-infected and uninfected Vero 023 and Vero KDELR2 cells were treated with anti-flag affinity gel for immuno-precipitation. Precipitated proteins were the separated on 10% SDS PAGE, blotted on nitrocellulose membrane and probed with anti MV-H, anti-Flag antibodies and respective secondary HRP conjugated antibodies. **(C)** To confirm the interaction of KDELR2-Flag and GRP78, same immuno-precipitated samples were probed with anti-GRP78 and anti-Flag antibodies. Representative images from three independent experiments.

4.9.4. Sub-cellular interaction between KDELR2 and ER Chaperones

It has been reported earlier that measles virus glycoproteins interact with various ER resident chaperones such as Calnexin, Calreticulin and GRP78 [31]. During MV infection, these chaperones are up-regulated which may play an important role in MV pathogenesis [31]. Interestingly, GRP78 and Calreticulin possess C-terminal KDEL tetra peptide signals [31].

Since KDELR2 was ectopically overexpressed in Vero cells, it was essential to confirm that it interacts with known interacting proteins. Co-immunoprecipitation of GRP78 with KDELR2-Flag was reported in a previous experiment **(Figure 4.26 C)**. Now, its interaction with cellular chaperones was further evaluated by confocal microscopy **(Figure 4.27 A)**.

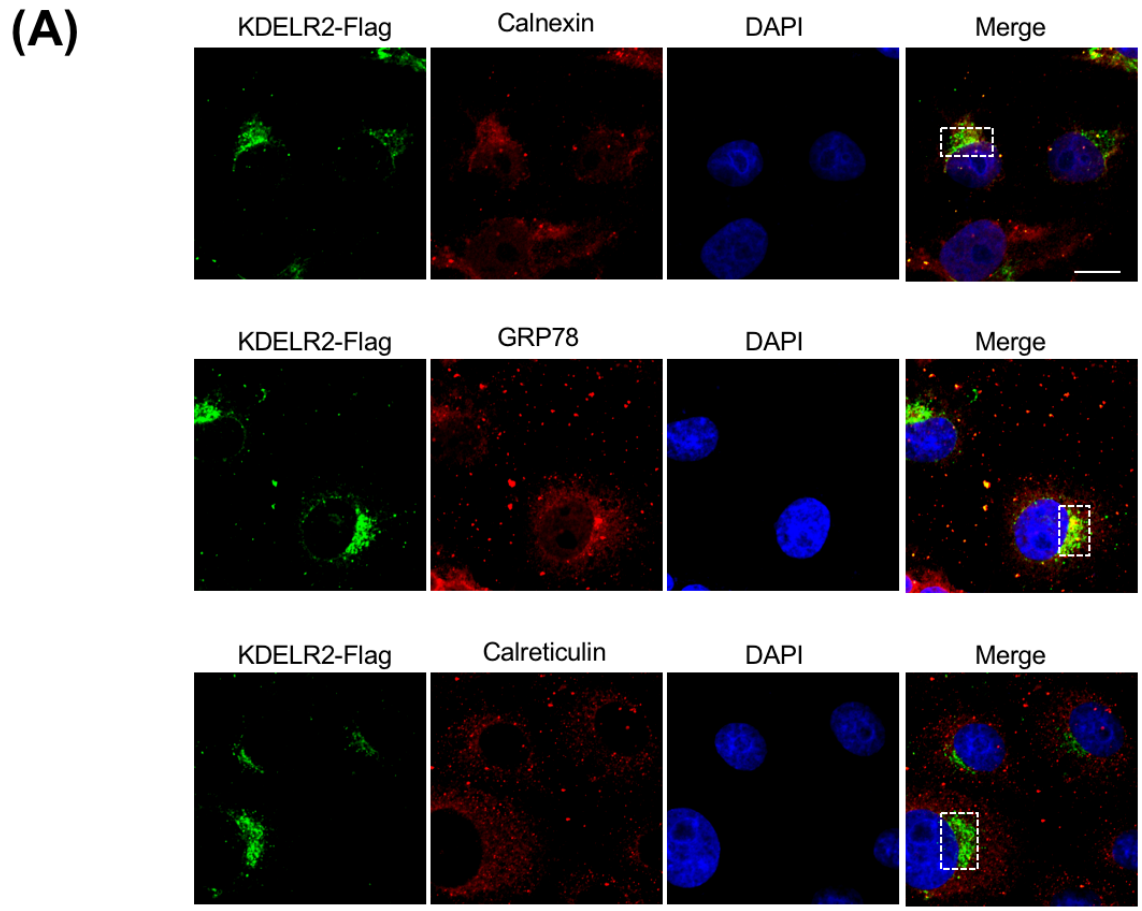

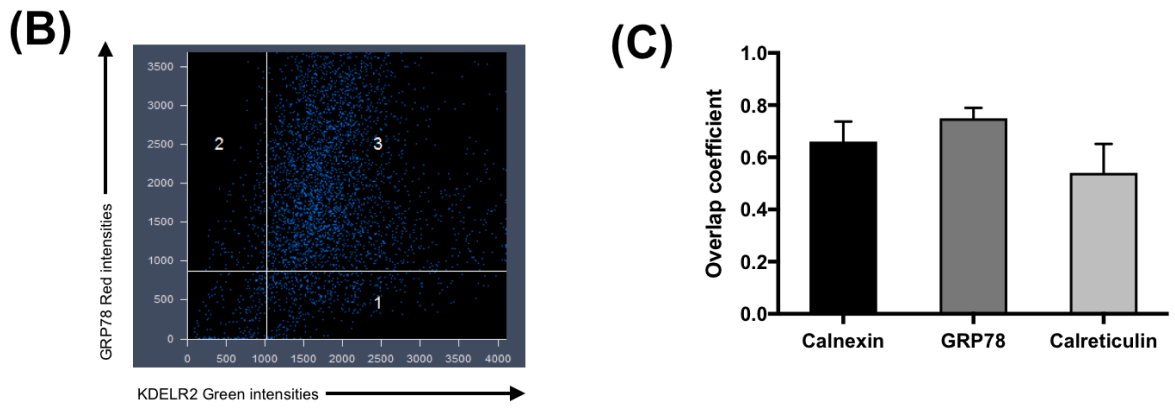

Figure 4.27: Sub-cellular interaction between KDELR2-Flag and Chaperones was evaluated by co-localization analysis
KDELR2 over-expressing Vero cells (1 x 10^4 cells) were seeded overnight in chamber slides. Cells were then fixed and stained with antibodies (primary: mouse anti-Flag, Rabbit Calnexin/GRP78/ Calreticulin and secondary: anti-mouse Alexa-488, anti-rabbit Alexa-594) and DAPI for nuclear staining. **(A)** Representative confocal images that were used for co-localization analysis (400x magnification; size bar = 20µm) **(B)** Representative scatter plot of individual red and green pixel intensities of KDELR2-Flag Green v/s Chaperons Red. **(C)** For analysis of co-localization between KDELR2 and Chaperones, Pearson's correlation coefficients were calculated in the region of interest ROI (represented by a square in above images) in each cell using Zen software. The data represents the overlap coefficient of 14-30 images.

Ectopically expressed KDELR2-Flag significantly co-localized with GRP 78 (correlation coefficient: 0.75), whereas Calnexin and Calreticulin showed moderate co-localization with KDELR2-Flag (correlation coefficient: 0.66 and 0.54, respectively). Thus, confirming a functional role of KDELR2-Flag in Vero cells.

4.9.5. Surface expression of ER chaperones was reduced significantly in MV infected KDELR2 expressing cells

As mentioned in above, MV infection results in increased surface expression of ER chaperones (Calnexin, Calreticulin and GRP78). This increased surface expression of chaperones was associated with an effective transport of MV glycoproteins to the cell surface [264]. As shown in **Figure 4.24**, surface expression of MV-H was significantly reduced in Vero-KDELR2 cells. These findings raised the important question if the inhibition of MV in KDELR2 expressing cells was attributed to a reduced function of chaperones. Therefore, the cell surface expression of Calnexin, GRP78 and Calreticulin was measured by FACS (Experimental setup **Figure 4.24A**). To prevent the MV-induced syncytium formation without affecting MV viral protein synthesis, we again added FIP after virus entry. This facilitated single-cell analysis of the chaperone expression on MV-

GFP positive cells **(Figure 4.28 A)**. Relative MFI of surface and total expression of chaperones was determined.

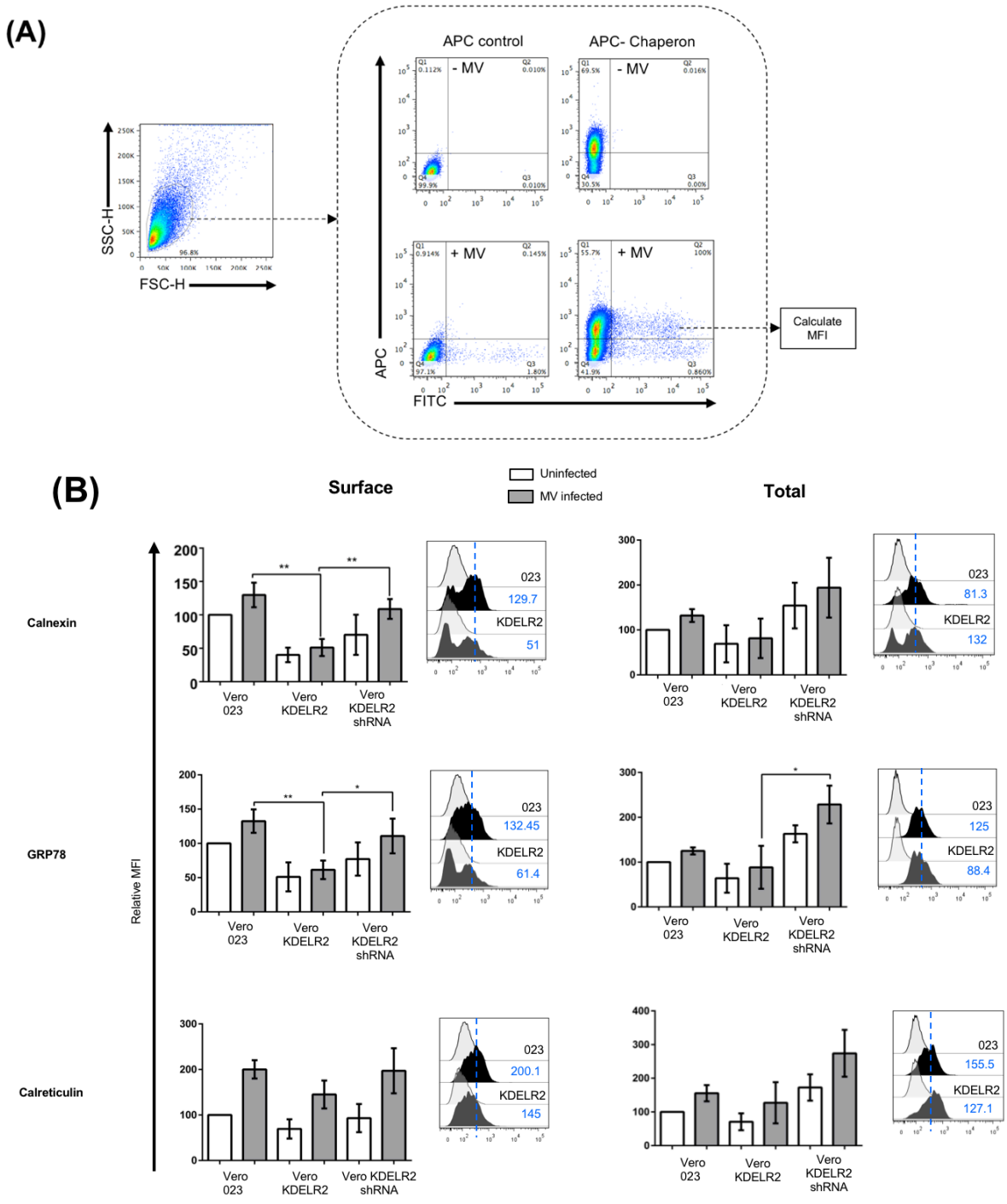

Figure 4.28: Surface expression of Chaperones is significantly reduced in KDELR2 expressing cells
Vero 023, Vero KDELR2 and Vero KDELR2 shRNA expressing cells (3 x 10^5 cells) were infected with rMV ^{Edtag} eGFP with MOI of 0.1 for 48 hrs. For single cell analysis of infected cells Fusion inhibitory peptide (FIP) 200 µM was added. Cells were stained with respective antibodies and then fixed for surface expression or fixed, permeabilized and stained for total expression. Cells were then analysed by FACS. **(A)** Dot-plots shows surface/total expression of Cellular chaperones Calnexin, GRP78, Calreticulin (APC labelled) in uninfected (upper panel) and MV-infected (lower panel) cells. The double positive population was used to calculate MFI. **(B)** Representative histograms show MFI in infected Vero 023 and Vero KDELR2 cells. Mean fluorescence intensities (MFI) ± SEM were presented as percent of control normalized to values of Vero-023 cells of three independent experiments. Statistical significance was calculated using the Student's t-test (*p< 0.05, **p < 0.01, ***p<0.001).

KDELR2 overexpression significantly reduced the surface expression of Calnexin and GRP78 in uninfected as well as in MV-infected cells as compared to control Vero-023 cells. In contrast, in KDELR2 depleted cells the surface expression was similar to control cells. In other words, MV infection failed to increase the Calnexin and GRP78 surface expression in KDELR2 expressing cells. **(Figure 4.28 B: Left panel).** Interestingly, the total levels of Calnexin and GRP78 were not affected in control and Vero-KDELR2 cells **(Figure 4.28 B: right panel)**. A similar trend was seen also for the third chaperone, Calreticulin. However, in this case, the differences were not statistically significant.

Taken together, microscopic and FACS analysis of viral and cellular chaperones revealed a correlation between MV-H and Chaperone surface expression resulting in less surface MV-H expression upon KDELR2 overexpression. Furthermore, our findings showed that overexpressed KDELR2 competes with MV-H for binding to Calnexin and GRP78. This binding results in ER retention of these chaperones and curtails their subsequent surface transport.

DISCUSSION

5. Discussion

With more than 90,000 deaths reported worldwide in 2016, measles remains the leading cause of vaccine-preventable disease. MV incident rates are notably increasing in developed countries due to personal, parental, religious and philosophical beliefs. Whereas, in developing countries of Africa and Asia people do not have access to vaccination due to the lack of health infrastructures. Therefore, to achieve the goal of MV eradication a combination of vaccination and therapeutic strategies are required. This highlights the need for an effective post-exposure antiviral drug. Directing an antiviral strategy towards viral proteins is more beneficial than targeting host proteins to avoid any cytotoxic effects. Hence, it is important to understand the role of viral proteins and their interaction with host proteins. This may help in designing novel and effective target-specific inhibitors with potent antiviral activity. The aim of this study was to thoroughly understand the role of APOBEC3G (A3G) regulated novel host factors in restricting MV.

5.1. A novel function of A3G: regulation of cellular gene expression

APOBEC proteins have been known to induce cytidine deamination in viral cDNA. The C-terminal is responsible to perform cytidine deaminase functions resulting in hypermutated viral genomes and for a long time, these functions were studied in excessive details. Various evidence has suggested that deamination alone is not sufficient to restrict viral replication. Catalytically inactive mutants of A3G were shown to have considerable antiviral activity [159]. Specifically, these mechanisms prevent accumulation of reverse transcription products [161]. The N-terminal domain binds to viral nucleic acids and is involved in several deaminase independent functions which are still poorly understood. It is yet to determine if these are the only deaminase independent functions of APOBEC proteins. Overall, cytidine independent mechanisms also equally contribute to the cumulative antiviral effect mediated by A3G.

A3G recruitment in HMM and LMM complexes is responsible for its catalytic and antiviral functions. In the HMM complex, the enzymatic functions of A3G are significantly diminished. The HMM-RNP complex contains a variety of cellular proteins especially those that are involved in RNA metabolism. Also, a significant amount of A3G was detected in cytoplasmic P bodies and stress granules, which regulate cellular mRNA translation and processing [182]. The exact mechanism of A3G interaction with cellular RNAs and proteins in these cytoplasmic structures is not known. However, based on these findings it has been speculated that A3G plays an important role in cellular RNA function.

Usually, the overexpression of a gene of interest is extensively used to analyse its biological function. Parallel to overexpression, loss of function studies is also required for complete understanding of gene functions. Previous studies in our group were based on A3G overexpression in IFN deficient Vero cells (Vero-A3G). Studies in Vero-A3G cells showed that A3G can mediate the inhibition of MV, MuV and RSV and this effect was independent of catalytic activity of A3G [192]. These findings contributed to the list of viruses that are restricted due to A3G. Based on the results of this study, we hypothesised that A3G may alter the expression of cellular genes.

The human genome contains more than 20000 protein-encoding genes. Simultaneous and parallel analysis of such a number of genes is quite challenging. A microarray analysis is a universal and powerful tool used to study the expression of numerous genes at a time. It is the easiest and quickest way to provide a composite image of cells under a particular condition. Overexpression of a gene followed by microarray can help to understand the broader physiological role of this single gene [265].

Therefore, our group studied the cellular gene expression in the presence and absence of A3G using a microarray. This experiment revealed significant differential regulation of around 1500 genes in Vero cells [266]. Interestingly, in parallel with our finding another group has shown the differential expression of 7500 genes in 293T cells upon A3G overexpression [267]. A3G induced site-specific mutations in more than 600 mRNA transcripts and these transcripts were

specifically involved in HIV-1 infection [267]. Similarly, it was also reported that A3A can edit more than hundreds of cellular transcripts in monocytes and macrophages [268]. From these findings, it appears that, apart from editing viral nucleic acid, A3G may alter the cellular host environment by RNA editing to retaliate against viral invasion. Here we reported for the first time a novel function of A3G in regulating cellular gene expression [266].

The microarray study revealed various interesting candidate genes as shown in **Figure 5.1.** Because post-translational mechanisms are known to control protein turnover in cells, mRNA levels seldom predict corresponding protein levels [269]. Protein expression analysis by western blot demonstrated that REDD1 and KDELR2 proteins levels were significantly increased due to A3G expression **(Figure 4.2)**. Interestingly, REDD1 is a stress response protein known to negatively regulate mTORC1 **(1.4.2)** and recently was shown to act as a host defence factor against Influenza [223]. KDELR2 has also been found to influence viral replication **(1.5.1)**. Therefore, we more closely investigated the role of these two proteins in A3G mediated inhibition of MV.

Upregulated	Ratio	Adjusted P-value
IL-1α (Interleukin 1 alpha)	4.5	1.65^{-10}
REDD1 / DDIT4	3.5	7.71^{-10}
ADRB2 (β2-adrenergic receptor)	3.0	2.29^{-9}
SPINK5 (Serine peptidase inhibitor, kazal type 5)	2.9	1.03^{-8}
SPINK6 (Serine peptidase inhibitor, kazal type 6)	2.8	3.38^{-9}
KDLER2 (ER lumen protein retaining receptor 2)	2.8	3.47^{-9}
IL-1β (Interleukin 1 beta)	2.8	3.70^{-9}
LOXL1 (Lysyl oxidase like 1)	2.7	5.61^{-9}
Protocadherin 9	2.3	1.54^{-7}
hDkk-1 (Dickkopf-related protein 1 precursor)	2.3	3.68^{-8}
Kynureninase	2.2	1.37^{-6}

Downregulated	Ratio	Adjusted P-value
PRDX2 (Peroxiredoxin 2)	0.28	$6{,}06^{-10}$
MOSC2/mARC-2	0.30	$2{,}93^{-9}$
ACY1 (Aminoacyclase 1)	0.42	$3{,}69^{-8}$
Collectrin precursor (Transmembrane protein 27)	0.43	7.02^{-5}
Collagen type VIII alpha 1 chain precursor	0.44	1.10^{-7}
TXNIP (Thioredoxin-interacting protein)	0.44	$4{,}77^{-8}$
Chloride intracelluler channel 6	0.45	3.65^{-8}
LGR5	0.47	1.85^{-7}
PP2A, subunit B	0.47	7.88^{-8}

Figure 5.1. list of differentially regulated genes in A3G expressing Vero cells

5.2. REDD1 and KDELR2 expression inhibited MV infection

In the first part of this thesis, the preparation of REDD1 and KDELR2 overexpressing Vero and CEMSS cells is described **(Figure 4.3-4.5)**. REDD1-Flag Vero cells showed significant expression of the 24 kDa REDD1-Flag protein **(Figure 4.3C)** and cytoplasmic distribution of REDD1 in Vero cells **(Figure 4.3B).** Similarly, KDELR2-Flag Vero cells also showed significant expression of KDELR2 in the ER

(Figure 4.5B and C). KDELRs are known to be localized in the Golgi complex in low amounts. Increased expression of KDELRs results in ligand-independent activation of KDELRs and in the increased retrograde transport of KDELRs to the ER [228].

Expression of REDD1 and KDELR2 regulates crucial signalling events in cells. Therefore, it was important to assess the effect of ectopic expression of these proteins on cell proliferation before evaluating their impact on viral replication. The Assessment of the proliferative ability of transduced Vero cell using eFluor670 showed no significant impact on cell division at 48 and 72 hrs timepoint **(Figure 4.6A)**. However, cell proliferation was partially affected at the 24 hrs time point in Vero-A3G cells **(Figure 4.6A and B)**. The APOBEC family of proteins A3A, A3C and A3H have shown to have nuclear localization and may have access to cellular chromatin network during mitosis [270]. Specifically, A3A and A3B have been shown to alter the cell cycle profile and trigger DNA damage response [271]. Interestingly, the cytidine deaminase A3G is excluded from cellular chromatin throughout mitosis [270] [272]. It is not known how A3G influences cell proliferation or the cell cycle. On the other hand, KDELR2 and REDD1 expressing Vero cells proliferated equally as compared with parent cells.

After infection with rMV^{Edtag}eGFP, REDD1 expressing cells showed a substantial decrease in viral-induced syncytium formation **(Figure 4.11B)** and 90% reduction of the viral titre **(Figure 4.11C)** as compared to control cells, and shRNA-mediated silencing of REDD1 abolished these negative effects **(Figure 4.15B)**. MV is known to form giant multinucleated cells in Vero [273] as well as in small airway epithelial cells [274]. Interactions between MV H and F are required for the formation of syncytia and for efficient virus replication [260]. An alteration in MV-H impairing this interaction with MV-F leads to decreased syncytium formation [275]. Currently, there is no evidence of a direct interaction between MV proteins and REDD1. However, the cellular stress response in Vero cells induced by hyperthermia and heavy metal exposure was shown to lead to a larger plaque phenotype mainly by induction of HSPs (heat shock proteins) [276]. Interestingly, REDD1 is also known to induce a stress response in cells, especially during hypoxic conditions. However, we observed a decrease in syncytium formation upon

overexpression of REDD1, which might be due to reduced viral protein expression, especially of MV-H. If there is no direct interaction of REDD1 with viral proteins or nucleic acid, it might influence viral replication also via indirect mechanisms involving other host factors. Recently, REDD1 was shown to act as host defence factor against influenza virus with concomitant inhibition of mTORC1 [223]. Therefore, the role of REDD1 mediated inhibition via mTORC1 was investigated.

The second A3G regulated gene of interest was KDELR2. MV induced syncytium formation in Vero-KDELR2 cells was reduced significantly **(Figure 4.12A)** with 85% decrease in virus titre **(Figure 4.12B)**. shRNA mediated ablation of KDELR2 restored the virus titre to control cells **(Figure 4.12 A and B)**. It has been shown that addition of the KDEL motif to the F protein of HPIV3 (Human Parainfluenza virus) resulted in ER retention of this protein and subsequently reduced surface expression [277], whereas DENV requires KDELR1 and KDELR2 for the viral export across ER and Golgi. The prM protein of DENV interacts with KDELRs in the ER [243], although there is no KDEL motif present in DENV proteins. However, in contrast to MV, membranous web structures of the ER are replication and assembly sites of various viruses such as HCV, DENV, Vaccinia Virus and Rota virus. In addition, viral glycoproteins undergo folding and oligomerization in the ER similar to cellular proteins. Therefore, viruses have evolved to use ER membranes and ER proteins efficiently for their own benefit in very virus-specific ways [240].

MV is known to induce cell type-specific changes in lymphoid and non-lymphoid cell lines [278]. Therefore, we evaluated REDD1 and KDELR2 mediated inhibition of MV not only in Vero cells but also in a lymphoid cell type. CEMSS cells are susceptible to MV infection and earlier we reported that A3G expression in CEMSS cells also inhibited MV replication [192]. It is a human lymphosarcoma T cell line used for HIV-1 studies. Here we showed that ectopic expression of REDD1 and KDELR2 in CEMSS cell effectively reduced MV titres **(Figure 4.13)**. These findings confirm that REDD1 and KDELR2 mediated inhibitory effects on MV are a cell type independent phenomenon.

We first showed that individual overexpression of REDD1 and KDELR2 was sufficient to inhibit MV replication. These findings raised an important question of whether these factors contribute to A3G mediated inhibition of MV. To answer this question, REDD1 and KDELR2 expression were targeted individually or together by shRNA. Knockdown of these mRNAs and effects on protein expression were confirmed by western blot and a substantial decrease in expression of REDD1 and KDELR2 was observed **(Figure 4.14D)**. MV induced syncytium formation in REDD1 and/or KDELR2 depleted Vero-A3G cells were similar to that of control cells **(Figure 4.15A)** and the virus titre was restored in these cells **(Figure 4.15B)**. Therefore, this study clearly showed that the A3G mediated antiviral effect on MV is mediated by REDD1 and KDELR2.

5.3. REDD1 exerts its antiviral effect via inhibition of mTORC1

REDD1 mediated inhibition of mTORC1 has been reported to be a cell type -dependent phenomenon [279]. In renal cancer cells, constitutively upregulated REDD1 levels failed to inhibit mTORC1 [280], whereas in other cells during hypoxic and stress conditions REDD1 inhibits mTORC1 signalling in a TSC2 dependent manner **(1.4.2)**. To validate role of mTORC1 in MV replication, we used the pharmacological inhibitor rapamycin **(1.4.2)**. As determined by viability staining with propidium iodide, control and transduced Vero cells tolerated 1μM concentration of rapamycin without any impact on cell proliferation **(Figure 4.16A)**. We observed a strong dose-dependent decrease in MV syncytium formation as well as in titre upon rapamycin treatment in Vero-023 cells. A similar trend of dose-dependent decrease was seen in Vero-KDELR2 cells. However, no additive effect of rapamycin was seen in Vero-REDD1 cells **(Figure 4.17)**. This demonstrated that rapamycin and REDD1 act on the same pathways.

Unstimulated peripheral blood mononuclear cells (PBMC) support replication of wildtype MV only on a very low level. Usually, less than 20% PBMC are infected with MV [281]. In contrast, mitogen stimulation of lymphocytes leads to effective viral replication and release of infectious virus [282][283]. CD150/SLAM is known to be expressed on stimulated lymphocytes and APCs and

is used as an entry receptor by WT MV **(1.1.4)**. Corroborating with earlier findings, MV titre was increased by 1 log upon stimulation in three donors that we tested. Additionally, we found that pharmacological inhibition of mTORC1 by rapamycin effectively reduced viral giant cell formation and MV replication in PHA stimulated human PBL **(Figure 4.21)**. This demonstrated that mTORC1 signalling is required for active replication of not only lab adapted strain but also for WT MV in primary human cells. Similar to our findings, rapamycin has been shown to reduce MV syncytium formation in NSCLC (non-small-lung carcinoma cells) [284]. In contrast, one study reported that rapamycin treatment led to more virus production in HeLa cells with increased expression of MV-N and MV-P proteins [262]. This may be due to the fact that in this experiment a low concentration of Rapamycin (0.125nM) was used against very high MOI of MV and also no dose-dependent effect was studied. Interestingly, rapamycin has also been shown to effectively target HIV-1 replication in PBL [285], which suggested a role of mTORC1/2 in the maintenance of HIV1 latency [286].

Phosphorylation of TOR by upstream signalling results in activation of S6 kinases which regulate mRNA translation and ribosomal biogenesis [215]. A complex series of phosphorylation events regulate activation of p70S6K [287]. Phosphorylation at Thr389 is often used as a marker of active mTOR1 signalling. Rapamycin inhibits phosphorylation signals for activation of p70S6K [288]. We observed a significant reduction of the p70S6K phosphorylation in untreated Vero-A3G and in Vero-REDD1 cells. These levels were further diminished by rapamycin treatment. Interestingly, Vero-KDELR2 cells showed decreased p70S6K levels only after rapamycin treatment **(Figure 4.19 A and B)**. These findings further highlighted the following facts: first, in Vero-A3G cells REDD1 levels are induced which is responsible for decreased mTORC1 signalling, second, this decrease in mTORC1 signalling is responsible for the observed inhibitory effect on MV replication in Vero-A3G and Vero-REDD1 cells **(Figure 4.11C)**, third, REDD1 and rapamycin act upstream of mTORC1 signalling, and fourth, in KDELR2 overexpressing cells a mTORC1 independent mechanism is responsible for the observed antiviral activity. It would be worth investigating the effect of rapamycin on mTORC1 signalling in PBL, which would help to strengthen the role of

mTORC1 in MV replication. Importantly, S6K1 is not the only protein affected by mTORC1 activation. Several other complex signalling events govern overall cellular metabolism, protein and mRNA turnover (as summarized in **Figure 1.16**). Further investigations focused on these signalling events are also required to determine the exact consequence of A3G and REDD1 expression on these signalling events.

Our group and several other groups have reported increased A3G expression upon stimulation of human PBL [192][164]. Upregulated REDD1 levels were observed in activated T cells without significant impact on T cell activation [257]. Here we showed that upon stimulation with PHA and IL-2 not only A3G and REDD1 levels were increased, but also KDELR2 expression was increased **(Figure 4.20)**. Further, we found that siRNA mediated knockdown of A3G in PHA and IL-2 stimulated PBL resulted in reduced REDD1 expression with corresponding increased MV titres as compared to non-targeted siRNA application (**Figure 4.22C and D**). This finding indicates that in stimulated PBL, REDD1 was induced due to the expression of A3G. To understand the antiviral role of REDD1 in human PBL, REDD1 levels were also directly targeted by REDD1-specific siRNA. MV titres were found to be improved upon depletion of REDD1. These findings corroborate with our earlier results as discussed above and show that high mTORC1 activity is important for the replication of lab-adapted and wildtype MV. At this point, we did not determine the corresponding effect on mTORC1 activity. However, transient transfection of siREDD1 was shown earlier to hinder dephosphorylation of p70S6K which impedes subsequent inhibition of mTORC1 [289].

In summary, as shown in **Figure 5.2**, we can state that A3G up-regulates REDD1 expression in Vero cells and PBL. REDD1 expression and rapamycin treatment exerted strong antiviral effects on MV replication. Interestingly, the combination of both did not had any additive antiviral effect. These findings underlined the role of active mTORC1 signalling in MV replication.

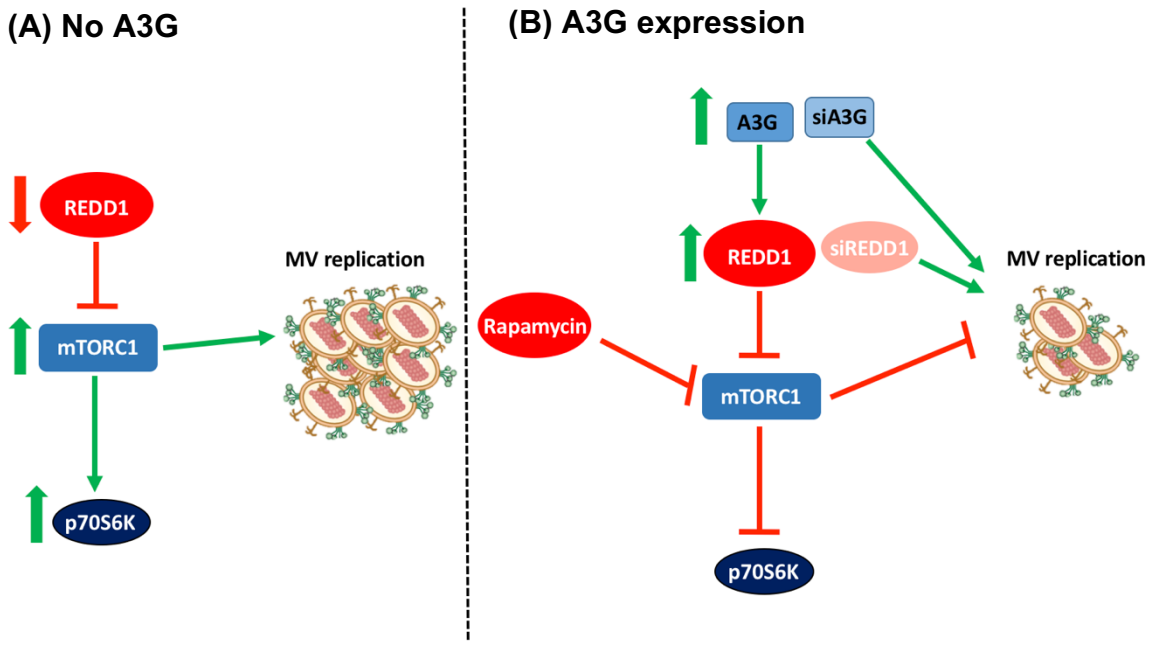

Figure 5.2. Schematic summary of A3G mediated inhibition of MV
(A) Under physiological condition mTORC1 signalling in absence of REDD1 results in active MV replication. **(B)** Increased A3G expression induces REDD1, which results in inhibition of mTORC1 and downstream signalling of p70S6K. The reduced mTORC1 levels are responsible for reduced MV replication and siRNA mediated silencing of REDD1 and A3G rescue this inhibitory block on MV replication.

5.4. KDELR2 expression affects MV spread

KDELR2 functions in retrograde transport of chaperones from the Golgi to the ER. Apart from transport functions, KDELRs have been shown to stimulate Golgi SFKs and cellular MAPK (1.5.1). Knowledge about the role of KDEL receptors in viral egress has developed recently. Flaviviruses such as DENV and JEV were shown to exploit the KDELR function for viral particle transport across Golgi and ER (1.5.2). As defined by the name itself, KDELRs are known to bind with proteins containing KDEL motifs. Although no such motif was found in Flaviviruses, the DENV prM protein was shown to interact with KDELRs and disruption of this interaction affected DENV egress [243]. Interestingly, prM assists in folding and maturation of the DENV envelope protein E in such a way that it can be released after maturation [290]. Details about the role of KDERLs in benefiting these interactions are not yet investigated. Only FIPV proteins have been shown to possess the retention signal KTEL, which is required for the extremely slow release of viral proteins across the ER [246].

MV H and F proteins are oligomers. Cleavage of the F protein inactive precursor (F_0) by cellular enzymes in trans-Golgi network is required for trimerization of this protein. Similarly, H protein glycosylation and oligomerization occurs in the ER **(1.1.3)**. MV H and F have been shown to interact with ER chaperones for the maturation and transport of viral proteins to the plasma membrane. To meet the excessive requirement of chaperones during active viral replication, MV induces the expression of Calreticulin, Calnexin and GRP78. A significant amount of these chaperones is expressed on the infected cell surface [264]. Here, we showed using FACS analysis that in KDELR2 expressing cells the surface expression of H and F proteins **(Figure 4.24)** and simultaneously the surface expression of GRP78, Calnexin and CRT was reduced **(Figure 4.28)**. A significant degree of colocalization between overexpressed KDELR2 and Calreticulin/ GRP78 was observed **(Figure 4.27)** and overexpressed KDELR2 immunoprecipitated with its known interacting partner GRP78 **(Figure 4.16C)**. These results further confirmed previous findings that ER chaperons contain KDEL motifs for their retrieval [291]. Interestingly, no interaction of MV-H with KDELR2 was observed **(Figure 4.26A and B)**. As mentioned earlier, the ER appears to be the most probable site for interaction of KDELR2 with Chaperones and for Chaperones with MV. The finding that overexpression of KDELR2 results in its redistribution to the ER [292] suggests that KDELR2 competes with MV-H proteins for binding to chaperones. Since these chaperons contain KDEL binding motifs they may be quickly occupied by overexpressed KDELR2 making them unavailable for MV H and F proteins to assist their maturation and transport to the infected cell surface **(Figure 5.3).**

Interestingly, when MV spread was restricted by the addition of FIP, an increased accumulation of MV-H was observed in Vero-KDELR2 cells. Using same MOI, Vero-KDELR2 cells showed less expression of MV-H in absence of FIP **(Figure 4.25)**. Similarly, the MV GFP expression remained similar in Vero-KDELR2 cells for 48 hrs whereas Vero-REDD1 cells showed a significantly decreased MV GFP expression after 24 hr **(Figure 4.24E)**.

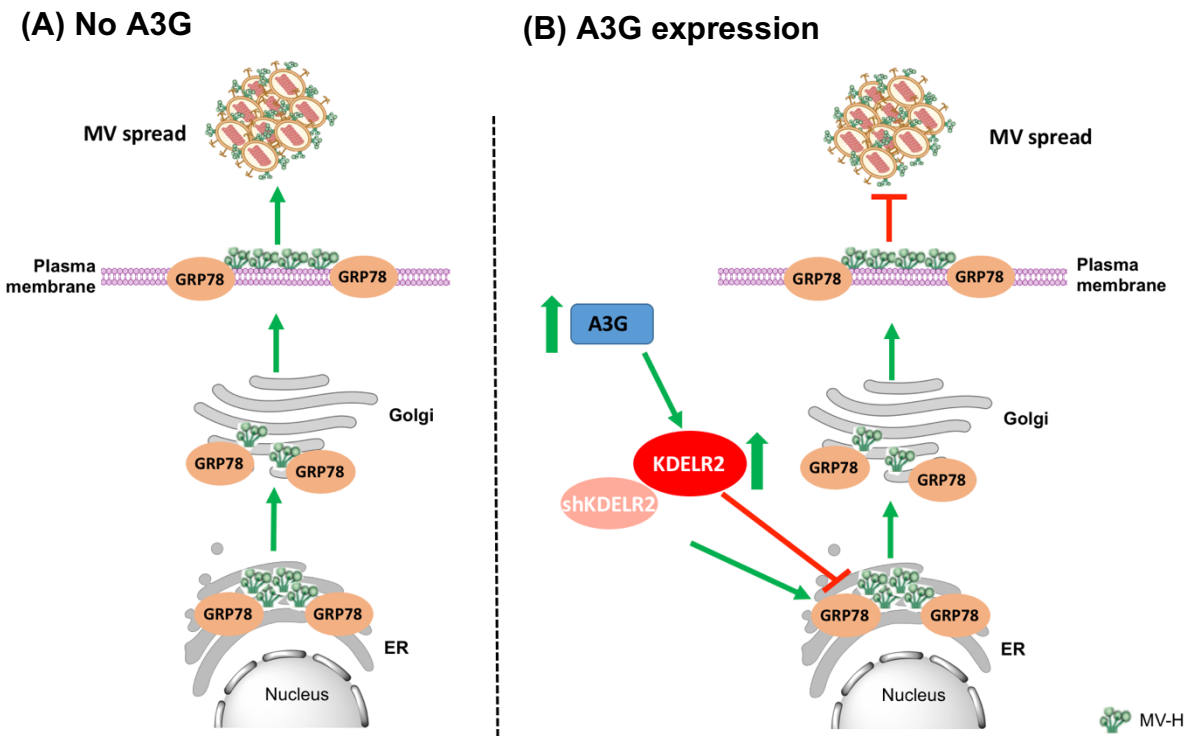

Figure 5.3. Schematic summary of KDELR2 mediated indirect effect on MV H surface transport.
(A) Under physiological condition, MV infection increases ER chaperones and chaperones mediated surface expression of MV-H. This results in efficient MV spread. **(B)** Increased A3G induces KDELR2 and this KDELR2 competes with MV-H for binding with ER chaperones such as GRP78. Thus, results in decreases surface expression of MV-H and GRP78 and diminished MV spread.

Taken together, in KDELR2 cells it appears that only the viral spread is affected without significant impact on viral replication **(Figure 5.3).** Due to overexpression of KDELR2 chaperones are no longer available for MV glycoprotein maturation. Therefore, MV H and F although translated from the viral genome are not transported to the cell surface for final assembly and egress. To determine if the H and F proteins are degraded in the ER or simply accumulate requires further investigation. Similarly, quantification of the outcoming amount of MV using different MOI would help to confirm if the viral release is affected upon expression of KDELR2.

Targeting GRP78 by chemical inhibitors or depletion of KDER2 would help further to confirm these dynamic interactions between chaperones, KDELR2 and MV. The GRP78 inhibitor IT-139 is a ruthenium-based anticancer drug which is used to increase the efficacy and to overcome chemo-resistance in certain cancer therapies [293]. However, considering the crucial role of chaperones and KDELRs in cellular signalling it would be challenging to target these molecules to hinder MV replication without evident cytotoxic effect on cells.

BIBLIOGRAPHY

Bibliography

[1] S. J. Anthony *et al.*, "A strategy to estimate unknown viral diversity in mammals," *MBio*, vol. 4, no. 5, pp. e00598-13, 2013.

[2] Y. Furuse, A. Suzuki, and H. Oshitani, "Origin of measles virus: divergence from rinderpest virus between the 11th and 12th centuries," *Virol J*, vol. 7, p. 52, 2010.

[3] G. A. Marsh *et al.*, "Cedar virus: a novel Henipavirus isolated from Australian bats," *PLoS Pathog*, vol. 8, no. 8, p. e1002836, 2012.

[4] D. E. Griffin, "Fields Virology," in *Fields Virology. Vol. 1*, 6th ed., vol. 1, D. M. Knipe, Ed. Philadelphia: Lippincott Williams & Wilkins, 2013, pp. 1042–1069.

[5] Y. Yanagi, M. Takeda, and S. Ohno, "Measles virus: Cellular receptors, tropism and pathogenesis," *J. Gen. Virol.*, vol. 87, no. 10, pp. 2767–2779, 2006.

[6] P. Plattet, L. Alves, M. Herren, and H. C. Aguilar, "Measles virus fusion protein: Structure, function and inhibition," *Viruses*, vol. 8, no. 4, 2016.

[7] Y. Jiang, Y. Qin, and M. Chen, "Host-Pathogen Interactions in Measles Virus Replication and Anti-Viral Immunity," *Viruses*, vol. 8, no. 11, 2016.

[8] W. J. Moss and D. E. Griffin, "Global measles elimination.," *Nat. Rev. Microbiol.*, vol. 4, no. 12, pp. 900–908, 2006.

[9] B. K. Rima and W. P. Duprex, "New concepts in measles virus replication: Getting in and out in vivo and modulating the host cell environment," *Virus Res.*, vol. 162, no. 1–2, pp. 47–62, 2011.

[10] S. M. Beaty and B. Lee, "Constraints on the genetic and antigenic variability of measles virus," *Viruses*, vol. 8, no. 4, pp. 1–20, 2016.

[11] I. Takayama *et al.*, "The nucleocapsid protein of measles virus blocks host interferon response," *Virology*, 2012.

[12] J.-M. Bourhis *et al.*, "The intrinsically disordered C-terminal domain of the measles virus nucleoprotein interacts with the C-terminal domain of the phosphoprotein via two distinct sites and remains predominantly unfolded," *Protein Sci.*, 2005.

[13] S. Longhi *et al.*, "The C-terminal domain of the measles virus nucleoprotein is intrinsically disordered and folds upon binding to the C-terminal moiety of the phosphoprotein," *J. Biol. Chem.*, 2003.

[14] M. Ito, M. Iwasaki, M. Takeda, T. Nakamura, Y. Yanagi, and S. Ohno, "Measles virus nonstructural C protein modulates viral RNA polymerase activity by interacting with host protein SHCBP1.," *J. Virol.*, 2013.

[15] W. J. Bellini, G. Englund, S. Rozenblatt, H. Arnheiter, and C. D. Richardson, "Measles virus P gene codes for two proteins," *J. Virol.*, 1985.

[16] P. Devaux and R. Cattaneo, "Measles Virus Phosphoprotein Gene Products : Conformational Flexibility of the P / V Protein Amino-Terminal Domain and C Protein Infectivity Factor Function Measles Virus Phosphoprotein Gene Products : Conformational Flexibility of the P / V Protein Amino," *J. Virol.*, vol. 78, no. 21, pp. 11632–11640, 2004.

[17] F. Radecke and M. A. Billeter, "The nonstructural C protein is not essential for multiplication of Edmonston B strain measles virus in cultured cells," *Virology*, 1996.

[18] K. Takeuchi *et al.*, "Stringent requirement for the C protein of wild-type measles virus for growth both in vitro and in macaques," *J. Virol.*, 2005.

[19] C. Pohl, W. P. Duprex, G. Krohne, B. K. Rima, and S. Schneider-Schaulies, "Measles virus M and F proteins associate with detergent-resistant membrane fractions and promote formation of virus-like particles," *J. Gen. Virol.*, 2007.

[20] T. Cathomen, H. Y. Naim, and R. Cattaneo, "Measles viruses with altered envelope protein cytoplasmic tails gain cell fusion competence.," *J. Virol.*, 1998.

[21] M. Iwasaki, M. Takeda, Y. Shirogane, Y. Nakatsu, T. Nakamura, and Y. Yanagi, "The matrix protein of measles virus regulates viral RNA synthesis and assembly by interacting with the nucleocapsid protein.," *J. Virol.*, 2009.

[22] D. E. Griffin, W. H. Lin, and C. H. Pan, "Measles virus, immune control, and persistence," *FEMS Microbiol Rev*, vol. 36, no. 3, pp. 649–662, 2012.

[23] C. K. Navaratnarajah, V. H. J. Leonard, and R. Cattaneo, "Measles virus glycoprotein complex assembly, receptor attachment, and cell entry," *Curr. Top. Microbiol. Immunol.*, vol. 329, pp. 59–76, 2009.

[24] D. Naniche *et al.*, "Human Membrane Cofactor Protein (CD46) Acts as a Cellular Receptor for Measles Virus .," *J. Virol.*, 1993.
[25] R. E. Dörig, A. Marcil, A. Chopra, and C. D. Richardson, "The human CD46 molecule is a receptor for measles virus (Edmonston strain)," *Cell*, 1993.
[26] H. Tatsuo, N. Ono, K. Tanaka, and Y. Yanagi, "Slam (CDw150) is a cellular receptor for measles virus," *Nature*, 2000.
[27] R. S. Noyce *et al.*, "Tumor cell marker pvrl4 (nectin 4) is an epithelial cell receptor for measles virus," *PLoS Pathog.*, vol. 7, no. 8, 2011.
[28] T. Hashiguchi *et al.*, "Crystal structure of measles virus hemagglutinin provides insight into effective vaccines," *Proc. Natl. Acad. Sci. U. S. A.*, 2007.
[29] R. K. Plemper, M. A. Brindley, and R. M. Iorio, "Structural and mechanistic studies of measles virus illuminate paramyxovirus entry," *PLoS Pathog*, vol. 7, no. 6, p. e1002058, 2011.
[30] R. K. Plemper, a L. Hammond, and R. Cattaneo, "Measles virus envelope glycoproteins hetero-oligomerize in the endoplasmic reticulum," *J Biol Chem*, vol. 276, no. 47, pp. 44239–44246, 2001.
[31] G. Bolt, "The measles virus (MV) glycoproteins interact with cellular chaperones in the endoplasmic reticulum and MV infection upregulates chaperone expression," *Arch. Virol.*, vol. 146, no. 11, pp. 2055–2068, 2001.
[32] Y. Shu *et al.*, "Plasticity in structural and functional interactions between the phosphoprotein and nucleoprotein of measles virus," *J. Biol. Chem.*, 2012.
[33] B. Cevik, D. E. Holmes, E. Vrotsos, J. A. Feller, S. Smallwood, and S. A. Moyer, "The phosphoprotein (P) and L binding sites reside in the N-terminus of the L subunit of the measles virus RNA polymerase," *Virology*, 2004.
[34] M. D. Mühlebach *et al.*, "Adherens junction protein nectin-4 is the epithelial receptor for measles virus," *Nature*, 2011.
[35] T. Seya, L. L. Ballard, N. S. Bora, V. Kumar, W. Cui, and J. P. Atkinson, "Distribution of membrane cofactor protein of complement on human peripheral blood cells. An altered form is found on granulocytes," *Eur. J. Immunol.*, 1988.
[36] M. Tahara, M. Takeda, F. Seki, T. Hashiguchi, and Y. Yanagi, "Multiple Amino Acid Substitutions in Hemagglutinin Are Necessary for Wild-Type Measles Virus To Acquire the Ability To Use Receptor CD46 Efficiently," *J. Virol.*, 2007.
[37] N. Ono, H. Tatsuo, Y. Hidaka, T. Aoki, H. Minagawa, and Y. Yanagi, "Measles Viruses on Throat Swabs from Measles Patients Use Signaling Lymphocytic Activation Molecule (CDw150) but Not CD46 as a Cellular Receptor," *J. Virol.*, 2001.
[38] R. S. Noyce and C. D. Richardson, "Nectin 4 is the epithelial cell receptor for measles virus," *Trends Microbiol.*, vol. 20, no. 9, pp. 429–239, 2012.
[39] C. Santiago, E. Björling, T. Stehle, and J. M. Casasnovas, "Distinct kinetics for binding of the CD46 and SLAM receptors to overlapping sites in the measles virus hemagglutinin protein," *J. Biol. Chem.*, 2002.
[40] I. C. Johnston, V. ter Meulen, J. Schneider-Schaulies, and S. Schneider-Schaulies, "A recombinant measles vaccine virus expressing wild-type glycoproteins: consequences for viral spread and cell tropism.," *J. Virol.*, 1999.
[41] C. Erlenhöfer, W. P. Duprex, B. K. Rima, V. ter Meulen, and J. Schneider-Schaulies, "Analysis of receptor (CD46, CD15O) usage by measles virus," *J. Gen. Virol.*, 2002.
[42] S. Ohno, F. Seki, N. Ono, and Y. Yanagi, "Histidine at position 61 and its adjacent amino acid residues are critical for the ability of SLAM (CD150) to act as a cellular receptor for measles virus," *J. Gen. Virol.*, 2003.
[43] N. Reymond, S. Fabre, E. Lecocq, J. Adelaide, P. Dubreuil, and M. Lopez, "Nectin4/PRR4, a New Afadin-associated Member of the Nectin Family that Trans-interacts with Nectin1/PRR1 through V Domain Interaction," *J. Biol. Chem.*, 2001.
[44] V. H. J. Leonard *et al.*, "Measles virus blind to its epithelial cell receptor remains virulent in rhesus monkeys but cannot cross the airway epithelium and is not shed," *J. Clin. Invest.*, 2008.
[45] L. M. Esolen *et al.*, "Brain endothelial cell infection in children with acute fatal measles.," *J. Clin. Invest.*, 1995.
[46] S. McQuaid and S. L. Cosby, "An immunohistochemical study of the distribution of the measles virus receptors, CD46 and SLAM, in normal human tissues and subacute sclerosing panencephalitis," *Lab. Investig.*, 2002.
[47] L. RA and P. GD, "Fields' Virology, Volume 1," in *Paramyxoviridae: the viruses and their replication*, 2007.
[48] L. A. Colf, Z. S. Juo, and K. C. Garcia, "Structure of the measles virus hemagglutinin," *Nat. Struct. Mol. Biol.*, 2007.

[49] M. A. Brindley, M. Takeda, P. Plattet, and R. K. Plemper, "Triggering the measles virus membrane fusion machinery," *Proc. Natl. Acad. Sci.*, 2012.
[50] S. P. J. Whelan, J. N. Barr, and G. W. Wertz, "Transcription and replication of nonsegmented negative-strand RNA viruses.," *Curr. Top. Microbiol. Immunol.*, 2004.
[51] J. Brunel *et al.*, "Sequence of Events in Measles Virus Replication: Role of Phosphoprotein-Nucleocapsid Interactions," *J. Virol.*, 2014.
[52] S. Plumet, W. P. Duprex, and D. Gerlier, "Dynamics of viral RNA synthesis during measles virus infection.," *J. Virol.*, 2005.
[53] F. El Najjar, A. P. Schmitt, and R. E. Dutch, "Paramyxovirus glycoprotein incorporation, assembly and budding: A three way dance for infectious particle production," *Viruses*, vol. 6, no. 8, pp. 3019–3054, 2014.
[54] L. Liljeroos and S. J. Butcher, "Matrix proteins as centralized organizers of negative-sense RNA virions.," *Front. Biosci. (Landmark Ed.*, 2013.
[55] H. Y. Naim, E. Ehler, and M. A. Billeter, "Measles virus matrix protein specifies apical virus release and glycoprotein sorting in epithelial cells," *EMBO J.*, 2000.
[56] M. Tahara, M. Takeda, and Y. Yanagi, "Altered Interaction of the Matrix Protein with the Cytoplasmic Tail of Hemagglutinin Modulates Measles Virus Growth by Affecting Virus Assembly and Cell-Cell Fusion," *J. Virol.*, 2007.
[57] M. Moll, H. D. Klenk, G. Herrler, and a Maisner, "A single amino acid change in the cytoplasmic domains of measles virus glycoproteins H and F alters targeting, endocytosis, and cell fusion in polarized Madin-Darby canine kidney cells.," *J. Biol. Chem.*, 2001.
[58] A. Salditt *et al.*, "Measles virus M protein-driven particle production does not involve the endosomal sorting complex required for transport (ESCRT) system," *J. Gen. Virol.*, 2010.
[59] J. L. G. Paul A. Gastañaduy, "Measles (Rubeola)." [Online]. Available: https://wwwnc.cdc.gov/travel/yellowbook/2018/infectious-diseases-related-to-travel/measles-rubeola.
[60] M. Ludlow *et al.*, "Wild-type measles virus infection of primary epithelial cells occurs via the basolateral surface without syncytium formation or release of infectious virus," *J. Gen. Virol.*, 2010.
[61] M. Ludlow, S. McQuaid, D. Milner, R. L. D. De Swart, and W. P. Duprex, "Pathological consequences of systemic measles virus infection," *J. Pathol.*, 2015.
[62] B. M. Laksono, R. D. de Vries, S. McQuaid, W. P. Duprex, and R. L. de Swart, "Measles virus host invasion and pathogenesis," *Viruses*, vol. 8, no. 8, pp. 1–13, 2016.
[63] R. L. De Swart *et al.*, "Predominant infection of CD150+ lymphocytes and dendritic cells during measles virus infection of macaques," *PLoS Pathog.*, 2007.
[64] "CDC Mealses Pinkbook." [Online]. Available: https://www.cdc.gov/vaccines/pubs/pinkbook/downloads/meas.pdf.
[65] S. Dittmar, H. Harms, N. Runkler, A. Maisner, K. S. Kim, and J. Schneider-Schaulies, "Measles Virus-Induced Block of Transendothelial Migration of T Lymphocytes and Infection-Mediated Virus Spread across Endothelial Cell Barriers," *J. Virol.*, 2008.
[66] K. B. Hummel, W. J. Bellini, and M. K. Offermann, "Strain-specific differences in LFA-1 induction on measles virus-infected monocytes and adhesion and viral transmission to endothelial cells.," *J. Virol.*, 1998.
[67] "Immunopaedia." [Online]. Available: https://www.immunopaedia.org.za/download/measles-virus/.
[68] M. Frenzke *et al.*, "Nectin-4-Dependent Measles Virus Spread to the Cynomolgus Monkey Tracheal Epithelium: Role of Infected Immune Cells Infiltrating the Lamina Propria," *J. Virol.*, 2013.
[69] R. E. Randall and S. Goodbourn, "Interferons and viruses: An interplay between induction, signalling, antiviral responses and virus countermeasures," *Journal of General Virology*. 2008.
[70] J. Schlender *et al.*, "Inhibition of toll-like receptor 7- and 9-mediated alpha/beta interferon production in human plasmacytoid dendritic cells by respiratory syncytial virus and measles virus.," *J. Virol.*, 2005.
[71] K. Childs, R. Randall, and S. Goodbourn, "Paramyxovirus V Proteins Interact with the RNA Helicase LGP2 To Inhibit RIG-I-Dependent Interferon Induction," *J. Virol.*, 2012.
[72] Y. Nakatsu, M. Takeda, S. Ohno, Y. Shirogane, M. Iwasaki, and Y. Yanagi, "Measles virus circumvents the host interferon response by different actions of the C and V proteins," *J. Virol.*, 2008.
[73] G. Caignard *et al.*, "Measles virus V protein blocks Jak1-mediated phosphorylation of STAT1 to escape IFN-α/β signaling," *Virology*, 2007.
[74] Y. Nakatsu, M. Takeda, S. Ohno, R. Koga, and Y. Yanagi, "Translational inhibition and increased interferon induction in cells infected with C protein-deficient measles virus.," *J.*

Virol., 2006.
[75] S. Ohno, N. Ono, M. Takeda, K. Takeuchi, and Y. Yanagi, “Dissection of measles virus V protein in relation to its ability to block alpha/beta interferon signal transduction,” *J. Gen. Virol.*, 2004.
[76] K. Takeuchi, S. I. Kadota, M. Takeda, N. Miyajima, and K. Nagata, “Measles virus V protein blocks interferon (IFN)-α/β but not IFN-γ signaling by inhibiting STAT1 and STAT2 phosphorylation,” *FEBS Lett.*, 2003.
[77] J. A. Shaffer, W. J. Bellini, and P. A. Rota, “The C protein of measles virus inhibits the type I interferon response,” *Virology*, 2003.
[78] J. M. Fontana, B. Bankamp, and P. A. Rota, “Inhibition of interferon induction and signaling by paramyxoviruses,” *Immunological Reviews*. 2008.
[79] H. H. Hoffmann, W. M. Schneider, and C. M. Rice, “Interferons and viruses: An evolutionary arms race of molecular interactions,” *Trends in Immunology*. 2015.
[80] D. E. Griffin, “The Immune Response in Measles: Virus Control, Clearance and Protective Immunity,” *Viruses*, vol. 8, no. 10, 2016.
[81] L. J. Kaplan, R. S. Daum, M. Smaron, and C. A. McCarthy, “Severe Measles in Immunocompromised Patients,” *JAMA J. Am. Med. Assoc.*, 1992.
[82] S. R. Permar *et al.*, “Prolonged measles virus shedding in human immunodeficiency virus-infected children, detected by reverse transcriptase-polymerase chain reaction.,” *J. Infect. Dis.*, 2001.
[83] R. A. Good and S. J. Zak, “DISTURBANCES IN GAMMA GLOBULIN SYNTHESIS AS "EXPERIMENTS OF NATURE",” *Pediatrics*, vol. 18, no. 1, p. 109 LP-149, Jul. 1956.
[84] S. R. Permar *et al.*, “Role of CD8+ lymphocytes in control and clearance of measles virus infection of rhesus monkeys,” *J. Virol.*, 2003.
[85] S. R. Permar *et al.*, “Limited contribution of humoral immunity to the clearance of measles viremia in rhesus monkeys,” *J. Infect. Dis.*, 2004.
[86] R. D. De Vries, S. Yüksel, A. D. M. E. Osterhaus, and R. L. De Swart, “Specific CD8+ T-lymphocytes control dissemination of measles virus,” *Eur. J. Immunol.*, 2010.
[87] R. Nanan, C. Carstens, and H. W. Kreth, “Demonstration of virus-specific CD8+ memory T cells in measles-seropositive individuals by in vitro peptide stimulation.,” *Clin. Exp. Immunol.*, 1995.
[88] W. J. Moss, J. J. Ryon, M. Monze, and D. E. Griffin, “Differential regulation of interleukin (IL)-4, IL-5, and IL-10 during measles in Zambian children,” *J. Infect. Dis.*, 2002.
[89] S. R. Permar, D. E. Griffin, and N. L. Letvin, “Immune containment and consequences of measles virus infection in healthy and immunocompromised individuals,” *Clinical and Vaccine Immunology*. 2006.
[90] H. S. El Mubarak *et al.*, “Measles Virus Protein-Specific IgM, IgA, and IgG Subclass Responses during the Acute and Convalescent Phase of Infection,” *J. Med. Virol.*, 2004.
[91] A. G. Wesley, H. M. Coovadia, and P. Kiepiela, “Further predictive indices of clinical severity of measles,” *South African Med. J.*, 1982.
[92] D. E. Griffin, W. H. W. Lin, and A. N. Nelson, “Understanding the causes and consequences of measles virus persistence [version 1; referees: 2 approved],” *F1000Research*, vol. 7, no. 237, 2018.
[93] E. Norrby and Y. Gollmar, “Appearance and persistence of antibodies against different virus components after regular measles infections.,” *Infect. Immun.*, 1972.
[94] F. B. Bouche, N. H. C. Brons, S. Houard, F. Schneider, and C. P. Muller, “Evaluation of hemagglutinin protein-specific immunoglobulin M for diagnosis of measles by an enzyme-linked immunosorbent assay based on recombinant protein produced in a high-efficiency mammalian expression system,” *J. Clin. Microbiol.*, 1998.
[95] R. S. Fujinami and M. B. Oldstone, “Alterations in expression of measles virus polypeptides by antibody: molecular events in antibody-induced antigenic modulation,” *J Immunol*, 1980.
[96] S. Schneider-Schaulies, U. G. Liebert, Y. Segev, B. Rager-Zisman, M. Wolfson, and V. ter Meulen, “Antibody-dependent transcriptional regulation of measles virus in persistently infected neural cells,” *J. Virol.*, 1992.
[97] A. P. Beckford, R. O. Kaschula, and C. Stephen, “Factors associated with fatal cases of measles. A retrospective autopsy study.,” *S. Afr. Med. J.*, 1985.
[98] P. Arneborn and G. Biberfeld, “T-lymphocyte subpopulation in relation to immunosuppression in measles and varicella,” *Infect. Immun.*, 1983.
[99] J. J. Ryon, W. J. Moss, M. Monze, and D. E. Griffin, “Functional and phenotypic changes in circulating lymphocytes from hospitalized zambian children with measles,” *Clin. Diagn. Lab. Immunol.*, 2002.
[100] R. D. de Vries *et al.*, “Measles Immune Suppression: Lessons from the Macaque Model,” *PLoS*

Pathog., 2012.
[101] T. Vuorinen, P. Peri, and R. Vainionpaa, "Measles virus induces apoptosis in uninfected bystander T cells and leads to granzyme B and caspase activation in peripheral blood mononuclear cell cultures," *Eur. J. Clin. Invest.*, 2003.
[102] E. Avota *et al.*, "Disruption of Akt kinase activation is important for immunosuppression induced by measles virus," *Nat. Med.*, 2001.
[103] M. Carsillo, K. Klapproth, and S. Niewiesk, "Cytokine Imbalance after Measles Virus Infection Has No Correlation with Immune Suppression," *J. Virol.*, 2009.
[104] D. E. Griffin, "Measles virus-induced suppression of immune responses," *Immunological Reviews*. 2010.
[105] R. Nardone, S. Golaszewski, E. Trinka, F. Tezzon, and G. Zuccoli, "Acute disseminated encephalomyelitis preceding measles exanthema," in *Journal of Child Neurology*, 2011.
[106] J. Schneider-Schaulies, S. Niewiesk, S. Schneider-Schaulies, and V. ter Meulen, "Measles virus in the CNS: the role of viral and host factors for the establishment and maintenance of a persistent infection.," *J. Neurovirol.*, vol. 5, no. 6, pp. 613–22, 1999.
[107] R. T. Johnson *et al.*, "Measles encephalomyelitis--clinical and immunologic studies.," *N. Engl. J. Med.*, 1984.
[108] R. K. Garg, "Subacute sclerosing panencephalitis.," *Postgrad. Med. J.*, 2002.
[109] A. F. Freeman *et al.*, "A new complication of stem cell transplantation: measles inclusion body encephalitis," *Pediatrics*, 2004.
[110] H. Budka, S. Urbanits, P. P. Liberski, S. Eichinger, and T. Popow-Kraupp, "Subacute measles virus encephalitis: A new and fatal opportunistic infection in a patient with AIDS," *Neurology*, 1996.
[111] E. Norrby and K. Kristensson, "Measles virus in the brain," *Brain Research Bulletin*. 1997.
[112] M. Dubois-Dalcq, J. M. Coblentz, and A. B. Pleet, "Subacute Sclerosing Panencephalitis: Unusual Nuclear Inclusions and Lengthy Clinical Course," *Arch. Neurol.*, 1974.
[113] N. A. Halsey, J. F. Modlin, J. T. Jabbour, L. Dubey, D. L. Eddins, and D. D. Ludwig, "Risk factors in subacute sclerosing panencephalitis: a case-control study.," *Am. J. Epidemiol.*, 1980.
[114] K. Schönberger, M. S. Ludwig, M. Wildner, and B. Weissbrich, "Epidemiology of Subacute Sclerosing Panencephalitis (SSPE) in Germany from 2003 to 2009: A Risk Estimation," *PLoS One*, 2013.
[115] B. K. Rima and W. P. Duprex, "Molecular mechanisms of measles virus persistence," *Virus Research*. 2005.
[116] J. Kirk, A. L. Zhou, S. McQuaid, S. L. Cosby, and I. V. Allen, "Cerebral endothelial cell infection by measles virus in subacute sclerosing panencephalitis: Ultrastructural and in situ hybridization evidence," *Neuropathol. Appl. Neurobiol.*, 1991.
[117] D. Reuter and J. Schneider-Schaulies, "Measles virus infection of the CNS: Human disease, animal models, and approaches to therapy," *Medical Microbiology and Immunology*. 2010.
[118] P. A. Rota *et al.*, "Global distribution of measles genotypes and measles molecular epidemiology," *J. Infect. Dis.*, 2011.
[119] L. Jin, S. Beard, R. Hunjan, D. W. G. Brown, and E. Miller, "Characterization of measles virus strains causing SSPE: A study of 11 cases," *J. Neurovirol.*, 2002.
[120] J. F. Enders, S. L. Katz, M. V Milovanovic, and A. Holloway, "Studies on an Attenuated Measles-Virus Vaccine," *N. Engl. J. Med.*, vol. 263, no. 4, pp. 153–159, Jul. 1960.
[121] D. E. Griffin and C. H. Pan, "Measles: Old vaccines, new vaccines," *Current Topics in Microbiology and Immunology*. 2009.
[122] J. L. Melnick, "Thermostability of poliovirus and measles vaccines.," *Dev. Biol. Stand.*, 1996.
[123] R. de Menezes Martins *et al.*, "Immunogenicity and safety of measles-mumps-rubella vaccine delivered by disposable-syringe jet injector in healthy Brazilian infants: A randomized non-inferiority study," *Contemp. Clin. Trials*, 2015.
[124] R. Reading, "A randomized, controlled trial of an aerosolized vaccine against measles," *Child: care, health and development*. 2015.
[125] M. M. Coughlin, A. S. Beck, B. Bankamp, and P. A. Rota, "Perspective on Global Measles Epidemiology and Control and the Role of Novel Vaccination Strategies," *Viruses*, vol. 9, no. 1, 2017.
[126] "Measles." [Online]. Available: http://www.who.int/immunization/monitoring_surveillance/burden/vpd/surveillance_type/active/measles/en/.
[127] "WHO 2016."
[128] P. M. Strebel *et al.*, "A world without measles," *Journal of Infectious Diseases*. 2011.
[129] P. A. Gastañaduy *et al.*, "A Measles Outbreak in an Underimmunized Amish Community in

Ohio," *N. Engl. J. Med.*, 2016.
[130] V. K. Phadke, R. A. Bednarczyk, D. A. Salmon, and S. B. Omer, "Association Between Vaccine Refusal and Vaccine-Preventable Diseases in the United States," *JAMA*, 2016.
[131] "European Centre for Disease Prevention and Control (ECDC)." [Online]. Available: https://ecdc.europa.eu/en/news-events/epidemiological-update-measles-monitoring-european-outbreaks-8-september-2017.
[132] "CDC update: Measles-United states," *MMWR Morb Mortal Wkly Rep. 2008*, 2008. .
[133] Y. Huiming, W. Chaomin, and M. Meng, "Vitamin A for treating measles in children," in *Cochrane Database of Systematic Reviews*, 2005.
[134] G. D. Hussey and M. Klein, "Routine high-dose vitamin a therapy for children hospitalized with measles," *J. Trop. Pediatr.*, 1993.
[135] J. A. Lecciones *et al.*, "A pilot double-blind, randomized, and placebo-controlled study of orally administered IFN-alpha-n1 (Ins) in pediatric patients with measles," *Journal of interferon & cytokine research : the official journal of the International Society for Interferon and Cytokine Research*. 1998.
[136] S. Hara *et al.*, "Combination therapy with intraventricular interferon-alpha and ribavirin for subacute sclerosing panencephalitis and monitoring measles virus RNA by quantitative PCR assay," *Brain Dev.*, 2003.
[137] H. Fernandez, G. Banks, and R. Smith, "Ribavirin: A clinical overview," *Eur. J. Epidemiol.*, 1986.
[138] A. Tomoda *et al.*, "Trial of intraventricular ribavirin therapy for subacute sclerosing panencephalitis in Japan," *Brain Dev.*, 2003.
[139] E. Freed and M. Martin, *Fields Virology*. 2013.
[140] N. K. Duggal and M. Emerman, "Evolutionary conflicts between viruses and restriction factors shape immunity.," *Nat. Rev. Immunol.*, vol. 12, no. 10, pp. 687–95, 2012.
[141] S. F. Kluge, D. Sauter, and F. Kirchhoff, "SnapShot: Antiviral Restriction Factors," *Cell*, vol. 163, no. 3, p. 774–774e1, 2015.
[142] A. M. Sheehy, N. C. Gaddis, J. D. Choi, and M. H. Malim, "Isolation of a human gene that inhibits HIV-1 infection and is suppressed by the viral Vif protein.," *Nature*, vol. 418, no. 6898, pp. 646–650, 2002.
[143] I. B. Rogozin *et al.*, "Evolution and diversification of lamprey antigen receptors: Evidence for involvement of an AID-APOBEC family cytosine deaminase," *Nat. Immunol.*, 2007.
[144] S. G. Conticello, "The AID/APOBEC family of nucleic acid mutators," *Genome Biology*. 2008.
[145] A. Jarmuz *et al.*, "An anthropoid-specific locus of orphan C to U RNA-editing enzymes on chromosome 22," *Genomics*, 2002.
[146] M. Muramatsu *et al.*, "Specific expression of activation-induced cytidine deaminase (AID), a novel member of the RNA-editing deaminase family in germinal center B cells," *J. Biol. Chem.*, 1999.
[147] M. T. Liddament, W. L. Brown, A. J. Schumacher, and R. S. Harris, "APOBEC3F properties and hypermutation preferences indicate activity against HIV-1 in vivo," *Curr. Biol.*, 2004.
[148] H. L. Wiegand, B. P. Doehle, H. P. Bogerd, and B. R. Cullen, "A second human antiretroviral factor, APOBEC3F, is suppressed by the HIV-1 and HIV-2 Vif proteins," *EMBO J.*, 2004.
[149] B. P. Doehle, A. Schäfer, and B. R. Cullen, "Human APOBEC3B is a potent inhibitor of HIV-1 infectivity and is resistant to HIV-1 Vif," *Virology*, 2005.
[150] J. D. Salter, R. P. Bennett, and H. C. Smith, "The APOBEC Protein Family: United by Structure, Divergent in Function," *Trends in Biochemical Sciences*. 2016.
[151] J. F. Hultquist *et al.*, "Human and Rhesus APOBEC3D, APOBEC3F, APOBEC3G, and APOBEC3H Demonstrate a Conserved Capacity To Restrict Vif-Deficient HIV-1," *J. Virol.*, 2011.
[152] B. R. Cullen, "Role and mechanism of action of the APOBEC3 family of antiretroviral resistance factors.," *J. Virol.*, 2006.
[153] F. Navarro *et al.*, "Complementary function of the two catalytic domains of APOBEC3G," *Virology*, 2005.
[154] J. S. Albin and R. S. Harris, "Interactions of host APOBEC3 restriction factors with HIV-1 in vivo: Implications for therapeutics," *Expert Reviews in Molecular Medicine*. 2010.
[155] C. Barnes and H. C. Smith, "Apolipoprotein B mRNA editing in vitro is a zinc-dependent process," *Biochem. Biophys. Res. Commun.*, vol. 197, no. 3, pp. 1410–1414, Dec. 1993.
[156] L. Betts, S. Xiang, S. A. Short, R. Wolfenden, and C. W. Carter, "Cytidine deaminase. the 2.3 Å crystal structure of an enzyme: Transition-state analog complex," *J. Mol. Biol.*, 1994.
[157] Q. Yu *et al.*, "Single-strand specificity of APOBEC3G accounts for minus-strand deamination of the HIV genome," *Nat. Struct. Mol. Biol.*, 2004.
[158] K. Shindo, A. Takaori-Kondo, M. Kobayashi, A. Abudu, K. Fukunaga, and T. Uchiyama, "The

Enzymatic Activity of CEM15/Apobec-3G Is Essential for the Regulation of the Infectivity of HIV-1 Virion but Not a Sole Determinant of Its Antiviral Activity," *J. Biol. Chem.*, 2003.
[159] E. N. C. Newman *et al.*, "Antiviral function of APOBEC3G can be dissociated from cytidine deaminase activity," *Curr. Biol.*, vol. 15, no. 2, pp. 166–170, 2005.
[160] Y. Iwatani *et al.*, "Deaminase-independent inhibition of HIV-1 reverse transcription by APOBEC3G," *Nucleic Acids Res*, 2007.
[161] R. K. Holmes, F. A. Koning, K. N. Bishop, and M. H. Malim, "APOBEC3F can inhibit the accumulation of HIV-1 reverse transcription products in the absence of hypermutation: Comparisons with APOBEC3G," *J. Biol. Chem.*, 2007.
[162] F. Guo, S. Cen, M. Niu, Y. Yang, R. J. Gorelick, and L. Kleiman, "The Interaction of APOBEC3G with Human Immunodeficiency Virus Type 1 Nucleocapsid Inhibits tRNA3Lys Annealing to Viral RNA," *J. Virol.*, 2007.
[163] S. Henriet, G. Mercenne, S. Bernacchi, J.-C. Paillart, and R. Marquet, "Tumultuous Relationship between the Human Immunodeficiency Virus Type 1 Viral Infectivity Factor (Vif) and the Human APOBEC-3G and APOBEC-3F Restriction Factors," *Microbiol. Mol. Biol. Rev.*, 2009.
[164] K. S. Stopak, Y. L. Chiu, J. Kropp, R. M. Grant, and W. C. Greene, "Distinct patterns of cytokine regulation of APOBEC3G expression and activity in primary lymphocytes, macrophages, and dendritic cells," *J Biol Chem*, vol. 282, no. 6, pp. 3539–3546, 2007.
[165] J. F. Kreisberg, W. Yonemoto, and W. C. Greene, "Endogenous factors enhance HIV infection of tissue naive CD4 T cells by stimulating high molecular mass APOBEC3G complex formation," *J. Exp. Med.*, 2006.
[166] A. G. Fisher *et al.*, "The sor gene of HIV-1 is required for efficient virus transmission in vitro," *Science (80-.).*, 1987.
[167] J. H. M. Simon, N. C. Gaddis, R. A. M. Fouchier, and M. H. Malim, "Evidence for a newly discovered cellular anti-HIV-1 phenotype," *Nat. Med.*, 1998.
[168] X. Yu *et al.*, "Induction of APOBEC3G Ubiquitination and Degradation by an HIV-1 Vif-Cul5-SCF Complex," *Science (80-.).*, 2003.
[169] R. K. Holmes, M. H. Malim, and K. N. Bishop, "APOBEC-mediated viral restriction: not simply editing?," *Trends in Biochemical Sciences*. 2007.
[170] S. Opi *et al.*, "Human Immunodeficiency Virus Type 1 Vif Inhibits Packaging and Antiviral Activity of a Degradation-Resistant APOBEC3G Variant," *J. Virol.*, 2007.
[171] K. M. Rose, M. Marin, S. L. Kozak, and D. Kabat, "Transcriptional regulation of APOBEC3G, a cytidine deaminase that hypermutates human immunodeficiency virus," *J. Biol. Chem.*, vol. 279, no. 40, pp. 41744–41749, 2004.
[172] H. Chen, L. W. Wang, Y. Q. Huang, and Z. J. Gong, "Interferon-alpha induces high expression of APOBEC3G and STAT-1 in Vitro and in Vivo," *Int. J. Mol. Sci.*, 2010.
[173] H. Muckenfuss *et al.*, "Sp1 and Sp3 regulate basal transcription of the human APOBEC3G gene," *Nucleic Acids Res.*, 2007.
[174] Y. Zeng, H. Li, X. Zhang, J. Shang, and Y. Kang, "Basal transcription of APOBEC3G is regulated by USF1 gene in hepatocyte," *Biochem. Biophys. Res. Commun.*, vol. 470, no. 1, pp. 54–60, 2016.
[175] B. D. Anderson and R. S. Harris, "Transcriptional regulation of APOBEC3 antiviral immunity through the CBF-β/RUNX axis.," *Sci. Adv.*, 2015.
[176] H. Oliva *et al.*, "Increased expression with differential subcellular location of cytidine deaminase APOBEC3G in human CD4+ T-cell activation and dendritic cell maturation," *Immunol. Cell Biol.*, 2016.
[177] L. S. Shlyakhtenko, A. Y. Lushnikov, M. Li, L. Lackey, R. S. Harris, and Y. L. Lyubchenko, "Atomic force microscopy studies provide direct evidence for dimerization of the HIV restriction factor APOBEC3G," *J. Biol. Chem.*, 2011.
[178] L. S. Shlyakhtenko, A. Y. Lushnikov, A. Miyagi, M. Li, R. S. Harris, and Y. L. Lyubchenko, "Nanoscale structure and dynamics of ABOBEC3G complexes with single-stranded DNA," *Biochemistry*, 2012.
[179] L. Chelico, E. J. Sacho, D. A. Erie, and M. F. Goodman, "A model for oligomeric regulation of APOBEC3G cytosine deaminase-dependent restriction of HIV," *J. Biol. Chem.*, 2008.
[180] H. Huthoff, F. Autore, S. Gallois-Montbrun, F. Fraternali, and M. H. Malim, "RNA-dependent oligomerization of APOBEC3G Is required for restriction of HIV-1," *PLoS Pathog.*, 2009.
[181] K. R. Chaurasiya *et al.*, "Oligomerization transforms human APOBEC3G from an efficient enzyme to a slowly dissociating nucleic acid-binding protein," *Nat. Chem.*, 2014.
[182] S. Gallois-Montbrun *et al.*, "Antiviral protein APOBEC3G localizes to ribonucleoprotein complexes found in P bodies and stress granules.," *J. Virol.*, vol. 81, no. 5, pp. 2165–78, 2007.
[183] Y.-L. Chiu *et al.*, "High-molecular-mass APOBEC3G complexes restrict Alu

retrotransposition," *Proc. Natl. Acad. Sci.*, 2006.
[184] S. L. Kozak, M. Marin, K. M. Rose, C. Bystrom, and D. Kabat, "The anti-HIV-1 editing enzyme APOBEC3G binds HIV-1 RNA and messenger RNAs that shuttle between polysomes and stress granules," *J. Biol. Chem.*, 2006.
[185] P. Villacé, R. M. Marión, and J. Ortín, "The composition of Staufen-containing RNA granules from human cells indicates their role in the regulated transport and translation of messenger RNAs," *Nucleic Acids Res.*, 2004.
[186] P. Turelli, B. Mangeat, S. Jost, S. Vianin, and D. Trono, "Inhibition of hepatitis B virus replication by APOBEC3G.," *Science*, 2004.
[187] R. Chen, X. Zhao, Y. Wang, Y. Xie, and J. Liu, "Hepatitis B virus X protein is capable of down-regulating protein level of host antiviral protein APOBEC3G," *Sci. Rep.*, 2017.
[188] R. Mahieux *et al.*, "Extensive editing of a small fraction of human T-cell leukemia virus type 1 genomes by four APOBEC3 cytidine deaminases," *J. Gen. Virol.*, 2005.
[189] Y. P. Zhu *et al.*, "Host APOBEC3G protein inhibits HCV replication through direct binding at NS3," *PLoS One*, vol. 10, no. 3, p. e0121608, 2015.
[190] H. Chen *et al.*, "APOBEC3A is a potent inhibitor of adeno-associated virus and retrotransposons," *Curr. Biol.*, 2006.
[191] C. M. Okeoma, N. Lovsin, B. M. Peterlin, and S. R. Ross, "APOBEC3 inhibits mouse mammary tumour virus replication in vivo," *Nature*, 2007.
[192] M. Fehrholz *et al.*, "The innate antiviral factor APOBEC3G targets replication of measles, mumps and respiratory syncytial viruses," *J. Gen. Virol.*, vol. 93, no. 3, pp. 565–576, 2012.
[193] A. Milewska *et al.*, "APOBEC3-mediated restriction of RNA virus replication," *Sci. Rep.*, 2018.
[194] S. Vega-Rubin-de-Celis, Z. Abdallah, L. Kinch, N. V. Grishin, J. Brugarolas, and X. Zhang, "Structural analysis and functional implications of the negative mTORC1 regulator REDD1," *Biochemistry*, 2010.
[195] T. Shoshani *et al.*, "Identification of a novel hypoxia-inducible factor 1-responsive gene, RTP801, involved in apoptosis.," *Mol. Cell. Biol.*, 2002.
[196] L. W. Ellisen *et al.*, "REDD1, a developmentally regulated transcriptional target of p63 and p53, links p63 to regulation of reactive oxygen species," *Mol. Cell*, 2002.
[197] Z. Wang, M. H. Malone, M. J. Thomenius, F. Zhong, F. Xu, and C. W. Distelhorst, "Dexamethasone-induced gene 2 (dig2) is a novel pro-survival stress gene induced rapidly by diverse apoptotic signals," *J. Biol. Chem.*, 2003.
[198] H.-O. Jin *et al.*, "Activating transcription factor 4 and CCAAT/enhancer-binding protein-beta negatively regulate the mammalian target of rapamycin via Redd1 expression in response to oxidative and endoplasmic reticulum stress.," *Free Radic. Biol. Med.*, 2009.
[199] N. K. McGhee, L. S. Jefferson, and S. R. Kimball, "Elevated corticosterone associated with food deprivation upregulates expression in rat skeletal muscle of the mTORC1 repressor, REDD1.," *J. Nutr.*, 2009.
[200] M. Lee, M. Bikram, S. Oh, D. A. Bull, and W. K. Sung, "Sp1-dependent regulation of the RTP801 promoter and its application to hypoxia-inducible VEGF plasmid for ischemic disease," *Pharm. Res.*, 2004.
[201] M. L. Whitney, L. S. Jefferson, and S. R. Kimball, "ATF4 is necessary and sufficient for ER stress-induced upregulation of REDD1 expression," *Biochem. Biophys. Res. Commun.*, 2009.
[202] S. R. Kimball, A. N. D. Do, L. Kutzler, D. R. Cavener, and L. S. Jefferson, "Rapid turnover of the mTOR complex 1 (mTORC1) repressor REDD1 and activation of mTORC1 signaling following inhibition of protein synthesis," *J. Biol. Chem.*, 2008.
[203] J. Brugarolas *et al.*, "Regulation of mTOR function in response to hypoxia by REDD1 and the TSC1/TSC2 tumor suppressor complex," *Genes Dev.*, 2004.
[204] K. Inoki, Y. Li, T. Xu, and K. L. Guan, "Rheb GTpase is a direct target of TSC2 GAP activity and regulates mTOR signaling," *Genes Dev.*, 2003.
[205] X. Long, Y. Lin, S. Ortiz-Vega, K. Yonezawa, and J. Avruch, "Rheb binds and regulates the mTOR kinase," *Curr. Biol.*, 2005.
[206] M. P. Deyoung, P. Horak, A. Sofer, D. Sgroi, and L. W. Ellisen, "Hypoxia regulates TSC1/2-mTOR signaling and tumor suppression through REDD1-mediated 14-3-3 shuttling," *Genes Dev.*, 2008.
[207] J. H. Reiling and E. Hafen, "The hypoxia-induced paralogs Scylla and Charybdis inhibit growth by down-regulating S6K activity upstream of TSC in Drosophila," *Genes Dev.*, 2004.
[208] M. N. Corradetti, K. Inoki, and K. L. Guan, "The stress-inducted proteins RTP801 and RTP801L are negative regulators of the mammalian target of rapamycin pathway," *J. Biol. Chem.*, 2005.
[209] M. Laplante *et al.*, "mTOR signaling at a glance.," *J. Cell Sci.*, 2009.
[210] R. J. O. Dowling, I. Topisirovic, B. D. Fonseca, and N. Sonenberg, "Dissecting the role of

mTOR: Lessons from mTOR inhibitors," *Biochimica et Biophysica Acta - Proteins and Proteomics*. 2010.
[211] Y. Zheng *et al.*, "A role for mammalian target of rapamycin in regulating T cell activation versus anergy.," *J. Immunol.*, 2007.
[212] D. S. Dos *et al.*, "Rictor, a novel binding partner of mTOR, defines a rapamycin-insensitive and raptor-independent pathway that regulates the cytoskeleton," *Curr. Biol.*, 2004.
[213] T. R. Peterson *et al.*, "DEPTOR Is an mTOR Inhibitor Frequently Overexpressed in Multiple Myeloma Cells and Required for Their Survival," *Cell*, 2009.
[214] R. A. Saxton and D. M. Sabatini, "mTOR Signaling in Growth, Metabolism, and Disease," *Cell*. 2017.
[215] X. M. Ma and J. Blenis, "Molecular mechanisms of mTOR-mediated translational control," *Nature Reviews Molecular Cell Biology*. 2009.
[216] S. Katiyar *et al.*, "REDD1, an inhibitor of mTOR signalling, is regulated by the CUL4A-DDB1 ubiquitin ligase.," *EMBO Rep.*, vol. 10, no. 8, pp. 866–872, 2009.
[217] C. Y. Tan and T. Hagen, "mTORC1 dependent regulation of REDD1 protein stability," *PLoS One*, vol. 8, no. 5, p. e63970, 2013.
[218] J. Chung, C. J. Kuo, G. R. Crabtree, and J. Blenis, "Rapamycin-FKBP specifically blocks growth-dependent activation of and signaling by the 70 kd S6 protein kinases," *Cell*, 1992.
[219] R. Stan, M. M. McLaughlin, R. Cafferkey, R. K. Johnson, M. Rosenberg, and G. P. Livi, "Interaction between FKBP12-rapamycin and TOR involves a conserved serine residue," *J. Biol. Chem.*, 1994.
[220] J. Chen, X. F. Zheng, E. J. Brown, and S. L. Schreiber, "Identification of an 11-kDa FKBP12-rapamycin-binding domain within the 289-kDa FKBP12-rapamycin-associated protein and characterization of a critical serine residue.," *Proc. Natl. Acad. Sci.*, 1995.
[221] E. Jacinto *et al.*, "Mammalian TOR complex 2 controls the actin cytoskeleton and is rapamycin insensitive," *Nat. Cell Biol.*, 2004.
[222] V. Le Sage, A. Cinti, R. Amorim, and A. J. Mouland, "Adapting the stress response: Viral subversion of the mTOR signaling pathway," *Viruses*, vol. 8, no. 6, pp. 1–19, 2016.
[223] M. A. Mata *et al.*, "Chemical inhibition of RNA viruses reveals REDD1 as a host defense factor," *Nat Chem Biol*, vol. 7, no. 10, pp. 712–719, 2011.
[224] S. Munro and H. R. B. Pelham, "A C-terminal signal prevents secretion of luminal ER proteins," *Cell*, 1987.
[225] K. G. Hardwick, M. J. Lewis, J. Semenza, N. Dean, and H. R. Pelham, "ERD1, a yeast gene required for the retention of luminal endoplasmic reticulum proteins, affects glycoprotein processing in the Golgi apparatus," *EMBO J*, 1990.
[226] J. C. Semenza, K. G. Hardwick, N. Dean, and H. R. B. Pelham, "ERD2, a yeast gene required for the receptor-mediated retrieval of luminal ER proteins from the secretory pathway," *Cell*, 1990.
[227] M. J. Lewis and H. R. B. Pelham, "A human homologue of the yeast HDEL receptor," *Nature*, 1990.
[228] M. Capitani and M. Sallese, "The KDEL receptor: new functions for an old protein.," *FEBS Lett.*, vol. 583, no. 23, pp. 3863–71, Dec. 2009.
[229] D. Kamimura *et al.*, "KDEL receptor 1 regulates T-cell homeostasis via PP1 that is a key phosphatase for ISR," *Nat. Commun.*, 2015.
[230] K. Yamamoto *et al.*, "The KDEL receptor mediates a retrieval mechanism that contributes to quality control at the endoplasmic reticulum," *EMBO J.*, 2001.
[231] M. J. Lewis and H. R. B. Pelham, "Ligand-induced redistribution of a human KDEL receptor from the Golgi complex to the endoplasmic reticulum," *Cell*, 1992.
[232] V. W. Hsu, N. Shah, and R. D. Klausner, "A brefeldin A-like phenotype is induced by the overexpression of a human ERD-2-like protein, ELP-1," *Cell*, 1992.
[233] D. W. Wilson, M. J. Lewis, and H. R. B. Pelham, "pH-dependent binding of KDEL to its receptor in vitro," *J. Biol. Chem.*, 1993.
[234] M. M. Wu, M. Grabe, S. Adams, R. Y. Tsien, H. P. H. Moore, and T. E. Machen, "Mechanisms of pH Regulation in the Regulated Secretory Pathway," *J. Biol. Chem.*, 2001.
[235] V. Saudek, "Cystinosin, MPDU1, SWEETs and KDELR belong to a well-defined protein family with putative function of cargo receptors involved in vesicle trafficking," *PLoS One*, vol. 7, no. 2, 2012.
[236] M. Giannotta *et al.*, "The KDEL receptor couples to Galphaq/11 to activate Src kinases and regulate transport through the Golgi," *EMBO J*, vol. 31, no. 13, pp. 2869–2881, 2012.
[237] K. Yamamoto, H. Hamada, H. Shinkai, Y. Kohno, H. Koseki, and T. Aoe, "The KDEL receptor modulates the endoplasmic reticulum stress response through mitogen-activated protein kinase signaling cascades.," *J. Biol. Chem.*, vol. 278, no. 36, pp. 34525–34532, 2003.

[238] C. Ruggiero *et al.*, "A Golgi-based KDELR-dependent signalling pathway controls extracellular matrix degradation," vol. 6, no. 5.
[239] V. Cherezov *et al.*, "High-resolution crystal structure of an engineered human beta2-adrenergic G protein-coupled receptor.," *Science*, 2007.
[240] T. Inoue and B. Tsai, "How viruses use the endoplasmic reticulum for entry, replication, and assembly," *Cold Spring Harb Perspect Biol*, vol. 5, no. 1, p. a013250, 2013.
[241] D. Egger *et al.*, "Expression of Hepatitis C Virus Proteins Induces Distinct Membrane Alterations Including a Candidate Viral Replication Complex," *J. Virol.*, 2002.
[242] S. Welsch *et al.*, "Composition and Three-Dimensional Architecture of the Dengue Virus Replication and Assembly Sites," *Cell Host Microbe*, 2009.
[243] M. Y. Li *et al.*, "KDEL Receptors Assist Dengue Virus Exit from the Endoplasmic Reticulum," *Cell Rep.*, vol. 10, no. 9, pp. 1496–1507, 2015.
[244] R. Wang, Y.-J. Wu, H.-S. Chen, and C.-J. Chen, "A KDEL Retrieval System for ER-Golgi Transport of Japanese Encephalitis Viral Particles," *Viruses*, vol. 8, no. 2, p. 44, 2016.
[245] L. Zhang *et al.*, "A role for the host coatomer and KDEL receptor in early vaccinia biogenesis," vol. 106, no. 1, pp. 163–168, 2009.
[246] H. Vennema, L. Heijnen, P. J. Rottier, M. C. Horzinek, and W. J. Spaan, "A novel glycoprotein of feline infectious peritonitis coronavirus contains a KDEL-like endoplasmic reticulum retention signal.," *Adv. Exp. Med. Biol.*, vol. 342, no. 8, pp. 209–214, 1993.
[247] L. Ellgaard and a. Helenius, "Quality control in the endoplasmic reticulum," *Nat. Rev. Mol. Cell Biol.*, vol. 4, no. 3, pp. 181–191, 2003.
[248] A. Bertolotti, Y. Zhang, L. M. Hendershot, H. P. Harding, and D. Ron, "Dynamic interaction of BiP and ER stress transducers in the unfolded-protein response," *Nat. Cell Biol.*, 2000.
[249] Q. J. Quinones, G. G. de Ridder, and S. V. Pizzo, "GRP78: A chaperone with diverse roles beyond the endoplasmic reticulum," *Histol. Histopathol.*, vol. 23, no. 11, pp. 1409–1416, 2008.
[250] C. Hetz, "The unfolded protein response: controlling cell fate decisions under ER stress and beyond," *Nat. Publ. Gr.*, vol. 13, no. 2, pp. 89–102, 2012.
[251] S.-W. Chan, "The unfolded protein response in virus infections," *Frontiers in Microbiology*, vol. 5. 2014.
[252] M. Zinke *et al.*, "Clearance of measles virus from persistently infected cells by short hairpin RNA," *J Virol*, vol. 83, no. 18, pp. 9423–9431, 2009.
[253] T. Dull *et al.*, "A third-generation lentivirus vector with a conditional packaging system," *J Virol*, vol. 72, no. 11, pp. 8463–8471, 1998.
[254] K. D. Shives, E. L. Beatman, M. Chamanian, C. O'Brien, J. Hobson-Peters, and J. D. Beckham, "West nile virus-induced activation of mammalian target of rapamycin complex 1 supports viral growth and viral protein expression," *J Virol*, vol. 88, no. 16, pp. 9458–9471, 2014.
[255] X. Fu, L. Tao, A. Rivera, and X. Zhang, "Rapamycin enhances the activity of oncolytic herpes simplex virus against tumor cells that are resistant to virus replication," *Int J Cancer*, vol. 129, no. 6, pp. 1503–1510, 2011.
[256] T. R. Fenton and I. T. Gout, "Functions and regulation of the 70kDa ribosomal S6 kinases," *Int J Biochem Cell Biol*, vol. 43, no. 1, pp. 47–59, 2011.
[257] E. L. Reuschel *et al.*, "REDD1 Is Essential for Optimal T Cell Proliferation and Survival," *PLoS One*, vol. 10, no. 8, p. e0136323, 2015.
[258] M. Y. Li, R. Bruzzone, and P. G. Wang, "New tricks for KDEL receptors," *Oncotarget*, vol. 6, no. 31, pp. 30425–30426, 2015.
[259] R. K. Plemper, a L. Hammond, and R. Cattaneo, "Measles virus envelope glycoproteins hetero-oligomerize in the endoplasmic reticulum," *J. Biol. Chem.*, vol. 276, no. 47, pp. 44239–44246, 2001.
[260] M. A. Brindley, S. Chaudhury, and R. K. Plemper, "Measles virus glycoprotein complexes preassemble intracellularly and relax during transport to the cell surface in preparation for fusion," *J Virol*, vol. 89, no. 2, pp. 1230–1241, 2015.
[261] C. B. Ruth Firsching Urs Schneider, Roberto Cattaneo, Volker ter Meulen, Jürgen Schneider-Schaulies, "Measles Virus Spread by Cell-Cell Contacts: Uncoupling ofContact-Mediated Receptor (CD46) Downregulationfrom Virus Uptake," *J. Virol.*, vol. Vol 73,No7, pp. 5265–5273, 1999.
[262] C. Richetta *et al.*, "Sustained Autophagy Contributes to Measles Virus Infectivity," *PLoS Pathog.*, vol. 9, no. 9, 2013.
[263] Y. Zhang, R. Liu, M. Ni, P. Gill, and A. S. Lee, "Cell surface relocalization of the endoplasmic reticulum chaperone and unfolded protein response regulator GRP78/BiP," *J Biol Chem*, vol. 285, no. 20, pp. 15065–15075, 2010.
[264] G. Bolt, "The measles virus (MV) glycoproteins interact with cellular chaperones in the endoplasmic reticulum and MV infection upregulates chaperone expression.," *Arch Virol*,

vol. 146, no. 11, p. 2055, 2001.
[265] G. Prelich, "Gene overexpression: Uses, mechanisms, and interpretation," *Genetics*. 2012.
[266] V. Tiwarekar, J. Wohlfahrt, M. Fehrholz, C.-J. Scholz, S. Kneitz, and J. Schneider-Schaulies, "APOBEC3G-regulated host factors interfere with measles virus replication: role of REDD1 and mTORC1 inhibition," *J. Virol.* , Jun. 2018.
[267] S. Sharma, S. K. Patnaik, R. T. Taggart, and B. E. Baysal, "The double-domain cytidine deaminase APOBEC3G is a cellular site-specific RNA editing enzyme," *Sci. Rep.*, 2016.
[268] S. Sharma *et al.*, "APOBEC3A cytidine deaminase induces RNA editing in monocytes and macrophages," *Nat. Commun.*, 2015.
[269] C. Vogel and E. M. Marcotte, "Insights into the regulation of protein abundance from proteomic and transcriptomic analyses," *Nat Rev Genet*, vol. 13, no. 4, pp. 227–232, 2012.
[270] L. Lackey, E. K. Law, W. L. Brown, and R. S. Harris, "Subcellular localization of the APOBEC3 proteins during mitosis and implications for genomic DNA deamination," *Cell Cycle*, vol. 12, no. 5, pp. 762–772, 2013.
[271] A. M. Green *et al.*, "APOBEC3A damages the cellular genome during DNA replication," *Cell Cycle*, 2016.
[272] Y. Wang, K. Schmitt, K. Guo, M. L. Santiago, and E. B. Stephens, "Role of the single deaminase domain APOBEC3A in virus restriction, retrotransposition, DNA damage and cancer," *Journal of General Virology*. 2016.
[273] B. Rentier, E. L. Hooghe-Peters, and M. Dubois-Dalcq, "Electron microscopic study of measles virus infection: cell fusion and hemadsorption.," *J. Virol.*, 1978.
[274] K. Takeuchi, N. Miyajima, N. Nagata, M. Takeda, and M. Tashiro, "Wild-type measles virus induces large syncytium formation in primary human small airway epithelial cells by a SLAM(CD150)-independent mechanism," *Virus Res.*, 2003.
[275] J. T. Roehrig, R. A. Bolin, and R. G. Kelly, "Monoclonal antibody mapping of the envelope glycoprotein of the dengue 2 virus, Jamaica," *Virology*, 1998.
[276] D. Vasconcelos, E. Norrby, and M. Oglesbee, "The cellular stress response increases measles virus-induced cytopathic effect," *J. Gen. Virol.*, vol. 79, no. 7, pp. 1769–1773, 1998.
[277] Y. Tanaka, B. R. Heminway, and M. S. Galinski, "Down-regulation of paramyxovirus hemagglutinin-neuraminidase glycoprotein surface expression by a mutant fusion protein containing a retention signal for the endoplasmic reticulum.," *J. Virol.*, vol. 70, pp. 5005–5015, 1996.
[278] H. Sato *et al.*, "Measles virus induces cell-type specific changes in gene expression," *Virology*, 2008.
[279] N. C. Wolff, R. M. McKay, and J. Brugarolas, "REDD1/DDIT4-independent mTORC1 Inhibition and Apoptosis by Glucocorticoids in Thymocytes.," *Mol. Cancer Res.*, 2014.
[280] B. Kucejova *et al.*, "Interplay Between pVHL and mTORC1 Pathways in Clear-Cell Renal Cell Carcinoma," *Mol. Cancer Res.*, 2011.
[281] R. Salonen, J. Ilonen, and A. Salmi, "Measles virus infection of unstimulated blood mononuclear cells in vitro: antigen expression and virus production preferentially in monocytes.," *Clin. Exp. Immunol.*, 1988.
[282] B. S. Joseph, P. W. Lampert, and M. B. Oldstone, "Replication and persistence of measles virus in defined subpopulations of human leukocytes," *J. Virol.*, 1975.
[283] J. R. Huddlestone, P. W. Lampert, and M. B. A. Oldstone, "Virus-lymphocyte interactions: Infection of TGand TMsubsets by measles virus," *Clin. Immunol. Immunopathol.*, 1980.
[284] M. R. Patel *et al.*, "Measles vaccine strains for virotherapy of non-small-cell lung carcinoma.," *J. Thorac. Oncol.*, 2014.
[285] J. Roy, J.-S. Paquette, J.-F. Fortin, and M. J. Tremblay, "The immunosuppressant rapamycin represses human immunodeficiency virus type 1 replication.," *Antimicrob. Agents Chemother.*, 2002.
[286] E. Besnard *et al.*, "The mTOR Complex Controls HIV Latency.," *Cell Host Microbe*, vol. 20, no. 6, pp. 785–797, 2016.
[287] L. A. Berven and M. F. Crouch, "Cellular function of p70(S6K): A role in regulating cell motility," in *Immunology and Cell Biology*, 2000.
[288] D. J. Price, J. R. Grove, V. Calvo, J. Avruch, and B. E. Bierer, "Rapamycin-induced inhibition of the 70-kilodalton S6 protein kinase," *Science (80-.).*, 1992.
[289] O. Decaux *et al.*, "Inhibition of mTORC1 activity by REDD1 induction in myeloma cells resistant to bortezomib cytotoxicity," *Cancer Sci.*, 2010.
[290] M. P. Courageot, M. P. Frenkiel, C. D. Dos Santos, V. Deubel, and P. Desprès, "Alpha-glucosidase inhibitors reduce dengue virus production by affecting the initial steps of virion morphogenesis in the endoplasmic reticulum.," *J. Virol.*, 2000.
[291] H. R. Pelham, "The dynamic organisation of the secretory pathway.," *Cell Struct. Funct.*, vol.

21, no. 5, pp. 413–419, 1996.
[292] V. W. Hsu, N. Shah, and R. D. Klausner, "A brefeldin A-like phenotype is induced by the overexpression of a human ERD-2-like protein, ELP-1," *Cell*, vol. 69, no. 4, pp. 625–635, 1992.
[293] J. B. Gifford *et al.*, "Expression of GRP78, Master Regulator of the Unfolded Protein Response, Increases Chemoresistance in Pancreatic Ductal Adenocarcinoma," *Mol. Cancer Ther.*, 2016.

APPENDICES

Appendices

A. Acronyms and symbols

°C	Centigrade
3D	3-Dimensional
A	Adenine
AAV	Adeno-Associated Virus
Abs	Antibody
ACY1	Aminoacylase 1
ADRB2	β2-Adrenergic Receptor
Ag	Antigen
AG	Arbeit Gruppe
AID	Activation-Induced Cytidine Deaminase
AIDS	Acquired Immunodeficiency Syndrome
Akt	Protein Kinases B
APC	Antigen Presenting Cell
APOBEC3G	Apolipoprotein B mRNA editing enzyme, catalytic peptide-like 3G
APS	Ammonium Per Sulphate
ARF1	ADP Ribosylation Factor
Asp	Aspartate
ATV	Antibiotic-Trypsin-Versene
b-TRCP	Beta-Transducin Repeat-Containing Protein
BALT	Bronchus-Associated Lymphoid Tissue
BCA	Bicinchoninic acid
bp	Base pair
BSA	Bovine serum albumin
BSS	Balanced salt solution
C-Terminus	Carboxy-Terminus
$CaCl_2$	Calcium chloride
CBF-b	Core-binding factor subunit beta
CD	Cluster of differentiation
cDNA	Complementary DNA
CDV	Canine distemper virus
CEM15	APOBEC3G
CIAP	Calf intestine alkaline phosphatase
cm	Centimetre
cm^2	Centimetre Square
CNS	Central nervous system

CoIP	Co-Immunoprecipitation
CPE	Cytopathic effect
CRT	Calreticulin
CSF	Cerebrospinal Fluid
CT	Cytoplasmic Tail
CTD	C-terminal Domain
CUL4A	Cullin 4A
$CuSO_4$	Copper Sulphate
DAPI	4',6-Diamidin-2-phenylindol
dATP	Deoxyadenosine-5'- triphosphate
DCs	Dendritic cells
dCTP	Deoxycytidin-5'- Triphosphate
DDB1	DNA damage-binding protein 1
DDIT4	REDD-1; DNA Damage Inducible Transcript 4
DENV	Dengue virus
Deptor	DEP domain containing mTOR-interacting protein
dGTP	Deoxyguanosin-5'- triphosphate
dH_2O	Distilled water
DMEM	Dulbecco's modified Eagle's medium
DMSO	Dimethyl sulfoxide
DNA	Deoxyribonucleic acid
dNTP	2'-Deoxyribonucleoside-5'- triphosphate
dpi	Days post infection
Dr.	Doctor
DTT	Dithiothreitol
ECDC	European Centre for Disease Prevention and Control
Edm	Edmonston
EDTA	Ethylenediaminetetraacetic acid
eGFP	Enhanced green fluorescent protein
EM	Electron microscopy
env	Envelop
ER	Endoplasmic reticulum
ERAD	ER-associated degradation
ESCRT	Endosomal sorting complexes required for transport
et al.	and others
F	Forward
F	MV Fusion protein
FACS	Fluorescence-activated cell sorting
FCS	Fetal calf serum

FIP	Fusion Inhibitory Peptide
FKBP12	FK506 binding protein of 12kDa
FP	Fusion peptide
FRB	FKBP12-rapamycin binding
FSC	Forward Scatter
gag	Group antigen
GAP	GTPase-activating proteins
GAPDH	Glyceraldehyde 3-phosphate dehydrogenase
Gly	Glycine
GPCR	G protein-coupled receptors
GRP78	78 kDa glucose-regulated protein
GRP94	Heat shock protein 90kDa beta member 1
GSK3b	Glycogen synthase kinase-3b
GTP	Guanosine triphosphate
GTP	Guanosine triphosphate
H	MV Hemagglutinin protein
HA	Hemagglutinin of Influenza virus
hA3G	Human APOBEC3G
HCl	Hydrogen chloride
HEK	Human Embryonic Kidney cell
HEPES	4-(2-hydroxyethyl)-1-piperazineethanesulfonic acid
HIV	Human Immunodeficiency Virus
HMM	High molecular mass complex of A3G
hpi	Hours post infection
HPLC	High performance liquid chromatography
HRA	Heptad repeat A
HRB	Heptad repeat B
HRP	Horseradish peroxidase
ICTV	International Committee on Taxonomy of Viruses
IFITIM	Interferon-induced transmembrane protein
IFN	Interferon
IgG	Immunoglobulin G
IgM	immunoglobulin M
IKKB	IκB kinase
Il-1α	Interleukin-1α
Il-1ß	Interleukin-1ß
IP	Immunoprecipitation
IRE1	Inositol-requiring protein 1
IRF-3	IFN regulatory factor-3

ISGs	Interferon-inducible genes
JAK	Janus kinase
JEV	Japanese encephalitis virus
KAP1	KRAB-associated protein 1
kb	Kilobase pair
KCl	Potassium chloride
kDa	Kilodalton
KDEL	Lysin-aspartic acid-glutamic acid-leucine
KDELR2	ER Lumen Protein Retaining Receptor 2
KH_2PO_4	Monopotassium phosphate
L	MV Large protein
LB	Luria-Bertani
LFA-1	Leucocyte function-associated antigen-1
LMM	Low molecular mass complex of A3g
log	Logarithm
LOXL 1	Lysyl-Oxidase
LTR	Long terminal Repeat
M	Molar
M-MLV	Moloney Murine Leukemia Virus
mA	Milliampere
mAb	Monoclonal antibody
MEM	Minimum essential medium
$MgCl_2$	Magnesium chloride
MIBE	Measles Inclusion Body Encephalitis
min	Minute
mLST8	Mammalian lethal with Sec13 protein 8
MLV	Murine leukemia virus
mM	Millimolar
mm	Millimetre
MMTV	Mouse mammary tumour virus
MOI	Multiplicity of infection
MOPS	3-Morpholinopropanesulfonic acid
MOSC	Molybdenum Cofactor Sulfurase C-terminal Domain
MOSC1	MOSC Domain-Containing Protein 1
MOSC2	MOSC-Domain-Containing Protein 2
mRNA	Messenger RNA
mTORC1	Mammalian Target of Rapamycin 1
MuV	Mumps virus
MV	Measles virus

MxB	Myxovirus resistance gene B
N	Nucleoprotein
N-Terminus	Amino terminus
N/A	Not applicable
Na_2 EDTA	EDTA disodium salt hydrate
NaCl	Sodium Chloride
NaF	Sodium fluoride
$NaHPO_4$	Sodium phosphate
NaOH	Sodium hydroxide
NC membrane	Nitrocellulose membrane
NF κB	Inducibility of κ-Immunoglobulin Enhancer-Binding Protein
ng	Nanogram
NK cell	Natural killer cell
NLRs	NOD-like receptors
nm	Nanometer
NP-40	Nonidet P-40
nt	Nucleotide
NTD	N-terminal domain
NTE	Sodium-Tris-EDTA
OD	Optical density
Oligo-dT	Oligodeoxy-thymidine nucleotides
OPD	o-Phenylenediamine
ORF	Open reading frame
P	Phospho protein (MV)
P-bodies	RNA processing bodies
PAGE	Polyacrylamide gel electrophoresis
PAMP	Pathogen associated molecular patterns
PAMPs	Pathogen associated molecular patterns
PBL	Peripheral blood lymphocytes
PBMC	Peripheral blood mononuclear cells
PBS	Phosphate Buffered Saline
PCR	Polymerase chain reaction
PCT	P-protein C-terminal domain
PEI	Polyethyleneimine
PERK	Protein kinase RNA-like endoplasmic reticulum kinase
PFA	Paraformaldehyde
pfu	Plaque forming unit
pH	power of hydrogen
PHA	Polyhydroxyalkanoates

Phe	Phenylalanine
PKR	(ds)RNA-dependent protein kinase R
pmol	Picomole
PNT	P protein N-terminal domain
pol	Polymerase
PP1	Protein phosphatase 1
PPRs	Pattern recognition receptors
PPRV	Peste's Petits Ruminants Virus
PRAS40	Proline-rich Akt substrate of 40 kDa
PRDX1	Peroxiredoxin 1
Prof.	Professor
PRRs	Pattern recognition receptors
PVRL-4	Polio virus receptor-like protein-4
R	Reverse
RBC	Red blood cells
RdRp	RNA dependent RNA polymerase
REDD-1	Regulated in Development and DNA Damage Responses 1
rev	Reverse
Rheb	Ras homolog enriched in brain
RIG-I	Retinoic acid-inducible gene I
RIPA	Radio-immuno precipitation assay
RISC	RNA-induced Silencing Complex
RLRs	RIG-I like receptors
rMV	Recombinant Measles Virus
RNA	Ribonucleic acid
RNP	Ribonucleoprotein
ROC1	Regulator of cullins 1
rpm	Rotations per minute
RPV	Rinderpest virus
RRE	Rev Responsive Element
RSV	Respiratory Syncytial Virus
RT	Room Temperature
RT-PCR	Reverse Transcriptase polymerase chain reaction
S6K1	Ribosomal protein S6 kinase beta-1
SAMHD	SAM domain and HD domain-containing protein 1
SDS	Sodium dodecyl sulphate
SERNIC5	Serine incorporator
SFKs	Src family kinases
shRNA	Small hairpin RNA

siRNA	Small interfering RNA
SIV	Simian Immunodeficiency Virus
SLAM	Signalling Lymphocytic Activation Molecule
Sp1	Specificity protein 1
Sp3	Specificity protein 3
SPINK5	Serine Peptidase Inhibitor, Kazal type 5
SPINK6	Serine Peptidase Inhibitor, Kazal type 6
ss	Single-stranded
SSC	Side scatter
SSPE	Subacute sclerosing pan encephalitis
STAT	Signal transducer and activator of transcription (STAT) protein
T	Thymidine
TAE	Tris-Acetate-EDTA
TAR	Transactivation response element
TCID50	Tissue Culture Infectious Dose
TE	Tris-EDTA
TEMED	Tetramethylethylenediamine
TGFβ1	Transforming Growth Factor
T_H1	Th1 helper cell
TLR	Toll-like receptor
TLRs	Toll-like receptors
TM	Transmembrane domain
TRIM5	Tripartite motif-containing protein 5
TRIS	Tris(hydroxymethyl)-aminomethan
tRNA	Transfer-RNA
TSC2	Tuberous sclerosis complex
TXNIP	Thioredoxin-Interacting Protein
U	Uracil
UPR	Unfolded protein response
USF1	Upstream regulatory factor 1
UTR	Untranslated region
UV	Ultraviolet
V	Voltage
Vif	Virion infectivity factor
VLP	Virus-like particle
vpr	Viral Protein R
vpu	Viral Protein U
VSV	Vesicular Stomatitis Virus
WBCs	White blood cells

WHO	World Health Organization
WT	Wild Type
$x\,g$	Gravitational Constant
ZAP	Zinc-finger antiviral protein
µg	Micro gram
µl	Micro litre
µM	Micro molar
µM	Micro meter

B. List of publications and Presentations

Research article

1. APOBEC3G-regulated host factors interfere with measles virus replication: role of REDD1 and mTORC1 inhibition

   Vishakha Tiwarekar, Julia Wohlfahrt, Markus Fehrholz, Claus-Jürgen Scholz, Susanne Kneitz, Jürgen Schneider-Schaulies. *Journal of Virology 92: e00835-18. https://doi.org/10.1128/JVI.00835-18.*

2. KDELR2 competes with measles virus hemagglutinin for cellular chaperones and reduces chaperone-mediated cell surface transport of the hemagglutinin

   Vishakha Tiwarekar, Markus Fehrholz, Jürgen Schneider-Schaulies. *Viruses. 2019 Jan 4;11, 27.*

Poster presentations

1. Analysis of Host factors in Measles virus replication.
   Vishakha Tiwarekar, Julia Wohlfahrt, Sabine Kendl, Markus Fehrholz, Jürgen Schneider-Schaulies. Eureka! 10th International GSLS Symposium, Rudolf-Virchow Center, University of Würzburg, Germany (2015).
2. Analysis of APOBEC3G-mediated inhibition of Measles virus replication.
   Vishakha Tiwarekar, Sabine Kendl, Julia Wohlfahrt, Markus Fehrholz, Jürgen Schneider-Schaulies. 26th Annual Meeting of the Society of Virology, Münster, Germany (2016).
3. Analysis of APOBEC3G-mediated inhibition of Measles virus replication.
   Vishakha Tiwarekar, Sabine Kendl, Julia Wohlfahrt, Markus Fehrholz, Jürgen Schneider-Schaulies. Eureka! 11th International GSLS Symposium, Rudolf-Virchow Center, University of Würzburg, Germany (2016).
4. Analysis of APOBEC3G-mediated inhibition of Measles virus replication.
   Vishakha Tiwarekar, Sabine Kendl, Julia Wohlfahrt, Markus Fehrholz, Jürgen Schneider-Schaulies. 11th Annual meeting of Immunology training network: Tübingen, Erlangen and Würzburg, Obertrubach, Germany (2016)

5. APOBEC3G-regulated host factors interfere with Measles Virus replication: Role of DDIT4/REDD1 and KDELR-2
   Vishakha Tiwarekar, Sabine Kendl, Julia Wohlfahrt, Markus Fehrholz, Jürgen Schneider-Schaulies. 6th European Congress of Virology, Hamburg, Germany (2016).
6. REDD1 and mTORC1 regulate measles virus replication in Vero and primary human peripheral blood lymohocytes
   Vishakha Tiwarekar, Sabine Kendl, Julia Wohlfahrt, Markus Fehrholz, Jürgen Schneider-Schaulies. 28th Annual Meeting of the Society of Virology, Würzburg, Germany (2018).

Oral presentations

1. Analysis of host factors in Measles virus replication. 10th Annual meeting of Immunology training network: Tübingen, Erlangen and Würzburg, Tagungszentrum Blaubeuren, Germany (2015).
2. Analysis of APOBEC3G mediated inhibition of Measles virus replication. GSLS winter Retreat, Lenggries, Germany (2016).
3. The host cell factors REDD1 and KDELR2 restricts measles virus replication in APOBEC3G expressing Vero cells. 12th Annual meeting of Immunology training network: Tübingen, Erlangen and Würzburg, Kloster Schöntal, Germany (2017).